

PROJECT ADMINISTRATION DATA SHEET

Project No. E25-669 (Subproject under B10-628) ORIGINAL REVISION NO. _____
 Project Director: Dr. William Z. Black GTRI/ GA DATE 5-29-84
 Sponsor: GTE Laboratories, 40 Sylvan Road, Waltham Mass 02254 School/ Mechanical Eng.
 Type Agreement: Basic Agreement B10-628, dated 5-3-84
 Award Period: From 4-1-84 To 12-31-85 (Performance) 12-31-84 (Reports)
 Sponsor Amount: This Change Total to Date
 Estimated: \$ _____ \$ _____
 Funded: \$ 50,000 \$ 50,000

Cost Sharing Amount: \$ None Cost Sharing No: _____
 Title: GTE Laboratories Microelectronics Research Program

ADMINISTRATIVE DATA
 OCA Contact Don Harty
 1) Sponsor Technical Contact: _____
 2) Sponsor Admin/Contractual Matters: _____

Dr. John Hooper
GA Dept.
(Main Project Director)

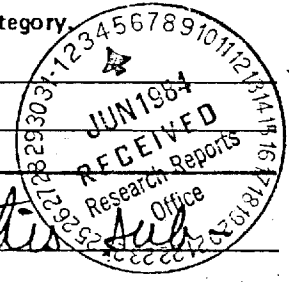
Defense Priority Rating: N/A Military Security Classification: N/A
 (or) Company/Industrial Proprietary: N/A

RESTRICTIONS
 Fee Attached N/A Supplemental Information Sheet for Additional Requirements.

Travel: Foreign travel must have prior approval - Contact OCA in each case. Domestic travel requires sponsor approval where total will exceed greater of \$500 or 125% of approved proposal budget category.

Equipment: Title vests with N/A

COMMENTS:
Reporting and budget to be under this subproject, but billing to be combined under B10-628



COPIES TO:
 Project Director
 Research Administrative Network - ME, OIP
 Research Property Management
 Accounting
 Procurement/EES Supply Services
 Research Security Services
 Reports Coordinator (OCA)
 Research Communications (2)
 GTRI
 Library
 Project File
 Other J. Hooper
02,206,000, E25669

SPONSORED PROJECT TERMINATION/CLOSEOUT SHEET

Date 2/3/87

Project No. E-25-669 (Sub under B-10-628) School/~~XXX~~ ME

Includes Subproject No.(s) N/A

Project Director(s) W. Z. Black GTRC / ~~GIT~~

Sponsor GTE Laboratories, 40 Sylvan Road, Waltham, Mass. 02254

Title GTE Laboratories Microelectronics Research Program

Effective Completion Date: 12/31/86 (Performance) 12/31/86 (Reports)

Grant/Contract Closeout Actions Remaining:

- None
- Final Invoice or Final Fiscal Report
- Closing Documents
- Final Report of Inventions
- Govt. Property Inventory & Related Certificate
- Classified Material Certificate
- Other _____

Continues Project No. _____ Continued by Project No. _____

COPIES TO:

Project Director
 Research Administrative Network
 Research Property Management
 Accounting
 Procurement/GTRI Supply Services
 Research Security Services
 Report Coordinator (OCN)
~~XXXXXXXXXX~~

Library
 GTRC
~~RESEARCH ADMINISTRATIVE NETWORK~~
 Project File
 Other Ina Lashley
Angela Jones
Russ Embry

Georgia Institute of Technology

A UNIT OF THE UNIVERSITY SYSTEM OF GEORGIA

SCHOOL OF MECHANICAL ENGINEERING

ATLANTA, GEORGIA 30332

November 27, 1984

Dr. William F. Nelson
Director, Collaborative Research Programs
GTE Laboratories, Inc.
40 Sylvan Road
Waltham, Massachusetts 02254

Subject: Quarterly Progress Report - August through October 1984, "Heat Transfer During the Manufacture of Fiber Optic Materials"

Dissertation Proposal

The dissertation proposal was submitted to the graduate committee and returned with comments. The proposal is being revised as recommended by the graduate committee and will be resubmitted in late November. A copy of the thesis proposal is attached to this report.

Summary of Progress on Analysis

The theoretical analysis which will eventually provide the temperature and velocity profiles within the fiber during the drawing process has progressed to a point where the governing differential equations have been formulated. Further simplification of the equations and eventual solutions are being postponed by a decision on the appropriate set of coordinates to use for the formulation of the equation for radiative transfer through the fiber.

The intensity of radiation is a function of both direction and location. Therefore five spatial variables are needed to specify the intensity. The selection of the coordinate system is important in determining the form of the equation of radiative transfer and the surface boundary condition of the incident radiation. A cylindrical coordinate system (r, θ, ϕ) is the obvious choice to specify an arbitrary point in the glass during the drawing process. To specify the direction of radiant intensity at any point, two more coordinates are needed. Two schemes for specifying these two variables are being considered at this time: 1) a spherical coordinate arrangement where the azimuthal angle is measured from the radial direction of the cylindrical coordinate system. This approach provides an advantage of simplifying the surface boundary conditions of the incident radiant energy. However, this method increases the complexity of the equations of radiative transfer. 2) a spherical coordinate arrangement where the azimuthal angle is measured from the axial direction of the cylindrical coordinate system. This method reduces the complexity of the equation of radiative transfer, but the formulation of the boundary conditions are now more difficult. Both schemes are currently being investigated.

Dr. William F. Nelson
November 27, 1984
page 2

The solution to the equation of radiative transfer is being investigated. Two methods are currently being considered. Application of Lie Group Theory to reduce the number of independent variables is being attempted. The method is first being applied to a simplified equation with azimuthal symmetry and no variation in the z (axial) direction. Hopefully this will provide insight into the different transformation groups that may be successful in reducing the number of independent variables.

The second method which is referred to as the normal-mode expansion technique is being reviewed. This method is similar to an eigenvalue problem where the solution is written as a linear sum of normal modes, and the expansion coefficients are determined from the boundary conditions. Although this method has been used successfully in "slab geometry" problems only, its use in other types of geometries is promising.

Additional Accomplishments

During the fall quarter of 1984 a Master's candidate has been added to the project. David Marcille, a graduate of Southeastern Massachusetts University, has agreed to work on the fiber optics problem as part of his Master's thesis requirement. Since additional funds are not available, he has agreed to join the project at no additional cost to GTE. To accommodate the addition of Mr. Marcille, the thermal analysis has been subdivided into two major segments. Mr. Parise continues to work on the thermal model of the fiber in the pre-melt and melt-zones, while Mr. Marcille will concentrate on formulating the basic conservation equations within the post-melt zone. Since the analysis is significantly less complex within the post-melt zone, it is anticipated the predicted fiber temperatures will be verified by an experimental program. At this time we feel that new infrared photographic equipment recently purchased by the School of Mechanical Engineering can be used to predict the glass fiber temperature in the post-melt region. The potential of the infrared equipment will be evaluated during the next several months of the project.

Respectfully submitted,



William Z. Black
Project Director

A HEAT TRANSFER AND FLUID FLOW MODEL
FOR THE DRAWING OF OPTICAL FIBERS

A THESIS PROPOSAL

Presented to

The Faculty of the School of Mechanical Engineering

By

Ronald J. Parise

In Partial Fulfillment

of the Requirements for the Degree

Doctor of Philosophy in the School of Mechanical Engineering

Georgia Institute of Technology

July 1984

TABLE OF CONTENTS

	Page
ABSTRACT	iii
NOMENCLATURE	V
Chapter	
I. LITERATURE REVIEW	1
Introduction	
Polymer and Glass Spinning	
Optical Fiber Drawing	
II. FORMULATION OF PROBLEM	15
Process Description	
Melt Zone	
III. PROPOSED INVESTIGATION	22
REFERENCES	25

ABSTRACT

The work described in this proposal has grown out of a research project funded by GTE Research Laboratories, Waltham, Massachusetts (E25-669). The manufacture of optical waveguides is a highly competitive industry, with a potential market of thousands of kilometers of fiber cable to be manufactured and installed over the next ten years, for both new installations and the replacement of existing copper conductors. As one of the major users of fiber optic materials in their communication network, GTE is concerned about obtaining fiber optic materials that have a low cost and yet a high quality. As a result, GTE has asked the School of Mechanical Engineering to thermally model the fiber drawing process in an attempt to more thoroughly understand those factors that influence the quality of the produced fiber.

This proposal describes a heat transfer and fluid flow analysis of the drawing of the optical fibers using the preform method. The early work in analyzing the drawing of optical fibers was based on existing analytical models and experimental data for the spinning of polymers and glass threads or fibers drawn from crucibles. For a fluid dynamics and heat transfer analysis, the region of cooling is the same for both fiber drawing methods. The cooling process was the common denominator for studying fiber spinning that provided a basis for analyzing the optical fiber drawing. However, the drawing of optical fibers requires a heat input along the surface of the preform to melt the glass, which is unique to the manufacture of optical fibers.

The thermal analysis of the drawing process will be developed for the melt zone region where the glass flows and the preform diameter attenuates to the fiber diameter. Due to the high temperatures required to melt the glass, the use of the equation of radiative transfer to account for the emission and absorption of radiant energy in the glass is necessary. Also, for the technique of drawing an optical fiber from a preform, the shape of the free surface is unknown. Therefore, the solution of the equations of motion with the free surface boundary conditions will be needed to determine the shape of the free surface at the glass-air interface.

The resulting model will provide a more thorough understanding of the drawing process and will result in the manufacture of higher quality fibers at increased production rates.

NOMENCLATURE

C	specific heat of glass
g	acceleration of gravity
h	convective heat transfer coefficient
I_{ν}	spectral radiation intensity
$I_{\nu b}$	spectral blackbody intensity
$k(T)$	thermal conductivity
P	pressure
\bar{q}^r	net radiative heat flux vector
r	radial direction
r_o	radius of glass in the drawdown region
s	arbitrary direction of I_{ν}
\bar{S}	direction of I_{ν}
t	time
T	temperature
v_r	radial velocity component
v_z	axial velocity component
$v_{r,0}$	upstream radial boundary velocity in the melt zone
$v_{z,0}$	upstream axial boundary velocity into the melt zone
V_o	preform velocity
\bar{x}	position vector of I_{ν}
z	axial direction

α_{ν}	glass spectral absorption coefficient
θ	angular direction
$\mu(T)$	glass viscosity
ν	frequency
ρ	glass density
ω	solid angle

CHAPTER I

LITERATURE REVIEW

Introduction

The earliest studies in the area of fibers considered the spinning (drawing) of threads through spinnerets or nozzles. The interest here was in the textile industry for the manufacture of manmade fibers for synthetic material or glass wool which were made from either polymers or glasses. The material to be drawn would originate in a crucible where the molten material would flow through an orifice or nozzle with the diameter of the fiber attenuated to the desired dimension as the fiber cooled. The fiber was then collected on a rotating drum, in a continuous process.

The techniques and experience gained in the textile industry can only be partially applied to the drawing of an optical fiber. The fundamental mechanisms of fluid mechanics and heat transfer downstream of the furnace are the same, but the physics of heat addition along the surface of the preform to melt the glass and allow the drawing of the fiber is very different (Figure 1-1). Therefore the experimental data and analytical work performed on fibers drawn from crucibles provide insight into the cooling of optical waveguides downstream of the furnace, but the region in the furnace is unique to optical fibers.

For the drawing of optical fibers, the complexity of the problem is threefold: (1) Having to consider the heat transfer mode of radiation as

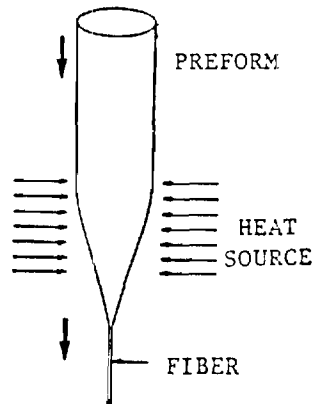


Figure 1-1. Neckdown Region for Drawing an Optical Fiber.

well as the modes of conduction and convection, the equations to solve are highly non-linear integrodifferential equations. (2) The solid preform in the furnace is transformed into a small diameter fiber within one or two preform diameters by heating the surface of the preform along its axis. The preform melts and the fiber is drawn, resulting in a drawdown ratio of up to (and sometimes more than) 100:1 in an axial direction. As a result of the radical change in the glass diameter during the drawdown process in the melt zone, the fiber is subjected to several forces including the drawing or tensile force on the fiber, and the viscous forces and surface tension stresses. These forces must be balanced to maintain diameter consistency of the fiber within 0.5%. (3) Properties of glass are dependent on the temperature field resulting in viscosity profiles in the melt zone, glass viscosity almost doubling for a 50-degree drop in temperature at the draw conditions, and the absorption coefficient varying with temperature as well, although not as drastically. Therefore the governing equations are coupled through temperature-dependent properties, further complicating the solution to the problem.

In the thermal model, the basic conservation laws of mass, energy, and momentum must be satisfied. Because the process involves such high temperatures, the equation of radiant energy transfer (for the glass media emitting and absorbing radiant energy) must also be satisfied to determine the intensity of the radiation field. With the radiation intensity not only a function of location but also of direction, the energy flux within the glass will also be a function of location and direction, complicating the analysis further.

The material of the fiber being spun, whether glass or polymer, affects the analytical model. Polymers and certain glasses are drawn at lower temperatures, hence radiation effects are less significant and frequently neglected. The fused silica used in optical fibers is drawn at a much higher temperature ($\sim 2000^{\circ}\text{C}$) than glass fibers drawn from crucibles, therefore the radiative mode of heat transfer is quite significant. References [1-13] discuss glass spinning while references [14-26] discuss the spinning of polymers, with some authors showing interest in both materials. Although the spinning of polymers and glass can differ significantly, the early studies provide an understanding of some of the fundamental physics involved in the drawing of the two types of materials.

During the drawing process, the fiber diameter is maintained by the tension of the take-up drum as the fiber is wound. Diameter control on polymers or glass drawn from nozzles is not critical. The primary concern is that the fiber does not break during spinning. For optical fibers, diameter control is one of the most critical draw parameters in the manufacture of low loss splices [27]. With draw speeds being important to production rates for the spinning of fibers, as with the drawing of optical fibers,

studies have been completed to predict the stability of draws to prevent breakage [13,19-22]. (Waveguides are drawn at 1 to 10 m/sec, polymer or glass spinning at 100 m/sec, and metal wires at 5 to 15 m/sec [28].)

Polymer and Glass Spinning

All of the early models of polymers and glasses drawn from spinnerets were concerned with fiber cooling time. Prior to 1964, all the models [1,2,5,14] were simple. Glicksman [6] was the first to solve the coupled energy, including radiation, and momentum equations for a cooling fiber for the one-dimensional case. His solution is valid in a region downstream of the nozzle where the slope of the boundary on the fiber is less than one-tenth. That is, the axial velocity, temperature, and pressure can be assumed constant over the cross-section normal to the jet axis, where the fiber slope is less than one-tenth. This has become the classic work for one-dimensional analysis of a cooling glass fiber, referred to as the small slope theory model.

Earlier works by Anderson [1] and Bateson [2] discussed the effect of cooling time on the strength of glass. They state that rapid cooling results in a higher fiber strength: the higher the rate of cooling, the stronger the fiber. But Glicksman's [3] analysis shows that cooling times are more than an order of magnitude greater than previously predicted. Glicksman attributed the higher strength of the fiber to both the fiber draw rate and the tension of the draw. If the flow rate is increased, or the tension is decreased, the fiber will cool faster. According to Glicksman, the rate of cooling increases to a value where the fiber reaches a tensile strength near the theoretical maximum strength. Increasing the cooling rate further

will no longer affect the tensile strength of the fiber. However, Burgman [4] reports that the rate of drawing affects the shape of the drawdown region as well. Therefore the relationship between the strength of the fiber and the drawing tension may be the shape of the melt zone that affects the cooling, consequently the strength. However, although Glicksman's [3] cooling model does show an increase in cooling time compared to the Anderson [1] or Bateson [2] solutions, it neglects radiative cooling. If Glicksman had considered radiative cooling, his predicted times may have been comparable to theirs.

Ben-Sabar [12] develops a two-dimensional model of a cooling fiber from a spinneret using a finite element program AXFIN. This model, described in reference [26], includes radiation cooling of the fiber. To account for the wavelength dependency of the radiant properties of glass on the emitted radiant energy, he uses a two-banded model, i.e., the properties are assumed constant over two different regions of the spectrum. The model includes an assumption that the glass is "optically thick" for the long wavelength (low frequency) energy and "optically thin" for the short wavelength (high frequency) energy. The optically thick band (Rosseland or diffusion) approximation is questionable, since its use near the boundary surface is not accurate [29]. Therefore, Ben-Sabar uses a blackbody approximation at the surface. For the equation of radiative transfer, the temperature in the jet is assumed to be a function of the axial direction only with radial temperature variations neglected. Essentially this is the small slope theory approximation for the equation of radiative transport in the upper neckdown region.

Ben-Sabar's finite element model, when compared with data by Glicksman [6], does not match well. Ben-Sabar's use of the one-dimensional model (small slope theory) as a matching downstream boundary condition imposes fixed conditions on the heat flux, axial stresses, and the draw force on the fiber at the point of take-up. The draw force was based on experimental measurements made by Glicksman [6] which included the aerodynamic drag force on the fiber. To properly match the conditions at the boundary between the upper jet region (where the flow is two-dimensional) and the one-dimensional region, the draw force must be reduced appropriately to account for the aerodynamic drag force on the fiber. Ben-Sabar estimated the drag force to be 40 percent of the measured draw force. Estimation of the drag force may be the reason Ben-Sabar's finite element model does not compare well with Glicksman's experimental data. Without experimental data, the draw force becomes an unknown parameter as well. Therefore Ben-Sabar forced his theoretical model to fit Glicksman's experimental data without consideration of the proper interaction of all the physical parameters.

Optical Fiber Drawing

The fluid mechanics and thermal models for drawing fibers from nozzles or spinnerets have been the basis of the early studies for drawing of optical waveguides. The effects of surface tension, gravity, air drag, viscous stresses, inertia, and tensile drawing force are important when fibers are drawn from both a nozzle and a preform. The drawdown occurs in such a small region (two or three preform diameters) that large temperature gradients will cause large property variations in a short axial and radial distance.

The current methods used for drawing the highly pure silica (semiconductor grade) fibers are similar in the basic principle of pulling the fiber from a glass rod or preform, but differ in the type of heating or furnace that is used. All fibers are drawn from a glass rod or preform, initially about a meter long and with a diameter that could vary from 0.5 cm to about 2.5 cm. The end of the preform is heated to the melting temperature of the glass and then is drawn from the preform diameter to the desired fiber diameter (Figure 1-1). The solid preform is manufactured so that the center or core of the rod has a higher index of refraction than the outer or cladding glass material. When the fiber is drawn from the preform, the fiber retains the desired optical properties of the preform, providing a better media to guide the light beam.

The drawing takes place in a device called a draw tower where the fiber, after being drawn in the furnace, is cooled, then passes through a coating process where a protective polymer coating is applied; the coating is dried, and the fiber is taken up on a spool in a continuous process. The tension on the fiber provided by the take-up spool controls the rate of pull and consequently the fiber diameter. The diameter is controlled by an optical scanner downstream of the furnace with feedback to the tensioner on the spool.

Problems with optical waveguides that occur as a direct consequence of the drawing process are dimensional (diameter) consistency, strength, and optical transmission [28,30]. Dimensional consistency of the fiber diameter is important since the outer fiber diameter serves as the reference surface for alignment during splicing, and misalignment is a major cause of signal loss as the lightwave leaves one fiber and enters the next at a splice [31-33]. The strength of the fiber is important in the handling, installation,

not agree. Glicksman [3] attributes the increased strength to the drawing tension on the fiber, as discussed earlier. But the graphite furnace provides the flexibility needed to control the energy input to the melting glass, influencing the shape of the melt zone which affects the cooling rate and possibly the strength of the fiber.

Payne and Gambling [42], Kobayashi et al. [43], and Nakahara et al. [44] present experimental data of fiber properties for fibers drawn in furnaces with carbon resistance heaters. They present no analytical work. Apparently no papers have analyzed the fiber drawing process for this type of heat source. Although the analytical model should be independent of the type of heat source used, the boundary conditions will be affected by the choice of heat source.

An accurate thermal model is needed to analyze the physical mechanisms involved to predict the stability of the drawing process. The stability analysis is useful in optimizing the control of the fiber diameter. Therefore the thermal model provides the information needed to determine the influence of the drawing process on the two major parameters affecting the quality of the optical fiber, the diameter and the fiber strength. Geyling [34,35] has developed stability models of fibers drawn from preforms based on Glicksman's [6] small slope theory. Geyling's stability analysis requires an analytical base flow. He performs some flow visualization studies [45] to justify the small slope theory approach. The visualization studies do show that there exists a hot zone at the surface of the preform that melts and flows more quickly than the rest of the glass forming a

"boundary layer" near the beginning of the drawdown region and also a hot zone on the axis further downstream. He indicates that these hot zones are due to radiation effects, and he concedes that more work is needed to include these radiation effects [46]. Geyling's experiments are based on a laser furnace where most of the energy is absorbed at the surface of the preform. This could explain the local heating effect at the surface. The downstream effect is due to internal reflection of the energy in the glass. Hence the radiation mode of exchange in the preform is considerable.

Geyling and Homsy [36] investigate the stability of a one-dimensional fiber draw that includes the effects of radiation heat transfer for a laser drawn fiber. They present a temperature profile along the axis of the fiber, combining Geyling's one-dimensional model from small slope theory with a thermal model including radiant energy from the laser in the melt zone. The thermal model used in the melt zone is based on a study by Homsy and Walker [47], where the laser furnace heats the preform to flowing conditions. The thermal model considers both conduction and radiation modes of heat exchange, using the Rosseland approximation (diffusion) for the absorption of radiant energy for a participating media, and only flow in the radial direction. The axial flow of energy is neglected. Also, the momentum equation is decoupled from the energy equation by assuming the form of the radial velocity and using an empirical formulation for the shape of the melt zone.

Paek and Runk [48] develop a one-dimensional model considering only axial gradients in the glass, using a zirconia oxide (ZrO_2) susceptor furnace as the heat source. They use the Rosseland approximation to simplify the radiation term in the energy equation, and neglect inertial terms in

the equation of motion. Hence, the analysis is good as a first approximation.

Sayles [49] develops a two-dimensional fluid dynamics and heat transfer model of a fiber being drawn, based on the finite element program AXFIN developed earlier [26]. To simplify the radiation analysis and to account for material properties dependent on wavelength, Sayles used a banded radiation model similar to Glicksman's [6] two-banded model. For the short wavelength bands (the optically thin limit), Sayles assumes that the absorption of radiation is negligible compared to emission, with the emitted radiation transmitted across boundaries where no reflection or re-emission occurs.

For the long wavelength band (the optically thick limit), the radiative transfer equation is approximated using the method of moments, since a larger portion of the energy is absorbed, and both emission and absorption of radiation in the glass must be considered. Sayles uses the first three moments which are the only moments that have a physical significance [50,51]. The zeroth moment is the mean radiation density, the first moment is the radiative energy flux, and the second moment is the radiation stress and pressure tensor.

Sayles' results show a localized heating at the surface, resulting in a large temperature gradient between the surface and the center of the preform. Hence his results justify the two-dimensional model in the melt zone and suggest that one-dimensional models will lead to inaccurate results.

Sayles' analysis considers only the upper jet region of the fiber draw. This is the region where there is fully two-dimensional flow, prior to the region where the one-dimensional assumptions are valid. This eliminates the problems Ben-Sabar [12] encountered by having to estimate the

aerodynamic drag force on the fiber or to consider the fiber drawing force as an unknown. Sayles uses Glicksman's [6] predicted velocity and stress fields and temperature distribution as the downstream boundary conditions, but Sayles' analysis does not include the one-dimensional region downstream or the fiber drawing force. Therefore Sayles' investigation is not a complete analysis of the fiber drawing process.

Sayles' work [49] represents the latest effort in developing a heat transfer model in fiber drawing. His two-dimensional model addresses the input of radiant energy as a heat source and simplifies the analysis to account for the radiation intensity attenuating as it travels through the media.

Oh [37] shows for a simplified model that the shape of the neckdown is dependent on the heat source, and verifies his conclusion experimentally. Figure 1-2 shows the neckdown shapes for the various heating methods, and Table 1-1 shows the time for the fiber to cool from the maximum temperature

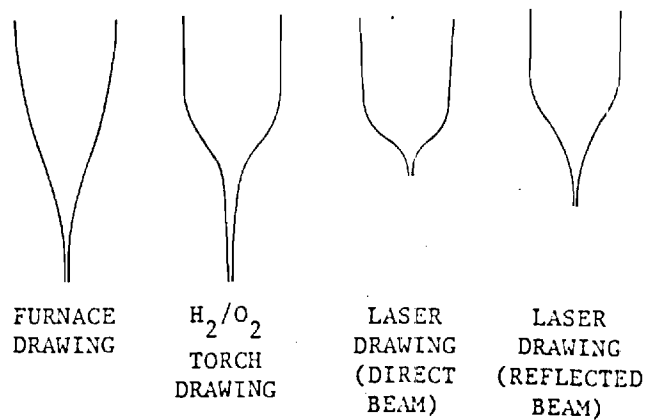


Figure 1-2. Neckdown Profiles of Optical Fibers Drawn from Preforms for Different Heat Sources (Oh [37]).

Table 1-1. Convective Heat Transfer Coefficient (h) and Cooling Times (t) (Oh [37]).

Heating Method	Convective Heat Transfer Coefficient (h) W/m ² °C	Time t, [ms], for a glass temperature drop of 400°C*
Graphite Furnace	49.40	522
Reflected Laser Beam	75.36	341
H ₂ O ₂ Torch	158.26	162
Direct Laser Beam	316.10	81

*Based on a glass temperature in the furnace of 1875 K and a minimum glass temperature for diameter attenuation of 1473 K.

in the furnace to the point at which the fiber reaches its final draw diameter. The shape of the neckdown also influences the heat transfer coefficient (shown in Table 1-1) which affects the cooling rate of the fiber. As a result the type of heat source used to melt the fiber can influence the cooling rate experienced by the fiber. In fact the directed beam CO₂ laser heat source provides for the most rapid cooling of the fiber. With an improved thermal model of the drawing process, and better understanding of the way the heat source shapes the drawdown region, an optimum heat input can be achieved that would shape the melt zone to yield maximum strength for the drawn fiber. Because the graphite furnace can be shaped to give any desirable heat flux, this promises to be the heat source with the greatest flexibility for optical fiber drawing.

Paek and Schroeder [52] reduced the cooling time of the fiber by increasing the convective heat transfer coefficient on the surface of the fiber. They increased the fiber draw rate twofold by forced convective

cooling of the fiber. They investigated heating by both CO₂ laser and zirconia furnace systems. No consideration was given to the effect of turbulence on the diameter tolerances of the fiber. Increased turbulence can introduce instabilities in the draw, creating problems with diameter control. Therefore this is not considered to be a desirable solution for increasing draw rates. Paek [54] did show that the flux distribution along the furnace wall influenced the shape of the melt zone. This agrees with the work by Oh [37] because the four types of furnaces that he compared provided different heat fluxes, producing the different shaped melt zones.

Having now addressed the literature for work in thermal modeling of the drawing process, we will look at the formulation of the problem.

CHAPTER II

FORMULATION OF PROBLEM

A thermal model will be developed for the glass preform as it melts in the furnace and is drawn to the fiber diameter. The physics of the problem indicates three zones of interest in the fiber drawing process (Figure 2-1): (1) the pre-melt zone, where the glass enters the furnace and is heated prior to melting; (2) the melt zone, where the glass starts to flow and is drawn to the fiber diameter; and (3) the post-melt zone, where the glass fiber solidifies and cools. The boundary between the pre-melt and melt zones is the point at which the glass starts to flow. The boundary between the melt and post-melt zones is not as well defined. The small slope theory, used by Glicksman [6], will be considered as a criterion to define the start of the post-melt zone. This is the region where the slope of the fiber boundary at the glass-air interface is one-tenth. The post-melt zone is then described by one-dimensional flow to the final fiber diameter and the subsequent cooling of the fiber. Although the interest of this study is in the melt zone only, a detailed description of the overall process will be given. The equations that characterize the process in the melt zone will then be presented.

Process Description

The pre-melt zone is characterized by "slug" flow of the preform entering the furnace. The surface of the preform is exposed to the ambient (room) temperature prior to entering the furnace. In the furnace, the

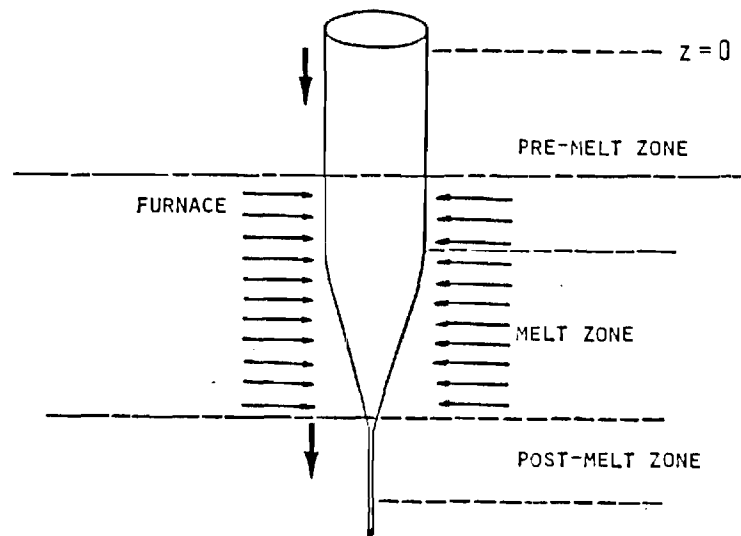


Figure 2-1. Three Zones of Interest to Model Optical Fiber Drawing Process.

glass is heated to the melting temperature. The flowing of the glass however occurs in the next region, the melt zone. From the surface, heat is transferred radially into the glass rod by both conduction and radiation. Internal to the glass preform, energy from the downstream boundary with the melt zone is transferred axially along the preform by both conduction and radiation.

In the melt zone, the glass diameter changes from that of the preform to approximately the final diameter of the finished fiber, in two or three preform diameters. The surface of the preform in the melt zone is exposed to the radiant energy flux from the heat source. As the glass is being drawn, heat continues to be added to the glass and convective cooling occurs due to natural convection in the furnace-glass surface annular region.

The third zone is the region where the slope of the fiber changes slowly enough so that radial velocity and temperature gradients in the

fiber are negligible. The one-dimensional assumptions that are applicable here were shown by Glicksman [6]. The surface will be exposed to the ambient (room) temperature. The glass solidifies, attaining the final fiber diameter, and continues to cool. The end boundary conditions are matched to the upstream melt zone conditions and the downstream fiber velocity, the fiber drawing force, and it will be assumed that the fiber is the same temperature as the ambient.

The zone boundaries have been selected to simplify the thermal model and to best represent the physical configuration of the drawing process. Now that the three zones have been described, the equations for the melt zone will be formulated.

Melt Zone

The initiation of the melt zone region occurs where the glass starts to flow. The large change of the preform diameter attenuating to the fiber diameter in a short axial direction dictates a two-dimensional flow problem and a two-dimensional variation in the temperature field.

The equations of conservation of mass, momentum, energy, and radiative transfer must be solved, all coupled because the properties are functions of the temperature field. The sensitivity of the viscosity to temperature changes will strongly affect the momentum equation; therefore knowledge of the temperature field is critical in this region. The conservation of mass and momentum equations require a two-dimensional treatment. The axial and radial velocity components, pressure gradients, and the viscous stress field must be taken into account. An order of magnitude analysis will be performed to determine which terms may be negligible.

Since the shape of the melt zone is unknown, a simultaneous solution with the free surface boundary conditions is necessary. The upstream and downstream boundary conditions for the two end surfaces in the melt zone, as yet to be determined, will be dictated by the conditions in the pre-melt zone and the downstream one-dimensional flow region, respectively.

For the equations of motion, we consider steady, axisymmetric flow, with the material properties functions of temperature. For constant density, the conservation of mass equation becomes

$$\frac{1}{r} \frac{\partial}{\partial r} (rv_r) + \frac{\partial v_z}{\partial z} = 0. \quad (2-1)$$

For the momentum equation, again the steady, axisymmetric flow assumptions apply. There are two component equations, for the r and z directions, with symmetry in the θ direction. For the r direction:

$$\begin{aligned} \rho(v_r \frac{\partial v_r}{\partial r} + v_z \frac{\partial v_r}{\partial z}) = & - \frac{\partial P}{\partial r} + \frac{2}{r} \frac{\partial}{\partial r} [\mu(T)r \frac{\partial v_r}{\partial r}] \\ & - 2\mu(T) \frac{v_r}{r^2} + \frac{\partial}{\partial z} [\mu(T)(\frac{\partial v_z}{\partial r} + \frac{\partial v_r}{\partial z})]. \end{aligned} \quad (2-2a)$$

For the z direction:

$$\begin{aligned} \rho(v_r \frac{\partial v_z}{\partial r} + v_z \frac{\partial v_z}{\partial z}) = & - \frac{\partial P}{\partial z} + \frac{1}{r} \frac{\partial}{\partial r} [\mu(T)r(\frac{\partial v_z}{\partial r} + \frac{\partial v_r}{\partial z})] \\ & + 2 \frac{\partial}{\partial z} [\mu(T) \frac{\partial v_z}{\partial z}] + \rho g. \end{aligned} \quad (2-2b)$$

The boundary conditions for the equations of motion are: (i) at the upstream boundary, the known axial velocity is $v_{z,0} = V_0$, and the radial velocity is $v_{r,0} = 0$; (ii) the pressure boundary condition is determined at the free surface from the free surface boundary conditions, which will

have to be determined; and (iii) at the downstream boundary, the known axial velocity is from the one-dimensional model and the radial velocity is zero (a basic assumption to the one-dimensional model).

Before considering the energy equation, the equation of radiative transfer will be discussed. The equation of radiative transfer must be solved to determine the divergence of the net radiative heat flux vector for the radiation term in the energy equation. The equation of radiative transfer is solved for the intensity of the radiation field. The equation of radiative transfer for a participating glass media involves both emission and absorption of radiant energy for a material in thermodynamic equilibrium. Using Kirchhoff's Law [53], the radiative transfer equation is

$$\frac{dI_{\nu}(\bar{x}, \bar{S})}{ds} = \alpha_{\nu}(\bar{x}) [I_{\nu b}(T) - I_{\nu}(\bar{x}, \bar{S})]. \quad (2-3)$$

The quantity I_{ν} is the monochromatic radiation intensity at frequency ν ; \bar{x} is the position vector of I_{ν} ; \bar{S} is the direction vector of I_{ν} ; $\alpha_{\nu}(\bar{x})$ is the glass spectral absorption coefficient; $I_{\nu b}(T)$ is the spectral blackbody intensity which is a function of temperature; and dI_{ν}/ds denotes the attenuation of I_{ν} along the path s .

Equation (2-3) can be written:

$$\nabla \cdot [\bar{S} I_{\nu}(\bar{x}, \bar{S})] = \alpha_{\nu}(\bar{x}) [I_{\nu b}(T) - I_{\nu}(\bar{x}, \bar{S})] \quad (2-4)$$

Integrating the spectral intensity over the entire spherical space and over all frequencies, the net radiative heat flux vector \bar{q}^R is obtained. Therefore if Equation (2-4) is integrated over the entire spherical space and

all frequencies, and applying the fact that the spectral blackbody intensity is independent of direction, we have:

$$\nabla \cdot \bar{q}^r = 4\pi \int_0^\infty \alpha_v(\bar{x}) I_{vb}(T) dv - \int_0^\infty \alpha_v(x) \left[\int_{4\pi} I_v(\bar{x}, \bar{S}) d\omega \right] dv. \quad (2-5)$$

The radiative term in the energy equation is the divergence of the net radiative heat flux vector, $\nabla \cdot \bar{q}^r$, Equation (2-5). This expression accounts for the net absorption or emission of radiation by the glass. In the furnace, there is a net absorption of radiation; when the fiber cools, there is a net emission of radiation. Note that the integration in Equation (2-5) requires knowledge of analytical expressions for the spectral absorption coefficient and the spectral radiation intensity field. The use of a banded model for $\alpha_v(\bar{x})$ to account for dependency on wavelength will be applied to simplify the analysis. Consideration will be given to the optical thickness assumptions if further simplification of the equation of radiative transfer is necessary to solve for the spectral radiation intensity field.

To determine the temperature field, the energy equation must be solved along with the equation of radiative transfer. For steady, axisymmetric flow, no internal energy generation, and the thermal conductivity as a function of temperature, the energy equation is:

$$\begin{aligned} \rho C(v_r \frac{\partial T}{\partial r} + v_z \frac{\partial T}{\partial z}) = \frac{1}{r} \frac{\partial}{\partial r} [rk(T) \frac{\partial T}{\partial r}] + \frac{\partial}{\partial z} [k(T) \frac{\partial T}{\partial z}] \\ + 2\mu(T) \left[\left(\frac{\partial v_r}{\partial r} \right)^2 + 2 \left(\frac{v_r}{r} \right)^2 \right] + \nabla \cdot \bar{q}^r \end{aligned} \quad (2-6)$$

where $\nabla \cdot \bar{q}^R$ is determined from Equation (2-5). The next to last term on the right side of Equation (2-6) is the viscous dissipation term. With the large velocity gradients in the flow field, an order of magnitude analysis will have to be performed to determine the significance of these terms.

The upstream and downstream boundary conditions will require matching the temperature and intensity fields in the melt zone to the pre-melt and post-melt zones, respectively.

Along the surface of the attenuating glass rod, the conduction of heat through the glass must be equal to the sum of the convection of heat from the surface to the surrounding gas and the net radiative energy exchange with the surroundings. The radiative boundary condition at the surface is dependent on both the angle of the incident energy on the outer surface of the glass and the reflected energy off the outer surface from within the preform region. Therefore, at the glass-air interface, the radiation intensity has two components, one for internally reflected energy, the other for absorbed energy from the surroundings.

CHAPTER III

PROPOSED INVESTIGATION

The work to be performed in this study will consist of developing and solving the two-dimensional radiative and conductive heat transfer problem in an absorbing and emitting glass media coupled with the two-dimensional conservation of mass and momentum equations for an attenuating glass jet where the free surface geometry of the jet is unknown and must be solved along with the conservation equations. The model will include the melting of the glass preform in the furnace with the attenuation of the preform diameter to the one-dimensional region or small slope region, developed by Glicksman [6]. The final result will entail an algorithm that predicts the temperature, velocity and intensity fields for the fiber drawing process in the melt zone.

For the heat addition in the furnace, the energy equation will be solved with the equation of radiative transfer. The attenuating cylindrical geometry will consider radial and axial variations of the temperature and intensity fields. The heating of the glass will include conduction and radiation heat transfer in the glass, including absorption and emission of the radiant energy. A banded model will be used to eliminate the dependency of the spectral absorptivity of the glass on wavelength. An attempt will be made to solve the equations without the restrictions imposed on the solution utilizing the optical thickness as a criteria to simplify the equation of radiative transport.

This approach is especially important in the melt zone since the glass preform diameter changes up to two orders of magnitude during the drawing process. Since the optical thickness assumptions are in part based on the diameter at the point of interest, some regions in the melt zone may imply an optically thick model while other regions may require an optically thin model. However, should the solution become too formidable without using the optical thickness simplifications, a banded model will then be employed to simplify the equation of radiative transfer as well.

The furnace heat flux is one of the parameters of major interest. Studies have shown that the type of heat source (affecting the flux distribution along the furnace wall [54]) and hence the shape of the melt zone affect the cooling rate of the fiber [37], and the cooling rate may affect fiber strength [1,2,37]. No previous studies were found that address modeling the fiber drawing process in a graphite furnace. The graphite furnace that is being modeled here can be fabricated to permit almost any desirable heat flux output. Therefore the algorithm will ultimately provide a means to optimize the flux and determine the effect of the flux on the drawing process.

Once the analytical model is completed, verification of the analysis will be performed by a comparison with the qualitative data presented by Oh [37]. The shape of the melt zone, as determined by Oh, for a fiber drawn in a graphite furnace will be compared with the shape of the melt zone predicted by the analytical model. An attempt will also be made to measure the surface temperature profile along the fiber in the melt zone with new infrared photography equipment recently

obtained by the School of Mechanical Engineering. GTE Laboratories has made available a draw tower where a limited experimental effort can be carried out to evaluate the influence of the furnace configuration on the quality of the finished fiber. The data obtained can then be used to compare with predicted temperatures provided by the analytical model. However, the main emphasis of this study is on the development of the analytical model. The majority of the experimental verification of the model will be completed in future research projects.

13. Chang, J. C., Denn, M. M., and Geyling, F. T. "Effects of Inertia, Surface Tension, and Gravity on the Stability of Isothermal Drawing of Newtonian Fluids." Industrial and Engineering Chemistry Fundamentals, Vol. 20, 1981.
14. Andrews, E. H. "Cooling of a Spinning Thread-Line." British Journal of Applied Physics, Vol. 10, January 1959.
15. Kase, S. and Matsuo, T. "Studies on Melt Spinning. I. Fundamental Equations on the Dynamics of Melt Spinning." Journal of Polymer Science, Part A, Vol. 3, 1965.
16. Kase, S. and Matsuo, T. "Studies on Melt Spinning. II. Steady-State and Transient Solutions of Fundamental Equations Compared with Experimental Results." Journal of Applied Polymer Science, Vol. 11, 1967.
17. Matovich, M. A. and Pearson, J. R. A. "Spinning a Molten Thread-Line. Steady-State Isothermal Viscous Flows." Industrial and Engineering Chemistry Fundamentals, Vol. 8, No. 3, August 1969.
18. Pearson, J. R. A. and Matovich, M. A. "Spinning a Molten Thread-Line. Stability." Industrial and Engineering Chemistry Fundamentals, Vol. 8, No. 4, November 1969.
19. Shah, Y. T. and Pearson, J. R. A. "On the Stability of Nonisothermal Fiber Spinning." Industrial and Engineering Chemistry Fundamentals, Vol. 11, No. 2, 1972.
20. Shah, Y. T. and Pearson, J. R. A. "On the Stability of Nonisothermal Fiber Spinning - General Case." Industrial and Engineering Chemistry Fundamentals, Vol. 11, No. 2, 1972.
21. Kase, S. "Studies on Melt Spinning. III. Velocity Field Within the Thread." Journal of Applied Polymer Science, Vol. 18, 1974.
22. Kase, S. "Studies on Melt Spinning. IV. On the Stability of Melt Spinning." Journal of Applied Polymer Science, Vol. 18, 1974.
23. Nickell, R. E., Tanner, R. I., and Caswell, B. "The Solution of Viscous Incompressible Jet and Free-Surface Flows Using Finite-Element Methods." Journal of Fluid Mechanics, Vol. 65 (Part I), 1974.
24. Fisher, R. J. and Denn, M. M. "Mechanics of Nonisothermal Polymer Melt Spinning." A.I.Ch.E. Journal, Vol. 23, No. 1, January 1977.
25. Jou, W.-H. "Boundary Layer Development and Heat Transfer for Fiber Spinning." Proceedings of the 1978 Heat Transfer and Fluid Mechanics Institute, Pullman, Washington, June 1978.

26. Ben-Sabar, E. and Caswell, B. "A Stable Finite Element Simulation of Convective Transport." International Journal for Numerical Methods in Engineering, Vol. 14, 1979.
27. Williford, T. L. Jr., Jackson, K. W., and Scholly, C. "Interconnection for Lightguide Fibers." The Western Electric Engineer, Vol. 24, No. 1, Winter 1980.
28. Miller, S. E. and Chynoweth, A. G. (Editors). Optical Fiber Telecommunications. Academic Press, New York, 1979.
29. Deissler, R. G. "Diffusion Approximation for Thermal Radiation in Gases with Jump Boundary Condition." Journal of Heat Transfer, Vol. 86, 1964.
30. Blyler, L. L. Jr. and DiMarcello, F. V. "Fiber Drawing, Coating, and Jacketing." Proceedings of the IEEE, Vol. 68, No. 10, October 1980.
31. Gambling, W. A. and Payne, D. N. "Optical Fibre Systems." Philosophical Transactions of the Royal Society of London. Series A, Vol. 289, 1978.
32. DiMarcello, F. V. and Williams, J. C. "Reproducibility of Optical Fibers Prepared by a Chemical Vapor Deposition Process." Optical Fibre Communication, First European Conference on, London, September 16-18, 1975.
33. DiMarcello, F. V. and Williams, J. C. "Reproducibility of Optical Fibers Prepared by a Modified Chemical Vapor Deposition Process." Bell System Technical Journal, Vol. 57, No. 6, July-August 1978.
34. Geyling, F. T. "Basic Fluid-Dynamic Considerations in the Drawing of Optical Fibers." Bell System Technical Journal, Vol. 55, No. 8, October 1976.
35. Geyling, F. T. "The Glass Fiber Drawing Process and Its Stability Characteristics." Unpublished paper presented at 14th International Congress of Theoretical and Applied Mechanics, Delft, The Netherlands, 1976.
36. Geyling, F. T. and Homsy, G. M. "Extensional Instabilities of the Glass Fibre Drawing Process." Glass Technology, Vol. 21, No. 2, April 1980.
37. Oh, S. M. "Cooling Rates of Optical Fibers During Drawing." Ceramic Bulletin, Vol. 58, No. 11, 1979.
38. Kaiser, P. "Drawing-Induced Coloration in Vitreous Silica Fibers." Journal of the Optical Society of America, Vol. 64, No. 4, April 1974.
39. Tariyal, B. K., Wright, J. G. and Iyengar, R. "The Production of Optical Fibers and Optical Fiber Cables." Unknown source, circa 1981.

40. Osanai, H. "Fabrication of Ultra-Low-Loss Low-OH-Content High Silica Optical Fiber." Electrochemical Society, Fall Meeting, Extended Abstracts, Pittsburgh, PA, 1978.
41. Smithgall, D. H. and Myers, D. L. "Drawing Lightguide Fiber." The Western Electric Engineer, Vol. 24, No. 1, Winter 1980.
42. Payne, D. N. and Gambling, W. A. "A Resistance-Heated High Temperature Furnace for Drawing Silica-Based Fibers for Optical Communications." American Ceramic Society Bulletin, Vol. 55, No. 2, 1976.
43. Kobayashi, T., Osanai, H., Sato, M., Takata, H. and Nakahara, M. "Tensile Strength of Optical Fiber by Furnace Drawing Method." The Transactions of the IECE of Japan, Vol. E61, No. 3, March 1978.
44. Nakahara, M., Sakaguchi, S., and Miyashita, T. "Drawing Techniques for Optical Fibers." In Review of the Electrical Communication Laboratories, Vol. 26, No. 3-4, March-April 1978.
45. Geyling, F. T. "Preliminary Flow Visualization Experiments for the Glass Fiber Drawing Process." Case 39092-3, Bell Laboratories Memorandum for File. October 25, 1976.
46. Geyling, F. T. "The Formation of Glass Fibers for Optical Communication." (Synopsis of Review Paper) Personal Communication, circa 1978.
47. Homsy, G. M. and Walker, K. "Heat Transfer in Laser Drawing of Optical Fibres." Glass Technology, Vol. 20, No. 1, February 1979.
48. Paek, U. C. and Runk, R. B. "Physical Behavior of the Neck-Down Region During Furnace Drawing of Silica Fibers." Journal of Applied Physics, Vol. 49, No. 8, August 1978.
49. Sayles, R. E. Jr. "A Finite Element Analysis of the Upper Jet Region of a Fiber Drawing Flow Field." Ph.D. Dissertation. Division of Engineering, Brown University, Providence, R.I., June 1982.
50. Siegel, R. and Howell, J. R. Thermal Radiation Heat Transfer, Second Edition. Hemisphere Publishing Corporation, McGraw-Hill Book Company, New York, 1981.
51. Ozisik, M. N. Radiative Transfer and Interactions with Conduction and Convection. John Wiley and Sons, New York, 1973.
52. Paek, U. C. and Schroeder, C. M. "Forced Convective Cooling of Optical Fibers in High-Speed Coating." Journal of Applied Physics, Vol. 50, No. 10, October 1979.
53. Condon, E. U. "Radiative Transport in Hot Glass." Journal of Quantitative Spectroscopy and Radiative Transfer, Vol. 8, 1968.
54. Paek, U. C. "Heat Transfer Aspects of Silica Lightguide Fiber Drawing and Coating." AIChE Symposium Series Number 236, Vol. 80, Nayeem M. Farukhi (editor), Niagara Falls, August 1984.



GEORGIA TECH 1885-1985

DESIGNING TOMORROW TODAY

March 11, 1985

Dr. William F. Nelson
Director, Collaborative Research Programs
GTE Laboratories, Inc.
40 Sylvan Road
Waltham, Massachusetts 02254

Pat Heitmuller - ppc
E25-669

SUBJECT: Quarterly Progress Report - November 1984 through January 1985,
"A Heat Transfer and Fluid Flow Model for the Drawing of Optical
Fibers"

Introduction

The following quarterly report was presented at GTE Laboratories in Waltham, Massachusetts, on February 22, 1985. The appendix shows the actual slides used in the presentation. A brief discussion is given that parallels the information provided in the talk.

Discussion

The analysis of the drawing of optical waveguides has been divided into three zones: the pre-melt zone, the melt zone, and the post-melt zone, as shown in Figure 1. The pre-melt zone is a two-dimensional heat transfer problem which includes conduction and radiative heat transfer in a cylindrical glass rod. The two equations to be solved, the energy equation and the equation of radiative transfer, are coupled, integro-differential equations. In the melt zone, the glass is flowing, and the two-dimensional equations of motion must be solved along with the two-dimensional energy equation and the equation of radiative transfer. Therefore, the equations to be solved consist of five coupled integro-differential equations. Ron Parise will carry out the analysis in the pre-melt and melt zones. Dave Marcille will perform

Georgia Institute of Technology
School of Mechanical Engineering Atlanta, Georgia 30332

the analysis in the third zone, the post-melt zone. From earlier work* in the post-melt zone, the flow is considered one-dimensional, based on a criterion where the slope of the surface of the fiber is less than one-tenth. The energy equation will be solved along with the equations of motion, resulting in three coupled equations to be solved. For the transport of radiative energy in the glass the Rosseland approximation will be considered. This provides a simple analytical expression to account for the attenuation of the energy as it is transported through the glass.

Due to the high temperatures involved, the equation of radiative heat transfer must be solved to account for the attenuation of the radiant energy as it travels in the glass (Figure 2). As the energy travels along some path s a distance ds in some elemental volume dAd_s , the radiant intensity is absorbed and re-emitted, with energy scattered into and out of the elemental volume. Therefore, the attenuation of the radiative intensity, dI_v/ds , can be expressed as shown in Equation 1. For glass, Rayleigh's ratio is of the order of 10^{-6} cm^{-1} , therefore the scattering terms are considered negligible. Based on the absorptivity of the glass, α_v , an expression can be determined for the attenuation of the energy in the glass (Equation 2). Now an analytical expression must be determined for dI_v/ds , based on a coordinate system chosen.

The coordinate system chosen is shown in Figure 3. Since the intensity I_v is not only a function of location, but direction as well, five spatial

*Glicksman, L. R., "An Investigation of the Shape, Temperature Distribution, and Tension of a Heat Free Jet at Ultra Low Reynolds Numbers." Ph.D. Dissertation, Massachusetts Institute of Technology, Cambridge, Massachusetts, September 1964.

coordinates are required: r, ψ, z represent a cylindrical coordinate system that specifies a location for \bar{S} ; Ψ, ϕ represent a spherical coordinate system at the location that defines a direction \bar{S} for the intensity.

From the coordinate system in Figure 3, the analytical expression for the equation of radiative transfer then becomes Equation 3. Considering symmetry with ψ , and letting $\mu \equiv \cos\phi$ and $\lambda \equiv \cos\Psi$, the equation can be rewritten as Equation 4. Therefore the equation of radiative transfer is a linear, first order, inhomogeneous partial differential equation with variable coefficients. Since I_b is a function of temperature, the equation must be solved simultaneously with the energy equation. The absorptivity, α_ν , is also a function of temperature slightly, but we will only consider effects due to frequency, ν . With this formulation, the equation of radiative transfer is considered to be two-dimensional in r and z . The directional dependency of I_ν at any location (r, z) is still determined by Ψ and ϕ . Therefore this equation can be used both in the pre-melt and melt zones for the intensity I_ν .

With the development of the two-dimensional (r, z) equation of radiative transfer, the equations can now be presented for the two zones. For the pre-melt zone, the energy and radiative transport equation are required. For a constant velocity rod translating into the furnace the two-dimensional energy equation is Equation 5. The term $\nabla \cdot \bar{q}^R$ is the divergence of the net radiative heat flux vector, determined from Equation 6, with the solution for the radiation intensity from Equation 4. The solution of these two equations in the pre-melt zone determines the radiation intensity and temperature fields in the glass rod in the furnace prior to melting.

At the point where the glass melts and starts to flow is the start of the melt zone. Now the equations of motion (Equation 7, the conservation of mass, and Equations 8, the momentum equations) must also be solved along with the energy and radiative transport equations. The equation of radiative transport is the same as in the pre-melt zone, but the energy equation now includes the convective energy terms. Due to the large turndown ratio of the preform diameter to the fiber diameter in such a short axial distance, the energy equation also includes the viscous dissipation terms. The momentum equations have the temperature dependent viscosity term and are therefore coupled to the energy equation. The pressure gradient is determined from the free surface boundary condition which includes the glass surface tension at the glass-air interface. This boundary condition is used to determine the shape of the free surface. Therefore the five equations must be solved simultaneously.

The basic outline to solve the equations in both the pre-melt and melt zones is shown in Figure 4. The method of solution includes:

1. Solve the equation of radiative transfer for the isothermal case, with no restrictions on the radiative model. In this way the equation can be solved independent of the temperature field and the solution compared with other known solutions.
2. With the solution to the equation of radiative transport verified, the equation can then be solved for the non-isothermal case, i.e., coupled to the energy equation. This would be the solution in the pre-melt zone.

3. The solution of the equations of motion coupled with the solution (slightly modified) in the pre-melt zone would be the solution to the drawing process in the melt zone.
4. The two solutions in the pre-melt and melt zones, compared with the solution provided by Dave Marcille in the post-melt zone, would then describe the drawing of an optical fiber using the preform method.

The first technique attempted in solving the equation of radiative transfer was similarity transformations, outlined in Figure 5a. The simplification of the partial differential equation to an ordinary differential would render a simplified numerical solution. However, the technique was abandoned when it proved fruitless.

The technique now being attempted for the first order partial differential equation, credited to Lagrange, is commonly referred to as method of characteristics. A functional form of the solution has been determined; now boundary conditions must be applied to determine this function. Some possible boundary conditions are outlined in Figure 6, but the actual form of the function is yet to be determined. This is presently being looked at on the project.

The work planned over the next months is outlined as shown in Figure 7 and as discussed earlier with respect to Figure 4, the method of solution. With a solution of the equation of radiative transfer complete, the equations in the pre-melt zone will then be solved. With these solved, the melt zone will then be attempted. The solutions will then be combined with the solution to the equations in the post-melt zone to describe the drawing process.

 3-11-85

Ronald J. Parise

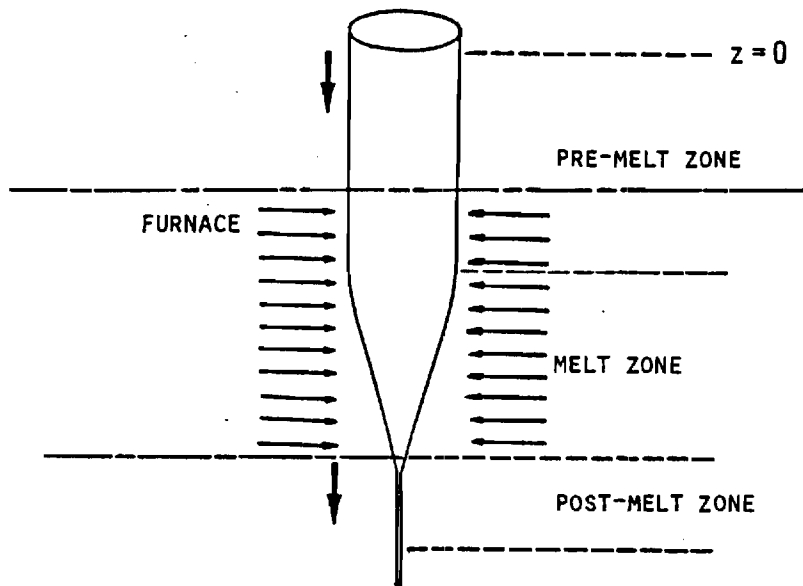
 3/11/85

William Z. Black

APPENDIX

A HEAT TRANSFER AND FLUID FLOW MODEL
FOR THE DRAWING OF OPTICAL FIBERS

RONALD J. PARISE
GEORGIA INSTITUTE OF TECHNOLOGY
SCHOOL OF MECHANICAL ENGINEERING



THREE ZONES OF INTEREST TO MODEL
OPTICAL FIBER DRAWING PROCESS

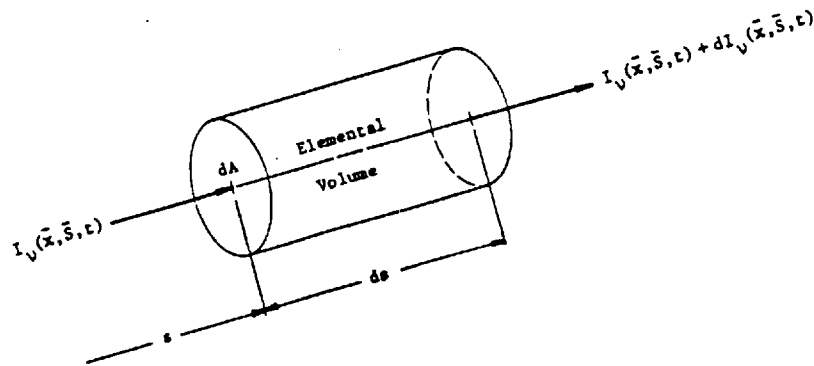
PRE-MELT ZONE: 2 EQUATIONS TO SOLVE

MELT ZONE: 5 EQUATIONS TO SOLVE

POST-MELT ZONE: 3 EQUATIONS TO SOLVE

FIGURE 1

RADIATIVE HEAT TRANSFER IN GLASS



BEAM ATTENUATION IN A PARTICIPATING MEDIA

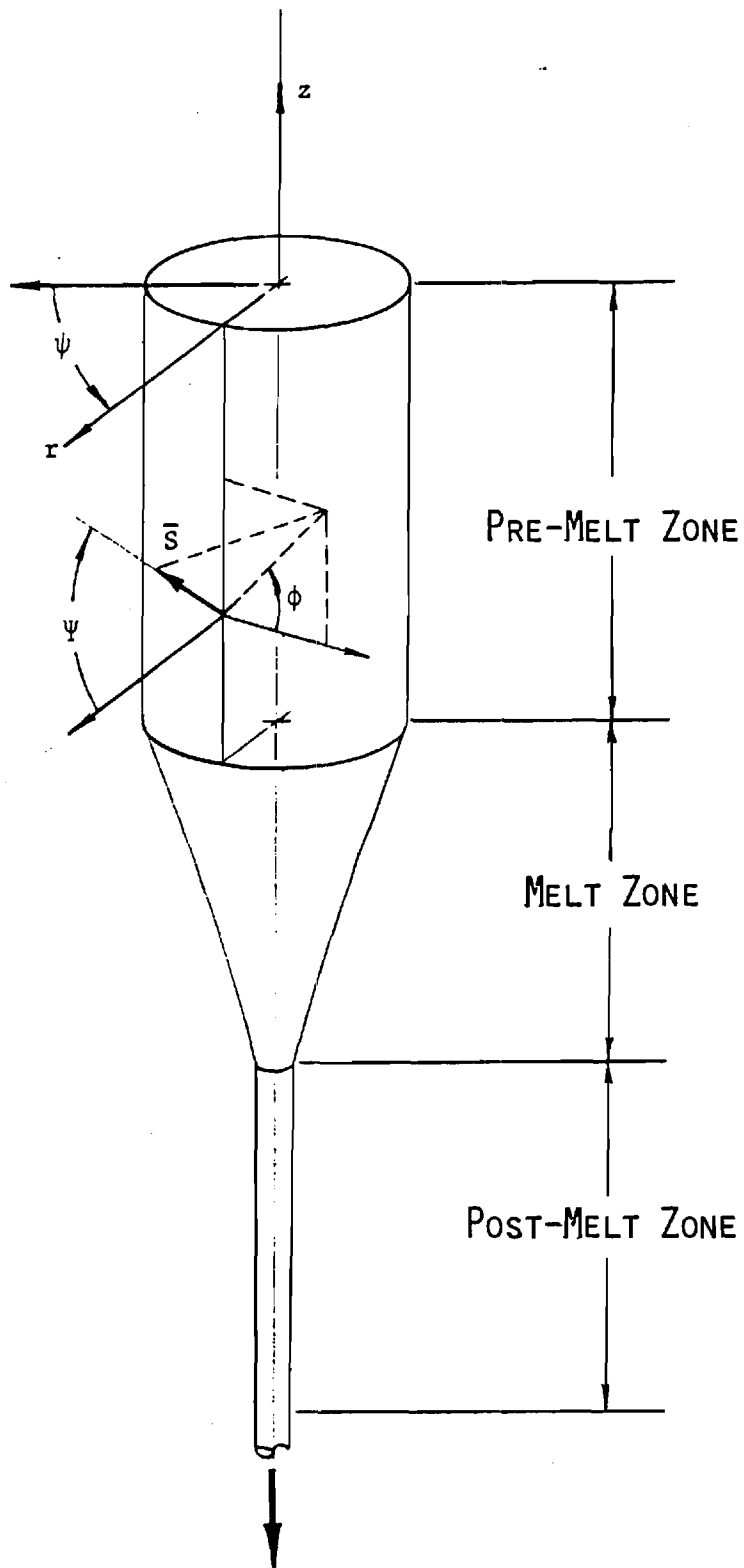
FIGURE 2

GENERAL RADIATION EQUATION

$$\frac{\partial I_{\nu}}{\partial s} = I_{\text{emission}} - I_{\text{absorption}} + I_{\text{in-scattering}} - I_{\text{out-scattering}} \quad (1)$$

NO SCATTERING

$$\frac{dI_{\nu}}{ds}(\bar{x}, \bar{s}) = \alpha_{\nu}(\bar{x}) [I_{\nu b}(T) - I_{\nu}(\bar{x}, \bar{s})] \quad (2)$$



COORDINATE SYSTEM

$$I_v = I_v(r, \psi, z, \Psi, \phi)$$

FIGURE 3

EQUATION OF RADIATIVE TRANSFER

$$\begin{aligned} \cos\psi \frac{\partial I}{\partial r} + \frac{\cos\phi}{r} (\sin\psi \frac{\partial I}{\partial \psi} + \sin\phi \cos\psi \frac{\partial I}{\partial \phi} - \cos\phi \sin\psi \frac{\partial I}{\partial \psi}) \\ + \sin\phi \sin\psi \frac{\partial I}{\partial z} = \alpha(I_b - I) \end{aligned} \quad (3)$$

where $I_b = I_b(T, \nu)$, black body spectral emissive energy

T = temperature

ν = frequency

Consider symmetric about ψ , i.e., $\frac{\partial}{\partial \psi} = 0$ and let $\mu \equiv \cos\phi$; $\lambda \equiv \cos\psi$

$$\lambda \frac{\partial I}{\partial r} + \frac{\lambda\mu}{r} (\mu^2 - 1) \frac{\partial I}{\partial \mu} + \frac{\mu^2}{r} (1 - \lambda^2) \frac{\partial I}{\partial \lambda} + [1 - \mu^2]^{1/2} [1 - \lambda^2]^{1/2} \frac{\partial I}{\partial z} + \alpha I = \alpha I_b \quad (4)$$

PRE-MELT ZONE:

ENERGY EQUATION:

$$\frac{1}{r} \frac{\partial}{\partial r} r k(T) \frac{\partial T}{\partial r} + \frac{\partial}{\partial z} k(T) \frac{\partial T}{\partial z} + \nabla \cdot \bar{q}^r = 0 \quad (5)$$

EQUATION OF RADIATIVE TRANSFER: $\mu \equiv \cos\phi$; $\lambda \equiv \cos\Psi$

$$\lambda \frac{\partial I}{\partial r} + \frac{\lambda \mu}{r} (\mu^2 - 1) \frac{\partial I}{\partial \mu} + \frac{\mu^2}{r} (1 - \lambda^2) \frac{\partial I}{\partial \lambda} + [1 - \mu^2]^{1/2} [1 - \lambda^2]^{1/2} \frac{\partial I}{\partial z} + \alpha I = \alpha I_b \quad (4)$$

$$\text{where } \nabla \cdot \bar{q}^r = 4\pi \int_0^\infty \alpha I_b dv + 2 \int_0^\infty \left\{ \alpha \int_{-1}^1 \left[\int_0^1 \frac{I d\mu}{[1 - \mu^2]^{1/2}} \right] d\lambda \right\} dv \quad (6)$$

NOTE: $I = I(r, z, \mu, \lambda, \nu)$; $T = T(r, z)$; $I_b = I_b(T, \nu)$

MELT ZONE:

CONSERVATION OF MASS:

$$\frac{1}{r} \frac{\partial}{\partial r} (rv_r) + \frac{\partial}{\partial z} v_z = 0 \quad (7)$$

MOMENTUM EQUATIONS:

r-DIRECTION:

$$\begin{aligned} \rho (v_r \frac{\partial v_r}{\partial r} + v_z \frac{\partial v_r}{\partial z}) = & - \frac{\partial P}{\partial r} + \frac{2}{r} \frac{\partial}{\partial r} \eta(T) r \frac{\partial v_r}{\partial r} \\ & - 2\eta(T) \frac{v_r}{r^2} + \frac{\partial}{\partial z} \eta(T) [\frac{\partial v_z}{\partial r} + \frac{\partial v_r}{\partial z}] \end{aligned} \quad (8A)$$

z-DIRECTION:

$$\begin{aligned} \rho (v_r \frac{\partial v_z}{\partial r} + v_z \frac{\partial v_z}{\partial z}) = & - \frac{\partial P}{\partial z} + \frac{1}{r} \frac{\partial}{\partial r} \eta(T) r [\frac{\partial v_z}{\partial r} + \frac{\partial v_r}{\partial z}] \\ & + 2 \frac{\partial}{\partial z} \eta(T) \frac{\partial v_z}{\partial z} + \rho g \end{aligned} \quad (8B)$$

ENERGY EQUATION:

$$\begin{aligned} \rho C (v_r \frac{\partial T}{\partial r} + v_z \frac{\partial T}{\partial z}) = & \frac{1}{r} \frac{\partial}{\partial r} rk(T) \frac{\partial T}{\partial r} + \frac{\partial}{\partial z} k(T) \frac{\partial T}{\partial z} \\ & + 2\eta(T) \{ (\frac{\partial v_r}{\partial r})^2 + 2(\frac{v_r}{r})^2 \} + \nabla \cdot \bar{q}^r \end{aligned} \quad (9)$$

EQUATION OF RADIATIVE TRANSFER: $\mu \equiv \cos\phi$; $\lambda \equiv \cos\psi$

$$\lambda \frac{\partial I}{\partial r} + \frac{\lambda \mu}{r} (\mu^2 - 1) \frac{\partial I}{\partial \mu} + \frac{\mu^2}{r} (1 - \lambda^2) \frac{\partial I}{\partial \lambda} + [1 - \mu^2]^{1/2} [1 - \lambda^2]^{1/2} \frac{\partial I}{\partial z} + \alpha I = \alpha I_b \quad (4)$$

$$\text{where } \nabla \cdot \bar{q}^r = 4\pi \int_0^\infty \alpha I_b dv + 2 \int_0^\infty \{ \alpha \int_{-1}^1 [\int_0^1 \frac{Id\mu}{[1 - \mu^2]^{1/2}}] d\lambda \} dv \quad (6)$$

METHOD OF SOLUTION: ANALYTICAL SOLUTION FOR EQUATION OF
RADIATIVE TRANSFER

- A. SOLVE EQUATION OF RADIATIVE TRANSFER TO ELIMINATE PHYSICAL CONSTRAINTS OF PREVIOUS MODELS
- B. SOLVE EQUATIONS IN PREMELT ZONE (ENERGY EQUATION AND RADIATION EQUATIONS)
- C. SOLVE EQUATIONS IN MELT ZONE (EQUATIONS OF MOTION, ENERGY AND RADIATION)

FIGURE 4

PROGRESS IN SOLUTION OF EQUATION OF RADIATIVE TRANSFER

I) SIMILARITY SOLUTION - LIE GROUP THEORY

A) METHOD DESCRIPTION:

- I) SYSTEM OF EQUATIONS IS INVARIANT UNDER VARIABLE TRANSFORMATION.
- II) EACH TRANSFORMATION RESULTS IN ONE LESS INDEPENDENT VARIABLE.
- III) RESULT IS ODE.
- IV) FINITE GROUPS TRIED TO REDUCE EQUATION - DILATATION GROUP (STRETCHING GROUP) OF THE FORM

$$r' = a^\beta r \quad \text{where } r' = \text{new variable}$$

a^β = "stretching" parameter to power β ;
 β to be determined

r = original variable

- B) INITIAL SUCCESS WITH SIMPLIFIED EQUATION PROVIDED ENCOURAGEMENT - PAPER BY STRIKWERDS ALSO WAS ENCOURAGING.
- C) ATTEMPTS AT FULL EQUATION WERE UNSUCCESSFUL USING FINITE GROUP METHOD.
- D) INFINITESIMAL GROUP TRANSFORMATION
 - I) MOST GENERAL METHOD USING GROUP THEORY - MAY GENERATE NEW GROUPS.
 - II) METHOD DIFFICULT TO APPLY - NOT RECOMMENDED BY PROFESSOR AMES, SCHOOL OF MATHEMATICS, GEORGIA TECH.

FIGURE 5A

II. METHOD OF CHARACTERISTICS -

A) METHOD DESCRIPTION:

- I) USE FIRST ORDER PDE THEORY TO GENERATE SURFACES OF CONSTANT OR CHARACTERISTIC CURVES.
- II) SOLVE HOMOGENOUS EQUATION USING THIS TECHNIQUE.
- III) FIND PARTICULAR SOLUTION FROM BOUNDARY CONDITIONS.
- IV) USING THIS TECHNIQUE, A HOMOGENOUS SOLUTION OF THE FORM HAS BEEN DETERMINED:

$$I_H = e^{-\alpha(1-\lambda^2)^{-1/2}(1-\mu^2)^{-1/2}z} f\left\{\frac{\lambda}{r^2\mu^2(1-\lambda^2)} + \frac{1}{r^2}, \frac{1-\mu^2}{r^2\mu^2}, (1-\mu^2)(1-\lambda^2)\right\}$$

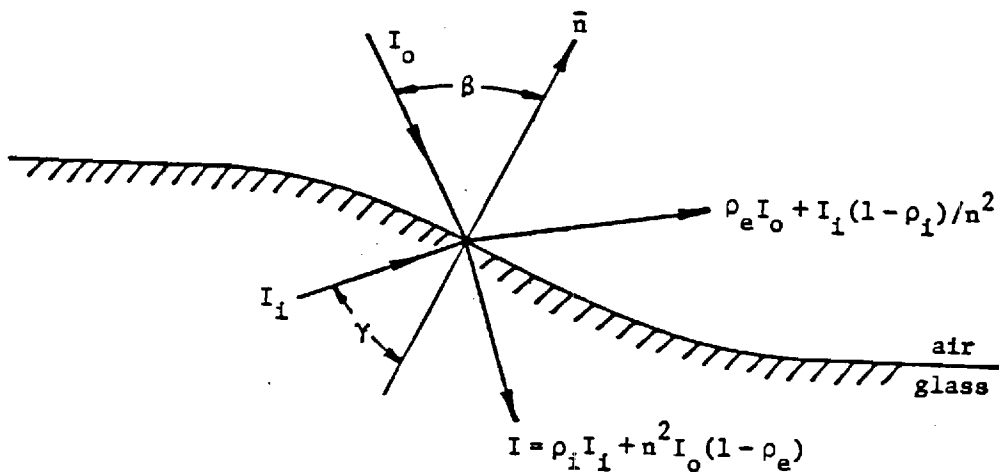
WHERE FUNCTION f HAS YET TO BE DETERMINED.

- B) ONCE f IS DETERMINED FROM BOUNDARY CONDITIONS, FULL SOLUTION MAY BE FOUND.
- C) BOUNDARY CONDITIONS MUST NOW BE DETERMINED.

FIGURE 5B

BOUNDARY CONDITIONS - RADIATION EQUATION: PREMELT ZONE

1. $z = 0; I = I_1(r, 0, \lambda, \mu)$
2. $r = 0, I$ is finite
3. $r = r_o, I(\lambda) = (1 - \rho_e(\beta))I_o n^2 + \rho_i(\gamma)I_i$
Also, $\lambda \geq \lambda^*; I = I$
4. $I(\mu) = I(-\mu)$



RADIANT ENERGY BOUNDARY CONDITION
AT THE GLASS-AIR INTERFACE

FIGURE 6

FUTURE WORK

- A) SOLVE EQUATION OF RADIATIVE TRANSFER.
- B) SOLVE EQUATIONS IN PREMELT ZONE.
- C) SOLVE EQUATIONS IN MELT ZONE.
- D) COMBINE SOLUTIONS WITH THOSE OF DAVE MARCILLE FOR FULL SOLUTION TO FIBER DRAWING PROCESS.

FIGURE 7



GEORGIA TECH 1885-1985

DESIGNING TOMORROW TODAY

September 9, 1985

Dr. William F. Nelson
Director, Collaborative Research Programs
GTE Laboratories Inc.
40 Sylvan Road
Waltham, Mass. 02254

Subject: Quarterly Progress Reports January-March and April-June, 1985
"Heat Transfer During Manufacture of Fiber Optic Materials"

Dear Dr. Nelson:

During the first six months of 1985 satisfactory progress has been made in two major areas. Mr. Ronald Parise, a Ph.D. candidate, has concentrated his effort in solving for the fiber temperature distribution in the pre-melt and melt zones. Mr. David Marcille, an M.S. candidate, has been added to the project during the summer quarter and his work involves determination of the temperature distribution of the fiber in the post-melt zone.

For the conditions that exist in the pre-melt zone, the equation of radiative transfer has been solved without making any simplifying assumptions regarding the optical thickness of the preform. Previous analyses have simplified the radiation equation by considering optically thick (Rosseland Approximation) and optically thin approximations, based on the wavelength of the incident radiant energy and the radius of the preform. During the fiber drawing operation, the diameter of preform changes several orders of magnitude, therefore, the optical thickness changes appreciably along the fiber. The solution obtained during the last six months does not depend on the optical thickness of the preform.

With the solution to the spectral equation of radiation transfer, the radiation heat flux and the divergence of the radiation heat flux vector have been obtained. The equation of radiation transfer provides the spectral intensity of radiation in an arbitrary direction. To determine the radiation heat flux, the spectral intensity is integrated over all directions, and over all wavelengths. These integrations are carried out numerically using a Gauss-Legendre Quadrature. The divergence of the heat flux vector is then performed and the result is used in the

Georgia Institute of Technology

School of Mechanical Engineering Atlanta, Georgia 30332

energy equation. Both algorithms have been written and debugged for syntax errors. There is a problem with stability in the output, because the data oscillates between negative and positive values. This problem will be eliminated in the next few weeks.

An algorithm for the radiation shape factor between the furnace and the preform is being developed. The shape factor, along with the furnace heat flux are important parameters which determine the influence of the furnace design on the quality of the fiber. Therefore, accuracy of the shape factor expression is considered important and will be given considerable attention.

The algorithm for the solution to the energy equation in the pre-melt zone will be expressed in a general form so that it will apply in the melt zone as well. Therefore, for the development of the temperature distribution in the melt zone, the only additional equations that must be solved are the conservation of mass and momentum equations. This work will be started in the next quarter.

Major progress has been made toward the solution of the fiber temperature in the post-melt region. The thermal model of an optical fiber in the post-melt region was developed during the Fall 84 and Winter 85 quarters. The analysis includes the formulation of the conservation of mass and energy equations. The energy equation takes into account the three modes of heat transfer: conduction, convection, and radiation, as well as the convective mass flow energy term. For the radiative heat transfer term, radiation from the surface of the fiber has been considered along with the axial radiative effect. For radiative heat transfer along the axis of the glass, the Rosseland or the diffusion approximation is used.

During the Spring 85 quarter a computer program was written to solve the coupled conservation of mass and energy equations. The program used a Runge-Kutta-Nystrom numerical scheme and for a given predicted fiber shape it will generate a fiber temperature profile for the post-melt region. During the summer quarter the computer program is being debugged and checked for accuracy. Thus far the program accurately reproduces known temperature profiles for radiating, conducting and convecting fins with constant properties. The program also provides values for the temperature distribution in an optical fiber for which the radiative and mass flux terms are absent. These checks provide confidence that the computer program is capable of predicting the fiber temperature when all of the significant energy terms are present. An

Dr. Nelson

-3-

September 9, 1985

order of magnitude calculation for each term in the energy equation has been performed in an attempt to determine the dominant factors which influence the heat transfer from the optical fiber.

Respectfully submitted,



William Z. Black
Project Director



Ronald J. Parise
Graduate Research Assistant



David F. Marcille
Graduate Research Assistant

WZB:pat

Georgia Institute of Technology

A UNIT OF THE UNIVERSITY SYSTEM OF GEORGIA
SCHOOL OF MECHANICAL ENGINEERING
ATLANTA, GEORGIA 30332

June 6, 1984

Dr. William F. Nelson
Director, Collaborative Research Programs
GTE Laboratories Inc.
40 Sylvan Road
Waltham, Mass. 02254

Subject: Quarterly Progress Report April - June 1984 E25-669, "Thermal Model for Microelectronic Chips."

ACCOMPLISHMENTS

Progress has been made in a number of areas during the first three months of the project. Wm. Z. Black traveled to Waltham on March 14, 1984 to discuss the initial planning stages of the project. During that trip he met with J. R. McColl and J. C. Gustafson. It was decided that initial work should focus on heat transfer from a single chip and work on the application to the larger scale system would be postponed until the results of the single chip study were completed. By concentrating effort on a thermal model from a single chip it is hoped that results will point to novel methods for cooling or suggestions for unique construction materials for integrated chip packages.

During the spring quarter 1984 Mr. Geow F. Heng started to work on the project. Mr. Heng is in his second quarter of his Ph.D. degree, majoring in the area of thermal sciences. The work that he performs on this project will form the framework for his Ph.D. thesis.

A comprehensive literature search was initiated during the first month of the project. Effort was concentrated on locating texts and articles which describe projects that thermally model the heat transfer from integrated chip packages. Also articles were sought which describe how heat is generated in a chip and how heat is dissipated from traditionally designed chip packages. The literature search uncovered a number of tests and technical papers which deal with the subject of heat transfer from VLSI packages. These references are listed at the end of this report. The following paragraphs briefly summarizes some of the results of these references.

A chip consists of microelectronic semiconductor components such as transistors, resistors, diodes and capacitors. It is called an integrated circuit because all the components are fabricated on a single substrate and cannot be separated from each other. The most widely used substrate material is silicon, although Gallium Arsenide is another common substrate material. N-type silicon is obtained by adding an

impurity from column V of the periodic table (called a donor). Similarly, p-type silicon is obtained by adding impurity from column III of the periodic table (called an acceptor). The microelectronic semiconductor components are assembled by diffusing the n-type and/or p-type region into a p-type or n-type substrate. Thus, logic gates or networks are implemented on a single chip.

When a single chip mounted on a ceramic substrate is encased into a single package, it is called a monolithic integrated circuit. When the package contains more than one chip and discrete components mounted on a large ceramic substrate, it is called a hybrid integrated circuit. Two common basic packaging configurations are the flat packs and the dual-in-line package (DIP). The pads on the chip (I/O, ground and power supply) are connected to the terminals of the pins of the container by means of lead wires made of gold. The IC packages are mounted by soldering the pins to the printed circuit (PC) boards. The PC boards are then plugged into drawer or rack-mounted back panels.

Integrated circuit performance, in terms of both speed and power has shown continuous improvement in the relatively brief period since its inception. Metal-oxide-semiconductor (MOS) and bipolar circuits are being combined on the same monolithic structure, and the number of active micro-devices on a chip has been steadily increasing. As the chip density increases, the number of I/O pins required for interconnection also increases. Greater pin densities result in chips which are larger and more pins can lead to breakage problems during assembly and during repairs. Also, for high-speed computers, pins of a container are undesirable because of parasitic capacitance which causes time delay (VLSI circuits are intolerant to the high output impedance). One approach to the problems is to assemble IC chips on a ceramic chip carrier which are then mounted on a ceramic mother carrier before placing them on a PC board. Another packaging configuration is the Multilayer Ceramic Multichip module.

The continuous increase in chip density (integration size) could inevitably pose a thermal failure of the chip microcomponents if the heat generated is not efficiently removed. The present day chip used in commercial equipment consists of almost half a million gates and is constrained by the available thermal design and heat removal techniques. The reliability of the microelectronic components typically decreases by 10 percent for every 2°C temperature increase.

Various literature is available which describes the possible methods of cooling microelectronic equipment. Different approaches are employed, including free/forced convection, metal-core conductive PCB/PWB, liquid cooled modules (from water coolant to cryogenic applications), evaporative cold plates, conduction modules.

Various numerical schemes for analyzing the thermal profile of microelectronic equipment have been developed. The approach that will be taken in this study on cooling microelectronic equipment can be itemized into the following three categories:

- i) microcomponent level
- ii) chip level
- iii) system level.

The analysis on the microcomponent level will be delayed temporarily until equipment for mapping temperature profiles of the microcomponents becomes available in the later stages of our research. The study will proceed at the chip level and will eventually built-up to a system level. Eventually a three-dimensional analysis will be required to predict the temperature distribution of the chip. However, initially a one-dimensional analysis is developed to provide an estimate of the governing modes of heat transfer from the chip.

During the literature survey, attention was focused on the packaging configuration of the chip. The geometry of a monolithic chip encapsulated in a DIP configuration was conceptualized as shown in Figure 4. The silicon chip is first mounted on the alumina substrate by eutectic bond. The substrate is then attached to the kovar carrier casing by conductive epoxy bonding. A kovar cover encapsulates the chip within the package, leaving an air gap between the chip and the top cover. Finally, the package is attached to the PC board heat sink and the heat conduction path completed by silicon grease

As part of the effort to thermally model the behavior of an integrated chip, a simplified one-dimensional, transient heat transfer formulation based on the geometry shown in Figure 1 has been completed. This model is highly simplified and it is intended to merely provide guidance in the initial stages of the project. It is hoped, for example, that this model will predict whether conduction of heat through the chip substrate is more significant than conduction through the metallic leads. Also this model should provide insight into whether radiation from the surface of the package is significant and whether radiation needs to be considered in future thermal models.

The geometry of the simplified analytical model consisting of only i) a top cover, ii) an air gap, iii) chip, and iv) a bottom cover was analyzed with convection and radiation heat loss from the top and bottom of the package to the ambient surrounding at 25°C. Heat loss through the leads was also considered. A finite difference method was used to solve the transient form of the energy equation. Starting at uniform ambient conditions, a step input of 1 W/cm² of chip area was used as the heat generated by the chip. The temperature history of the chip, bottom of base and top cover is given in Figure 2. Results from the simplified program are still preliminary at this time and they will be discussed in greater detail in future reports.

A separate study was also made to experimentally measure the temperature of a DIP monolithic integrated circuit. Two holes were drilled in the top plastic cover of Motorola 6800P chips. The holes were drilled to a depth of 55 mils, leaving a thickness of 5 mils before exposing the chip. One hole was drilled directly above the chip and the other was located near the edge of the chip. Copper-Constantan thermocouples were embedded in the holes to provide temperature readings. The chip was then energized with a step input and the voltage

and current measured to obtain the power input. Temperature readings were taken until a steady state condition was obtained. The chip was then reset and tests using voltages ranging from 2.3 to 15 volts were repeated. The plot of steady state temperature as a function of the power input is given in Figure 3 for the thermocouple located directly above the chip.

Currently, work is continuing in the development of a more accurate one-dimensional thermal model of the chip taking into consideration the geometry of the chip given in Figure 4. This model is being developed on a more general basis, keeping in mind that the model will eventually evolve into a three-dimensional analysis. The basis for the model and results predicted by the model will be described in future reports.

Plans are underway to purchase an imaging radiometer from Inframetrics in Bedford Mass. The equipment consists of a TV compatible imaging radiometer, interactive video system, 8 bit processor, IR telescope and microscope objective. This equipment will be used to verify the chip temperature predicted by the analytical model described in the previous section. The infrared camera equipment is capable of measuring the spot temperatures with a diameter of 0.001 inch. While this is not sufficient resolution to measure the temperature of an individual diode or transistor on a chip, it may be small enough to accurately verify the temperature predicted by the thermal model.

Respectfully submitted,



Wm. Z. Black
Project Director

WZB:maw

cc: Dr. John Hooper
Dr. John Brighton

TEXTS

1. Kraus, Allan D., and Bar-Cohen, Avram, "Thermal analysis and Control of Electronic Equipment," Hemisphere Publishing Corporation, Washington, 1983.
2. Seeley, J. H. and Chu, R. C., "Heat Transfer in Microelectronic Equipment", Marcel Dekker, New York, 1972.
3. Steinberg, D. S., "Cooling Techniques for Electronic Equipment," John Wiley & Sons, Inc., New York, 1980.
4. Muroga, S., "VLSI System Design", John Wiley & Sons Inc., New York, 1982.
5. Ellison, G. N., "Thermal Computations for Electronic Equipment", Van Nostrand Reinhold Company, New York, 1984.
6. Lenk, J. D., "Handbook of Integrated Circuits: For Engineers and Technicians," Reston Publishing Company, Reston, 1978.
7. Warner, R. M., Jr., "Integrated Circuits, Design Principles and Fabrication", McGraw-Hill Book Company, New York, 1965.
8. Mannasse, F. K., "Semiconductor Electronics Design", Prentice-Hall, Inc., Englewood Cliffs, 1977.
9. Bell, D. A. "Fundamentals of Electronic Devices," Reston Publishing Company, Inc., Reston, 1975.

PAPERS

1. Aung, W., Kessler, T. J., and Beitin, K. I., "Free Convection Cooling of Electronic Systems," IEEE Transactions on Parts, Hybrids and Packaging, June 1973.
2. Bauer, J. A., "Chip Carrier Packaging Applications" IEEE Transactions on Components, Hybrids, and Manufacturing Technology, March 1980.
3. Blodgett, A. J., and Barbour, D. R., "Thermal Conduction Module: A High-Performance Multilayer Ceramic Package", IBM Journal of Research and Development, January 1980.
4. Blodgett, A. J., "A Multilayer Ceramic Multichip Model", IEEE Transactions on Components, Hybrids, and Manufacturing Technology, December 1980.
5. Bar-Cohen, A., Kraus, A. D., and Davidson, S. F., "Thermal Frontiers in the Design and Packaging of Microelectronic Equipment," Mechanical Engineering, June 1983.
6. Ciccio, J. A., and Thun R. E., "Ultra-High Density VLSI Moduls", IEEE Transaction on Components, Hybrids, and Manufacturing Technology, September 1978.
7. Dance, F. J., and Wallace, J. L., "Clad Metal Circuit Board Substrates for Direct Mounting of Ceramic Chip Carriers", Electronic Packaging and Production, January 1982.
8. Jayo, J. S., "The Power of Microelectronics", Technology Review, January 1981.
9. McIver, C. H., "Flip TAB, Copper Thick Films Create the Micropackage," Electronics, November 1982.
10. Markoc, H. and Solomon, P. M., "The HEMT: A Superfast Transistor," IEEE Spectrum, February 1984.
11. Preston, G. W., "The Very Large Scale Integrated Circuit," American Scientist, September-October 1983.
12. Robinson, A. L., "Problems with Ultraminiatured Transistors", Science, Vol. 208, June 1980.
13. Robinson, A. L., "Are VLSI Circuits Too Hard to Design?", Technology Review, January 1981.
14. Refaie, M. E., "Chip-Package Substrate Cushions Dense, High-speed Circuitries," Electronics, July 1982.
15. Stafford, J. W., "Chip Carriers: Application and Future Direction," Electronic Packaging and Production, July 1980.

16. "Supercomputer" will use immersion cooling," Industrial Research and Development, p. 60, January 1982.
17. Tuckerman, D. B., and Pease, R. F. W., "High-Performance Heat Sinking for VLSI," IEEE Electronic Device Letters, May 1981.
18. Tuckerman, D. B., and Pease, R. F., "Microcapillary Thermal Interface Technology for VLSI Packaging".
19. Wilson, E. A., "A Liquid System Cools a Densely Packaged Computer."
20. Aung, W., "Fully Developed Laminar Free Convection Between Vertical Plates Heated Assymmetrically", Int. J. Heat Mass Transfer, 1972.
21. Levy, E. K., "Optimum Plate Spacings for Laminar Natural Convection Heat Transfer from Parallel Vertical Isothermal Flat Plates," Journal of Heat Transfer, November 1971.

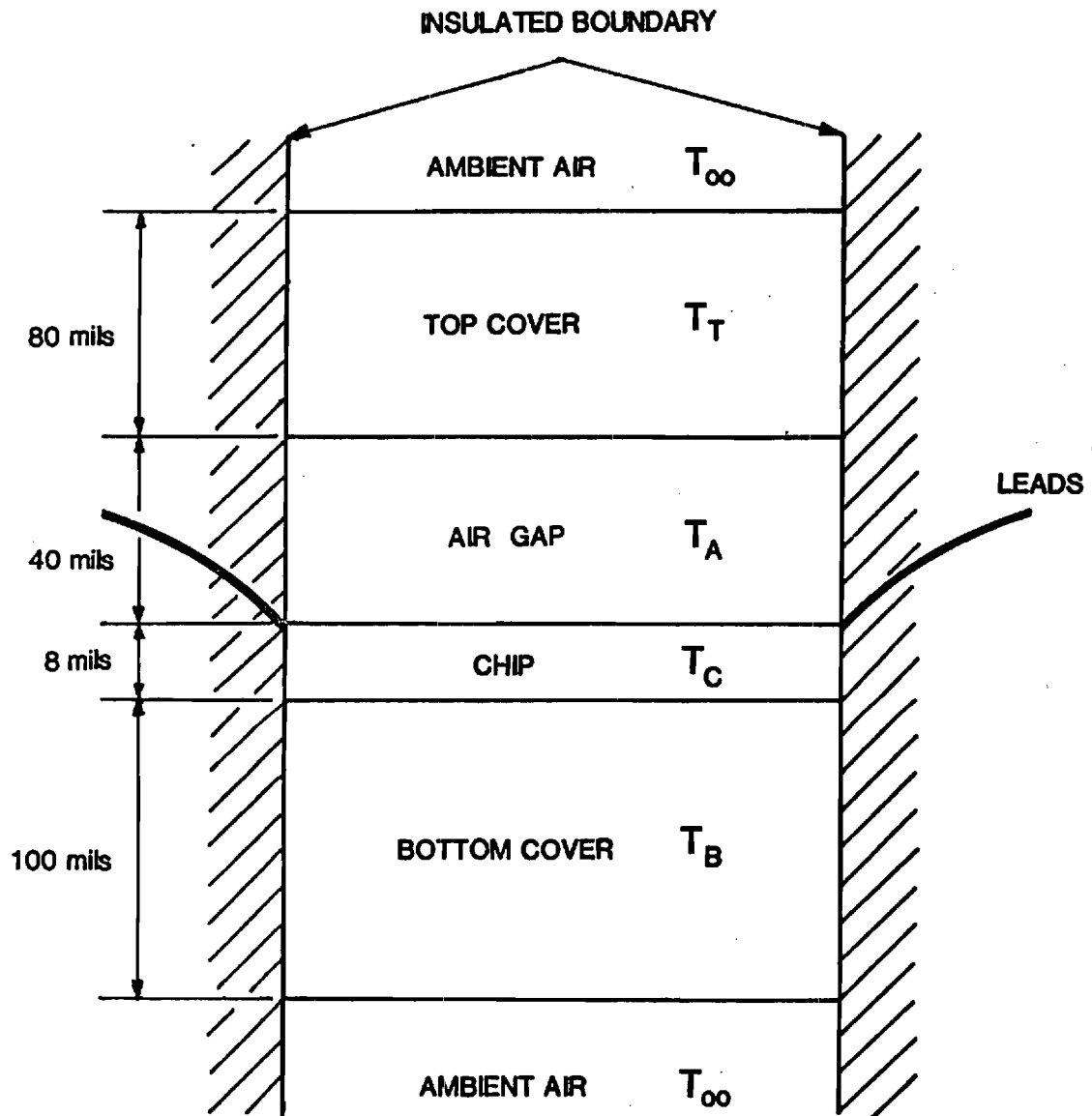


FIG. 1 SIMPLIFIED MODEL OF A CHIP
 (NOT TO SCALE)

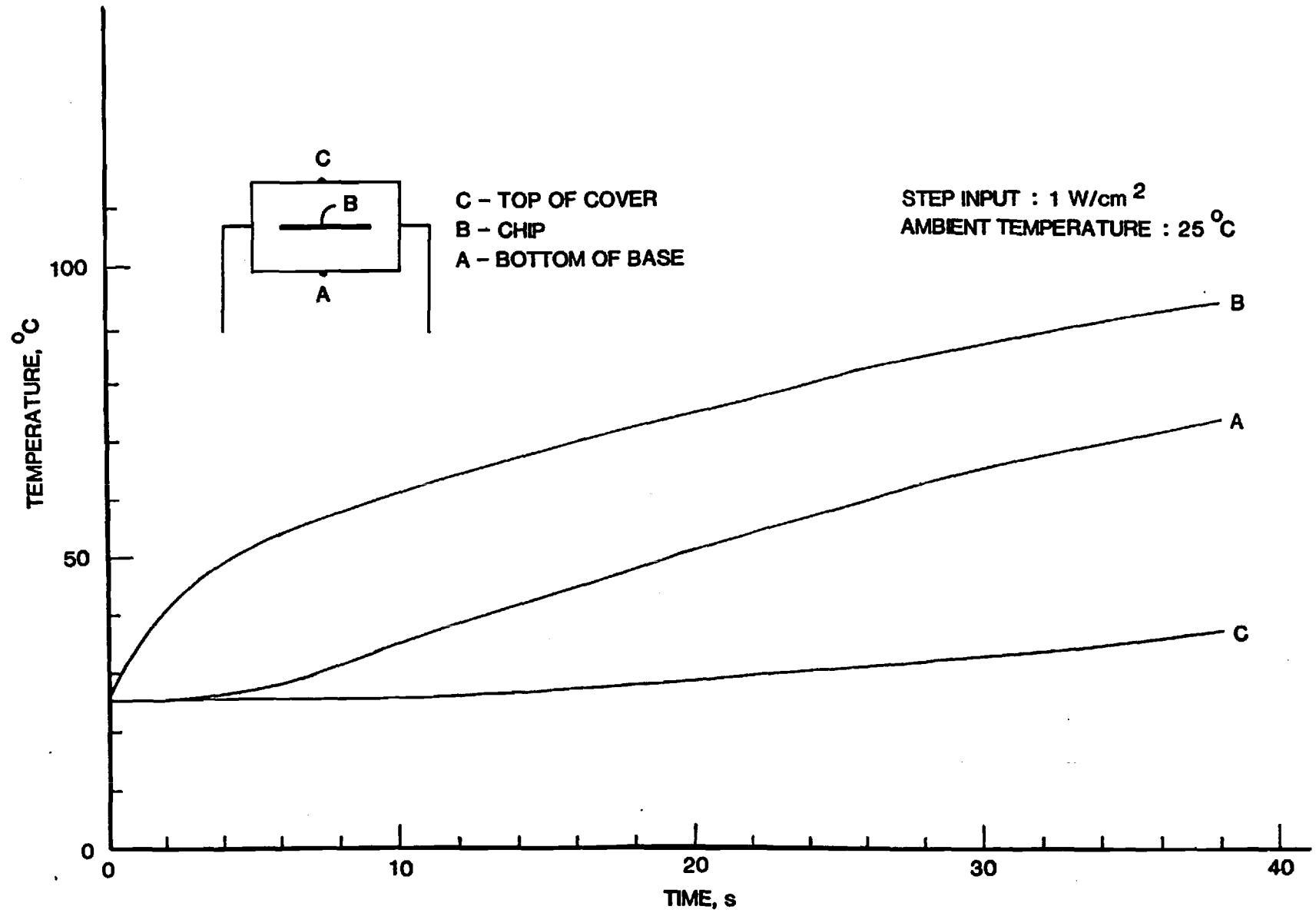


FIG. 2 CHIP TEMPERATURE VS TIME

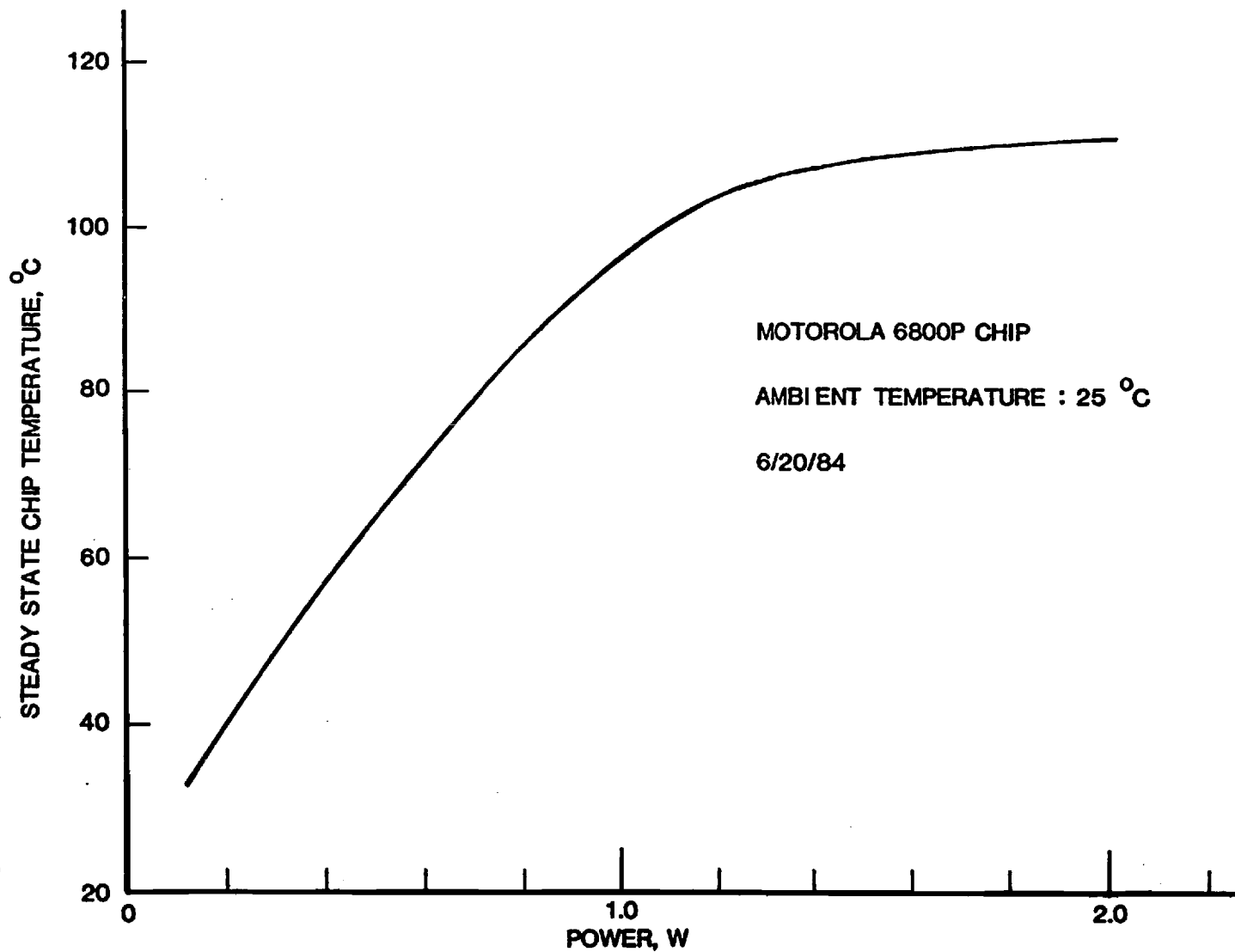


FIG. 3. MEASURED STEADY STATE CHIP TEMPERATURE VS POWER INPUT

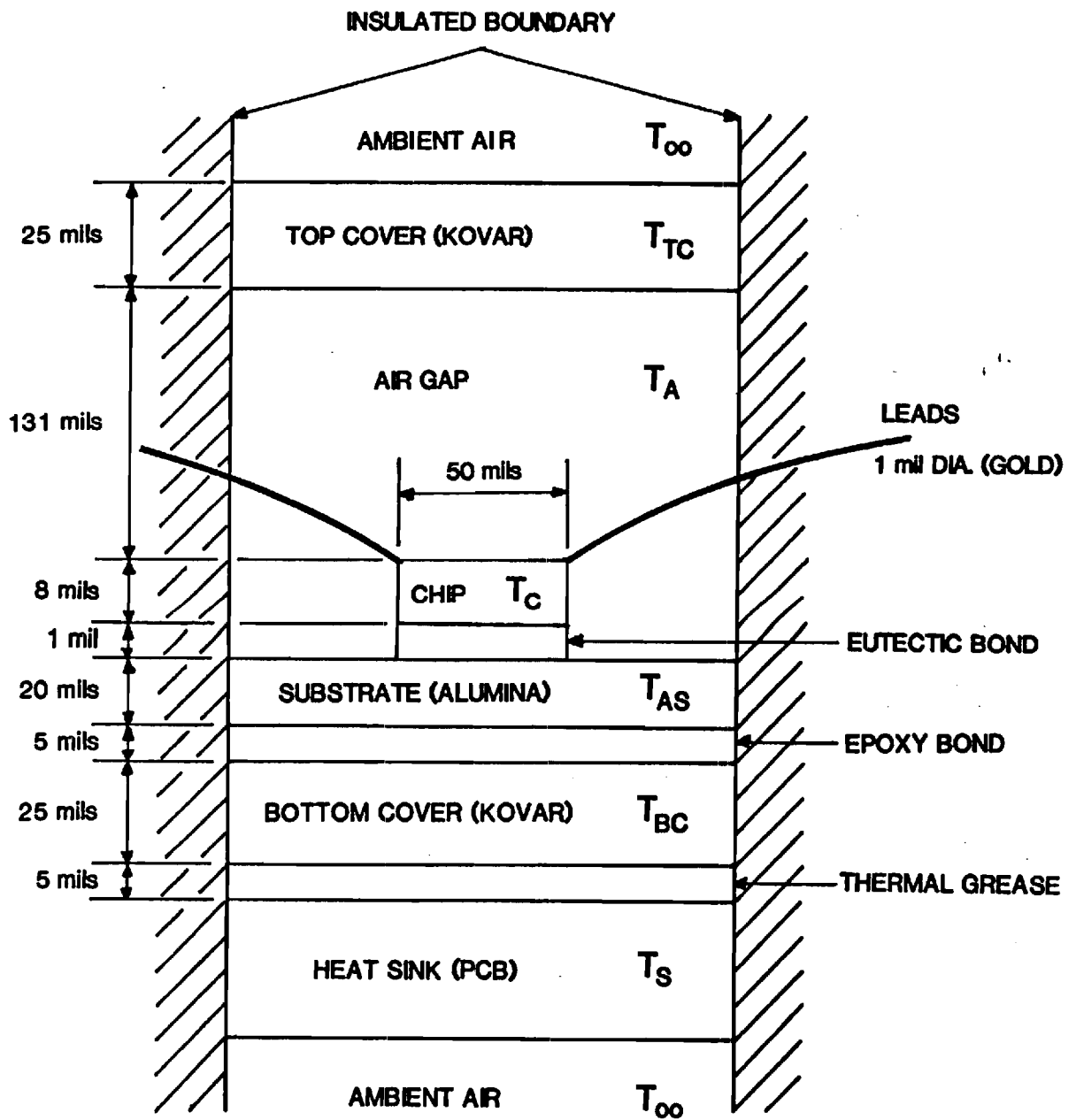


FIG. 4 ONE DIMENSIONAL CHIP CONFIGURATION
(NOT TO SCALE)

Georgia Institute of Technology

A UNIT OF THE UNIVERSITY SYSTEM OF GEORGIA

SCHOOL OF MECHANICAL ENGINEERING

ATLANTA, GEORGIA 30332

November 26, 1984

Dr. William F. Nelson
Director, Collaborative Research Programs
GTE Laboratories, Inc.
40 Sylvan Road
Waltham, Mass. 02254

Subject: Quarterly Progress Report - August through October 1984,
"Thermal Model for Microelectronic Chip".

Introduction

Heat is generated by the flow of electrical current in the microelectronic semiconductor components. The energy dissipated is associated with the passage of electrons through the transistor or diode emitter-base junction in a semiconductor device. This flow of current gives rise to the characteristic internal generation of heat in the chip, which must be effectively transferred to the environment to ensure reliable operation of the electronic system.

The heat dissipation must be accomplished to maintain the junction temperatures below the maximum allowable component temperature of the chip. To obtain the commonly accepted failure rates of 0.5 to 2.0% per thousand hours of operation, the semiconductor elements are generally operated at junction temperatures between 110 and 125°C. For systems with especially long operating life or with low maintenance and replacement-cost constraints, it is often desirable to have an average junction temperature as low as 60°C. A minor temperature increase above the maximum allowable component temperatures may result in a sharp decrease in reliability, while a large temperature excursion can produce a "thermal runaway" condition which may lead to catastrophic thermal failure of the device. Such thermal runaway can produce melting or even vaporization of the component, thermal fracture of the mechanical support element such as the case and substrate, separation between the leads and the external electrical network, plastic flow of printed circuits, and the deleterious migration of dopants in the semiconductor materials. Thus, the need for precise thermal analysis and thermal system design is apparent. The prevention of catastrophic thermal failure constitutes the primary motivation for the thermal control of semiconductor components.

The heat dissipation capability of semiconductor devices to a suitable heat sink (usually atmospheric air) is determined by the total thermal resistance of the heat flow path. The junction temperature is therefore directly dependent on the thermal resistance which is a function of material properties and the geometry of the device. In the case of microelectronic systems, the thermal resistance from the component junction to the environment can be classified into three levels: i) the component, ii) package, and iii) system. The component-level thermal resistance is due to the resistance of the microelectronic entity that exists between the junctions and the outside surface of the case. The package-level resistance consists of the resistance to heat flux from the surface of the case to a suitable reference point (e.g. temperature of air surrounding the component) in the entire system. The system-level resistance refers to the resistance to heat flux from the package-level to the ultimate heat sink which is the environment.

Current Project Status

Currently, the work on this research project is concentrating on the modeling of heat transfer from semiconductor devices at the component-level. A transient one-dimensional thermal model of a semiconductor chip encased in a dual in-line package (DIP) has been developed using a finite difference scheme (explicit forward difference formulation). A general model has been adopted to accommodate changes in geometry and variations in materials used in the fabrication of different microelectronic devices. The basic geometry of the DIP configuration used in the model is given in Figure 1. The semiconductor chip is first bonded to a ceramic or metallic substrate. The substrate is then bonded to the base of the component case. A casing cover encapsulates the chip within the package, leaving a gap between the chip and the top cover of the component case. This gap can be an air gap or it can be filled with a conductive material to increase conduction of heat from the chip to the top cover. Finally, the DIP is mounted onto a PC board. To decrease contact resistance, conductive thermal grease is often used as an interface between the package and the PC board.

At this point, the analysis suffers from a few weaknesses. Information regarding the material properties, geometry and thermal properties of semiconductor chips and their packaging are lacking in published literature. Semiconductor component manufacturers contacted decline to furnish the necessary information which is classified as an industrial trade secret. The geometry and material of the chip and packaging shown in Figure 1 is an approximate representation pieced together from scattered information in texts and from actually disassembling chip packages.

The material properties used in the model were obtained from the widely accepted Thermophysical Properties Research Center (TPRC) publications. For those materials not listed in this reference, the properties given in the CRC Handbook of Physics and Chemistry and in reference texts (by Kraus and Bar-Cohen, Steinberg, etc.) were used.

Nevertheless, thermal properties of bonding materials used in fabricating semiconductor devices are scarce and most bonding manufacturers contacted do not possess such information on their products.

The model assumes that the semiconductor chip is at a uniform temperature. An energy balance reveals that the heat generated in the chip is dissipated through combinations of series-parallel thermal resistances to the outside cover of the component package. See Figure 1 for the geometry of the chip package. Part of the heat is conducted in series through the substrate and the cover material before arriving at the outer surface of the bottom cover. Heat is also conducted from the chip through the lead wires. Lastly, the remaining heat is dissipated by conduction and radiation in parallel through the air gap and then by conduction through the cover material to the outer surface of the top cover. Due to the small spacing of the air gap, convective cells cannot develop, and heat transfer through the air gap occurs by conduction rather than convection. If the gap was filled with an opaque conductive solid, then heat is transfer by conduction only.

At the present time heat is assumed to be transferred at the outer surface of the top cover to the ambient surrounding by free convection and radiation. However the model can be easily modified to incorporate forced convection at this surface. Heat removal from the outer surface of the bottom cover is more complicated and is dependent on the mounting configuration of the DIP onto the PC board. In the model, the DIP is assumed to be mounted flush onto the PC board with a thin layer (0.005 to 0.010 in.) of conductive thermal grease between the surfaces to enhance conduction from the package (referred to as conductive cooled system). The thermal grease layer must be kept sufficiently thin to avoid high thermal resistance but it should also be thick enough to relieve stresses at solder joints resulting from expansion at high temperatures. When the power dissipation of a DIP is relatively low (< 0.2 watts), a controlled air gap may be used between the DIP and the PC board since air has relatively low resistance for a small air gap of less than 0.01 inch. Finally, the method used to cool the PC board will dictate the type of heat sink used in the model.

In the initial phase of the model, a semi-infinite conductive heat sink was assumed to be attached to the bottom of the DIP package. The heat sink was assumed to be maintained at a specified temperature. This assumption can be met by utilizing conduction cooled PC board heat sinks such as i) copper strips attached to the PC board that runs under the component package, ii) aluminum plate bonded to the back side of a thin PC board, and iii) aluminum plate with clearance holes for pins mounted onto the front side of the PC board. These metallic attachments of high thermal conductivity can be maintained at the specified temperature by conductive cooling at the package-level.

In the initial approach, a constant time step was used and all properties were assumed to be constant. The one-dimensional nodal

distribution of the DIP configuration is given in Figure 1; aside from the boundary nodes of each material the number of nodes in each material that comprises the package is as follows: i) 4 nodes in the top cover, ii) 8 nodes in the air gap, iii) 1 node in the chip, iv) 6 nodes in the substrate, and v) 4 nodes in the bottom cover. Even though the number of nodes has been specified for a given chip geometry the model is general and will accept any number of nodes desired by user.

The temperature-time history of any specified location on the semiconductor device can be obtained by using the thermal model. However, one major drawback results from the extremely small time steps needed to simulate temperature profiles that approach steady state conditions. Due to the small spatial dimensions encountered, very small time steps are necessary for the explicit finite different scheme to be numerically stable. As was discovered, the critical stability limit was reached in the eutectic bond region which has a nodal width of 1 mil. A time step of two ten-thousandth of a second must be used in order not to violate the Second Law of Thermodynamics. The criteria for numerical stability in an internal conduction node is such that Fourier Modulus must be less than or equal to one-half. Economics dictates that future modifications must be made to increase the efficiency of the model program. This problem will be addressed during the following months.

In the second phase of the development of the model, the program was modified in order to increase the time step size without causing the computations to become numerically unstable. This modification was accomplished by lumping the thin eutectic bond domain into the domain of the chip. Since the width of the eutectic bond is thin compared to the dimensions of its neighboring materials, a fairly accurate approximation can be made by assuming that the temperature of eutectic bond is equal to that of the chip. This assumption results in an increase in the time step by an order of magnitude (from 2×10^{-4} to 2×10^{-3} seconds) without affecting numerical instability. The larger time step affords a considerable saving in computing cost (ten fold reduction in CPU time) with only a slight change in the temperature profiles for the chip.

A analysis was also carried out to determine the effects on the temperature profiles when the number of nodes were increased. Doubling the number of nodes did not produce a significant change in the temperature profiles. However, the resulting decrease in spatial increments by half also necessitates a reduction in the time step by a factor of four in order to maintain numerical stability. Thus, it will not be cost effective to increase the number of nodes in the analysis, unless very accurate temperature profiles are required.

In the third phase of the modeling process, a convective heat sink PC board was adopted instead of the semi-infinite conduction cooled heat sink. The heat arriving at the front surface of the PC board is conducted through the PC board and then removed from the back surface by combined free convection and radiation to the surroundings. Due to the low convective heat transfer coefficient for the air, the temperature profiles obtained are considerably higher compared to profiles obtained with the semi-infinite conduction cooled heat sink.

An important improvement was made by introducing variable time steps into the model. The use of variable time steps eliminates the need to compromise accuracy which can arise when the eutectic bond layer is combined with the material in the chip. To obtain a variable time step, a routine was developed to subdivide the originally selected time step into smaller time steps whenever a numerical instability is encountered in the model. In other words, the model will proceed through the computations using the original time step until it encounters a thin layer that would be numerically unstable. At that point, the original time step is subdivided until new time step is obtained that will satisfy the stability criteria. The program then proceeds through the internal time loop based on this new time step. When the subtotal time of the inner loop equals the original time step, the program will return to the original time step loop. The same procedure is repeated for all the materials in the model. Thus, the variable time step concept offers accurate results while minimizing computing time.

In the latest phase of the thermal model, a more sophisticated approach was taken which incorporates temperature dependent properties into the program. A Least Square Fit routine was used in conjunction with the Gauss-Jordan Reduction routine to develop polynomial expressions for properties as a function of temperature. The polynomial expressions need to be determined only once and then properties which are functions of temperature can be evaluated from the algebraic equations.

Thermal Model Results

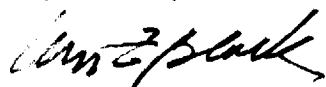
A temperature-time plot of the latest model is shown in Figure 2 for the following conditions; i) temperature dependent properties, ii) convective heat sink PC board, and iii) variable time steps. The package is originally at a temperature of 25°C and at time = 0, the chip is energized to a constant rate of 6.2 W/m². The geometry is illustrated in Figure 1 and the temperature results are shown in Figure 2. The temperature drop across each of the solid materials were small due to their relatively low thermal resistances. In the air gap, a large temperature gradient was obtained due to the low conductivity of air.

Future Work

The one-dimensional thermal model of the DIP has been carefully developed. This matured model has the flexibility to accept variations in geometry and material properties which may change for different DIP designs. At this stage of the model it is necessary to determine how well the theoretical results represent the actual heat transfer from a semiconductor component. The objective of the next phase of this research is to experimentally determine the temperature distribution in the DIP. Comparison of the theoretical results with the experimental data will provide an indication of the validity of the model. An imaging radiometer has been purchased from Inframetrics in Bedford, Massachusetts and this equipment will be used to measure the transient temperature of a chip under simulated operating conditions. This

equipment has recently been delivered and preliminary exposure to the infrared camera equipment as a tool for accurately measuring temperatures of semiconductor devices has been very encouraging. Details of the equipment, experimental procedures, and results will be given in future reports.

Respectfully submitted,

A handwritten signature in cursive script, appearing to read "Wm. Z. Black".

Wm. Z. Black
Project Director

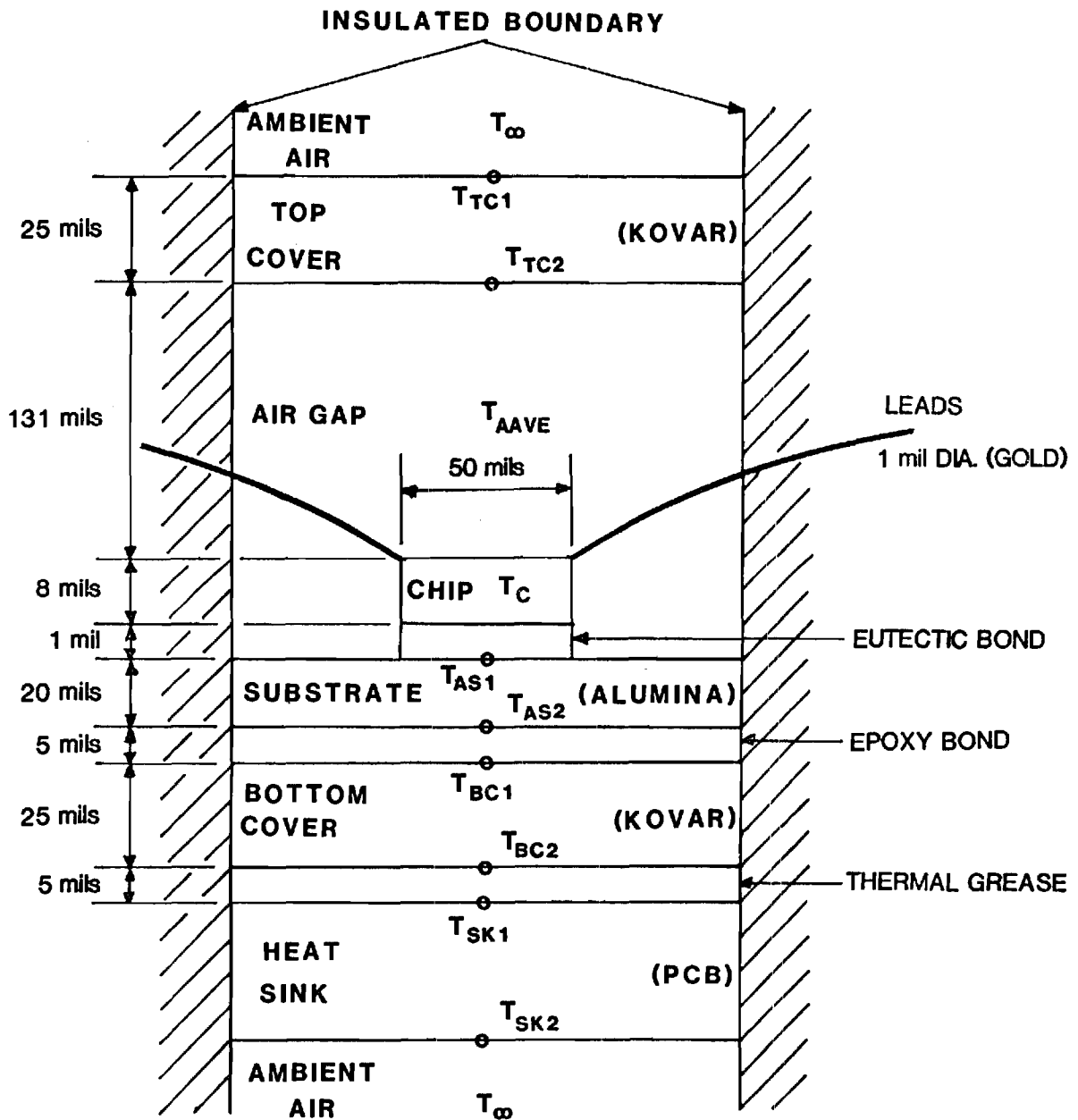


**FIG. 1 ONE DIMENSIONAL DIP PROFILE
(NOT TO SCALE)**

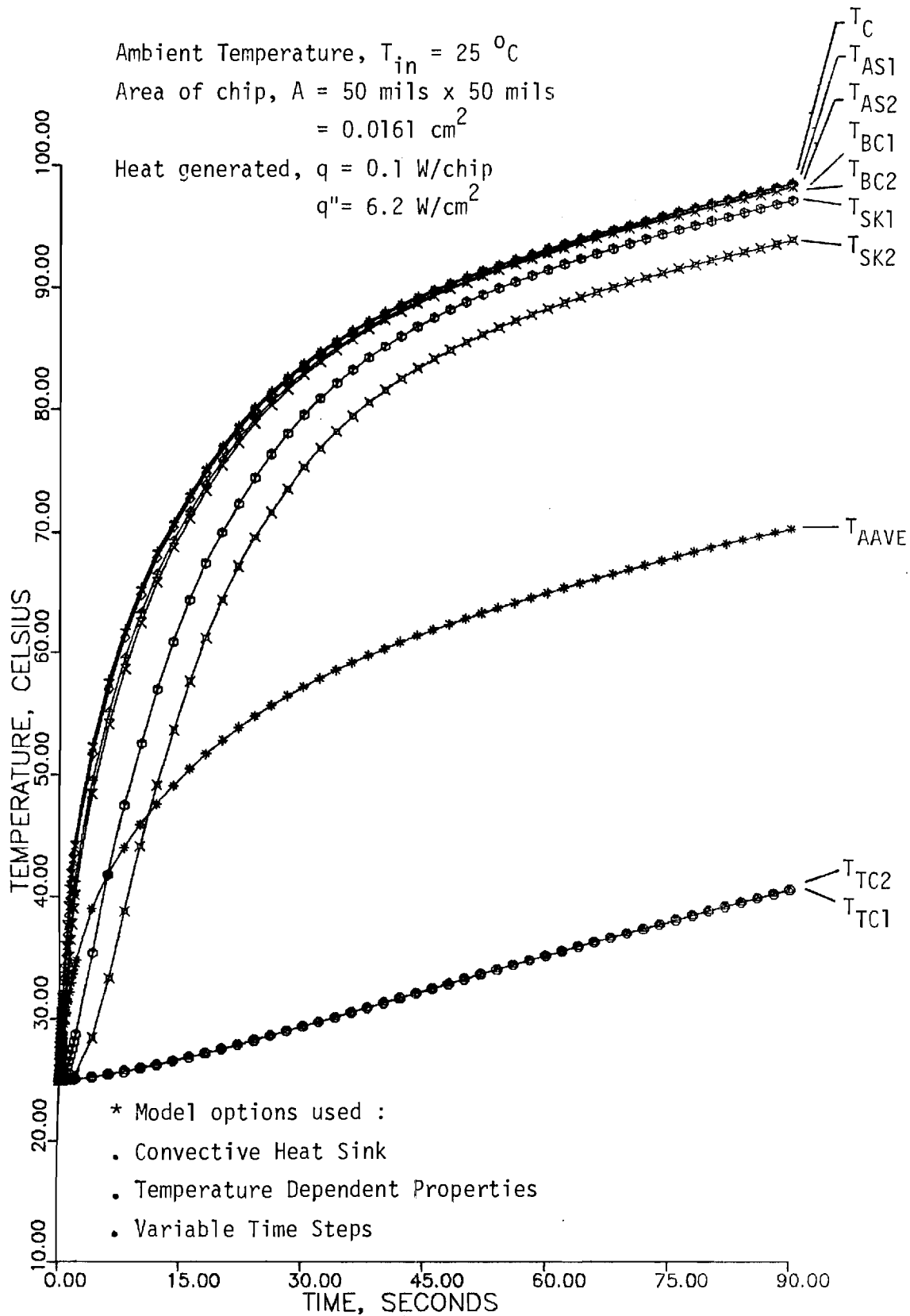


FIG. 2 TEMPERATURE DISTRIBUTIONS IN A DIP



GEORGIA TECH 1885-1985

DESIGNING TOMORROW TODAY

R 25-669

February 20, 1985

Dr. William F. Nelson
Director, Collaborative Research Programs
GTE Laboratories, Inc.
40 Sylvan Road
Waltham, Massachusetts 02254

SUBJECT: Quarterly Progress Report - November 1984 through January 1985, "Thermal Model for Microelectronic Chips."

This report briefly summarizes the accomplishments on the GTE Research Project entitled, "Thermal Model for Microelectronic Chips", achieved during the period between November 1984 and January 1985. Further details of project achievements will be reported during a visit to the GTE Laboratories on February 22, 1985.

COMPUTER PROGRAM

During the last three months less attention has been focused on the computer analysis pending experimental verification of the numerical results. The program has been organized to accept variations in chip and carrier geometries and variations in material properties. However a serious limitation arises from the use of the explicit finite difference scheme to solve the energy balance equations. In order to satisfy numerical stability, very small time steps are necessary. As a result, a very large computation time is required for the analysis to approach steady state. Furthermore a simplified analysis for heat transfer from electric lead wires will be replaced by one which more accurately models the heat loss. These weaknesses will be resolved in the future.

One of the major modifications to the thermal model will be to

Georgia Institute of Technology

School of Mechanical Engineering Atlanta, Georgia 30332

change the numerical scheme from an explicit to implicit technique which is more efficient on computation time. The use of an implicit scheme will provide unconditional stability, but it will lead to a discretization error of the order of $O(\Delta x^2 + \Delta \tau)$. Richardson's scheme is rejected because the scheme is always unstable for the heat equation. The numerical scheme that is being considered currently is the Crank-Nicholson Scheme. This method is unconditionally stable when applied to the heat equation and it leads to a discretization error of the order of $O(\Delta x^2 + \Delta \tau^2)$.

EXPERIMENTAL RESEARCH

Infrared Equipment Description

The temperatures predicted by the computer program will be verified by measuring the temperature distribution on the surface of an energized chip with an imaging radiometer. The Inframetrics' Model 525 Imaging Radiometer has been purchased by the School of Mechanical Engineering. This equipment is a compact, lightweight infrared thermal imaging system. The instrument produces a TV compatible video output signal of the thermal patterns radiated by the target. A scanner senses the infrared radiation emitted by the target which is then processed into a TV picture representing the temperature profile of the subject. The black-and-white "heat picture" generated permits quantitative data analysis by interpretation of gray tones or isotherm scale readings. In addition, a pseudo-color presentation of the scene can be obtained by superimposing eight discrete colors onto the black and white imagery.

Basically, the unit used at Georgia Tech consists of the following components:

- 1) An IR scanner

- 2) Control/Electronics Unit
- 3) Iso/Line Scan Colorizer
- 4) 5" Color TV Monitor
- 5) VHS format VCR
- 6) Power Supply/Charger
- 7) In addition to the normal lens,
 - a) 3X telescope
 - b) 1.8" microscope objective
 - c) 90° downlooker

Figure 1 shows the equipment layout for real-time processing, recording and processing of prerecorded black and white video tapes.

The Model 525 has a temperature measurement range of -20°C to 1300°C and a minimum detectable temperature of 0.1°C at $8-12\ \mu\text{m}$ and 0.2°C at $3-5.6\ \mu\text{m}$.* The Control/Electronics unit features three modes for analyzing the output:

- i) Image
- ii) Line Scan
- iii) Isotherm

In the Image mode, a black and white representation of the thermal pattern of the subject is presented on the screen. A Calibrated Gray scale is also superimposed across the bottom of the picture. This

*A liquid nitrogen cooled Mercury/Cadmium/Telluride detector, housed in the scanner, converts the incident infrared radiation to an electrical signal. This signal is then processed by the Control/Electronics unit into a TV picture.

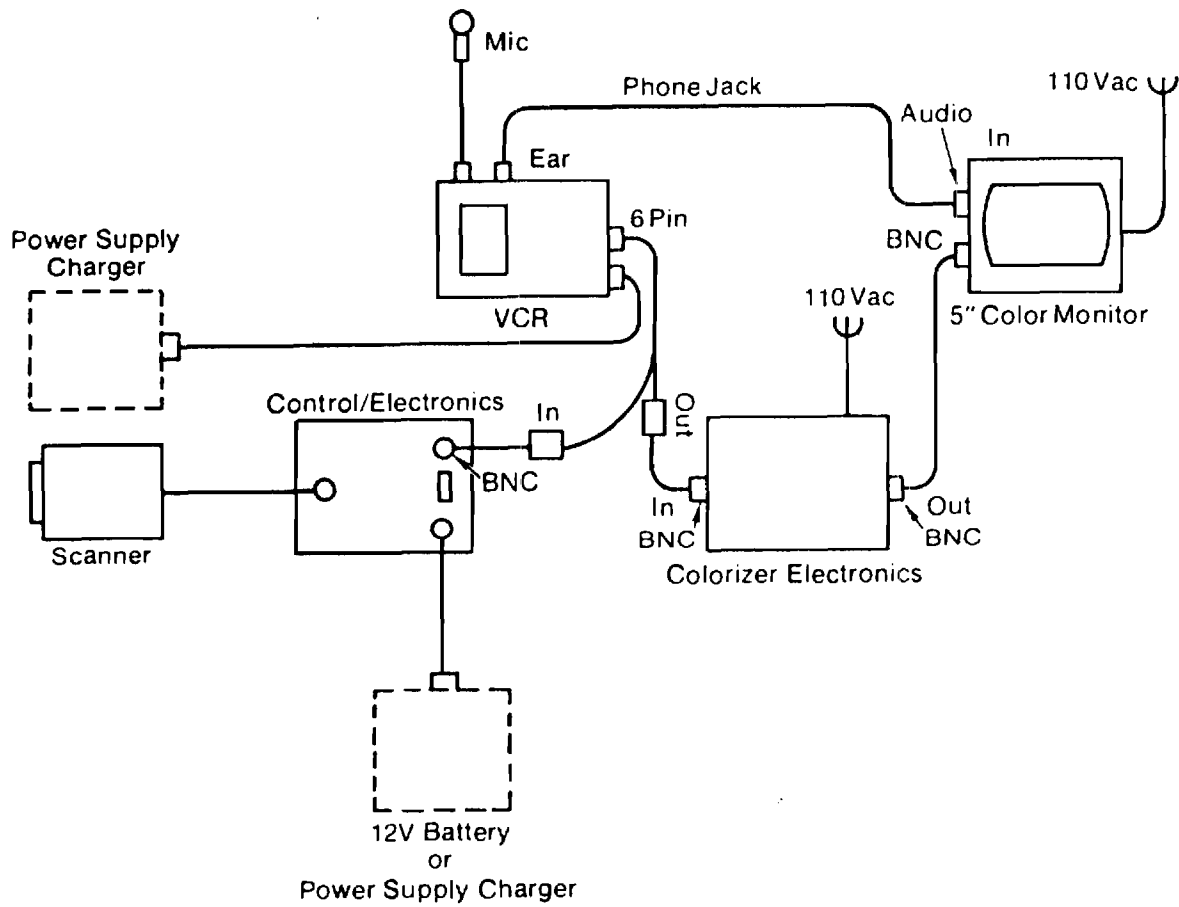


Fig. 1 Model 525 System With Colorizer for Real Time Processing, Record and Playback.

feature allows quantitative temperature difference measurements to be made in the Image mode by providing a relationship between the contrast in the display and the temperature difference. Another use of the Calibrated Gray scale is for color calibration with the colorizing system.

The Line Scan mode provides a thermal profile of any horizontal line in the scene which has previously been selected by using the Line Select mode. This feature provides a convenient means for quantitatively visualizing any apparent temperature distribution across a surface. Both absolute and differential temperatures can be obtained from the Line Scan mode.

The Isotherm mode can be used to measure absolute and differential temperatures of selected areas in the scene. Its use also allows the operator to visualize isotherm contours. Areas of the same temperature "sparkles" when the level of the display is adjusted.

The Control/Electronics unit has seven temperature ranges with full scale settings of 10⁰, 20⁰, 50⁰, 100⁰, 200⁰, 500⁰C, and an extended setting for 1300⁰C. This unit also features an Electro-Optic (E-0) Zoom scan ratio of 4 to 1. A polarity switch enables the operator to invert the picture from white "hot" to black "hot."

The Iso/Line Scan Colorizer generates a quantized color image in real-time processing of signals from the Control/Electronics unit or from VCR playback. Colorizing is a quantitative feature which enables the experimenter to continuously monitor temperature zones within the scene. Eight colors are superimposed on the Calibrated Gray scale of the video display and each represents a different isotherm range. These colors are black, blue, cyan, green, yellow, red, magenta, and white.

The colorizer unit also features a Range Multiplier switch with five calibrated widths which increases or decreases the image contrast by factors of 0.25, 0.5, 1.0, 2.0, and 5.0. For example, the 10-degree scale on the Control/Electronics unit, used in the color mode with the Range Multiplier set at 0.25, provides a more sensitive 2.5 degree scale.

Calibration of the Infrared Equipment

The Infrared Equipment is an ideal system for qualitatively detecting temperatures. "Hot spots" within the scene can readily be detected; however, in order to designate a numerical temperature value to a region of interest, an involved manipulation of the equipment and a complex analysis is required. The quantitative analysis is complicated by the non-blackbody characteristics of the surfaces of the computer chips. In reality the emissivities of these materials lie somewhere between 0 and 1.0 and are dependent upon the condition of the surface and surface temperature. An initial effort has been carried out in an attempt to calibrate the infrared equipment so that it can quantitatively measure temperature distribution of the surface of a DIP and of a thermal test chip mounted in 16-lead alumina chip carrier. The complexity of the calibration procedure is compounded by the unknown emissivities of the materials. These problems will be addressed further in the next quarterly report.

Six Motorola Thermal Test Die chips were obtained from the GTE Packaging Technology Center in Northlake. These chips consist of two heater implants (150Ω) and a centrally located NPN transistor. It has been decided that this chip will be used to evaluate the potential of the scanning radiometer for measuring the surface temperature of

chips. Prior to measuring the transistor temperature with the infrared camera, the emissivity of the chip as a function of temperature must first be established.

Leadless chip carrier holders were acquired for the necessary electrical connections. The resistance of the heater implant was first calibrated as a function of temperature. The test chip was placed in an oven, and resistance readings were taken after steady state temperature had been attained. In the next phase, the implant heater was powered and the chip scanned with the infrared equipment. With the normal lens an apparent uniform temperature was observed over the entire chip area. Since the glass window was still intact and glass is opaque to infrared radiation, the reading obtained with the IR equipment was due to IR radiation emitted by the heated glass.

Prior to the next test, the glass window was removed to expose the chip. With the implant heater energized, a relatively uniform temperature was observed over the chip area. Since the current through the heater and voltage drop across the heater implant can be readily measured, the resistance ($R = \frac{V}{I}$) can be calculated, and the temperature of the chip can be determined from the temperature-resistance calibration curve.

With the known chip temperature, a blackbody reference source is adjusted to the chip temperature and positioned beside the chip. Once steady state conditions have been obtained, both the blackbody reference source and the chip are scanned simultaneously with the infrared equipment. The relative intensity of the reference and the chip can be obtained with the infrared equipment and emissivity calculated from the following relationship:

$$\frac{\epsilon_c}{\epsilon_{ref}} = \frac{I_c}{I_{ref}}$$

I_c, I_{ref} = Intensity of chip and blackbody reference source respectively, when both are at the same temperature, T_t

ϵ_c = Emissivity of chip at T_t

ϵ_{ref} = Emissivity of the blackbody at $T_t = 1.0$

This procedure is then repeated for the entire temperature range of interest. At this time the procedure described above for measuring the emissivity of the chip material has not been carried out, but it will be evaluated in the next few months.

The procedure to determine the emissivity of a chip assumes the entire chip is at a uniform temperature. However, with the recent arrival of the microscopic objective, it has been observed that there is an apparent temperature variation on the chip arising from the different material used, particularly in the metallization regions. It is observed that the region near the perimeter of the chip is hotter than the middle. A possible explanation could be due to the location of the heater implants. The metallized regions are also observed to be colder than the rest of the chip. This would result from the lower emissivity of the metallized region. It would also be due to the reflective properties of the metallize region which reflects the colder radiation from the surrounding to the detector. Thus, with the higher resolution of the microscopic objective, a more detailed calibration of the various materials on the chip is necessary. With the normal lens these small scale variations have not been observed and the chip appears to have a

more uniform temperature. Once the emissivities of the materials on the chip are known, tests can then be performed to analyze the thermal characteristic of the transistor.

The following figures show the thermal images as recorded on the TV monitor with the infrared equipment set in the Color Mode. The temperature pattern of the exterior surface of an energized DIP scanned with the normal lens is shown in Figure 2. The chip is located at the central position of the package which is observed to be the hottest region. Figures 3, 4, and 5 are thermographs of the Motorola thermal test chip with the heater implants energized. Figure 3 was taken with the glass window intact, and the glass above the chip appears to be at a uniform temperature. With the glass window removed, as shown in Figure 4, variations in temperature were observed over the chip area. Both Figures 3 and 4 were thermographs recorded when the chip was scanned using the normal lens. To obtain a higher resolution picture, a 3X Telescope can be coupled to a Microscope objective and the two lenses can be used in place of the normal lens. Figure 5 is a high resolution TV picture showing a wide variation in surface temperatures that can exist in an energized chip.

FUTURE WORK

During the next several months two specific problems will be addressed. The first problem involves the analysis of heat transfer along the metallic lead wires which connect the chip carrier to the chip. The present analysis is only an approximate one and it does not consider the transient nature of the heat transfer along the leads and it does not include radiation from the surface of the leads. The present simplified analysis will be replaced by a more accurate one in the next few months.

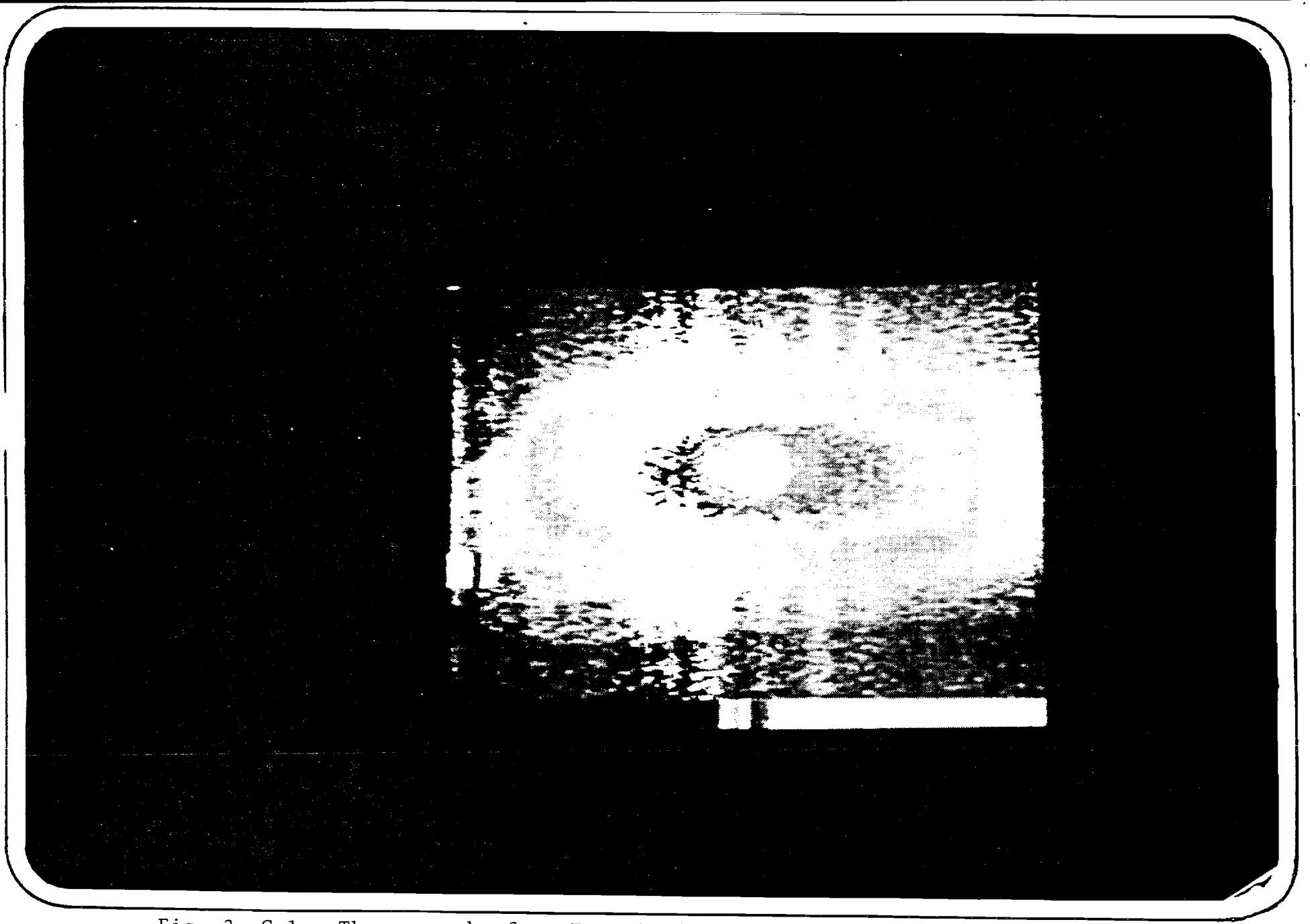


Fig. 2 Color Thermograph of an Energized DIP (scanned by normal lens).

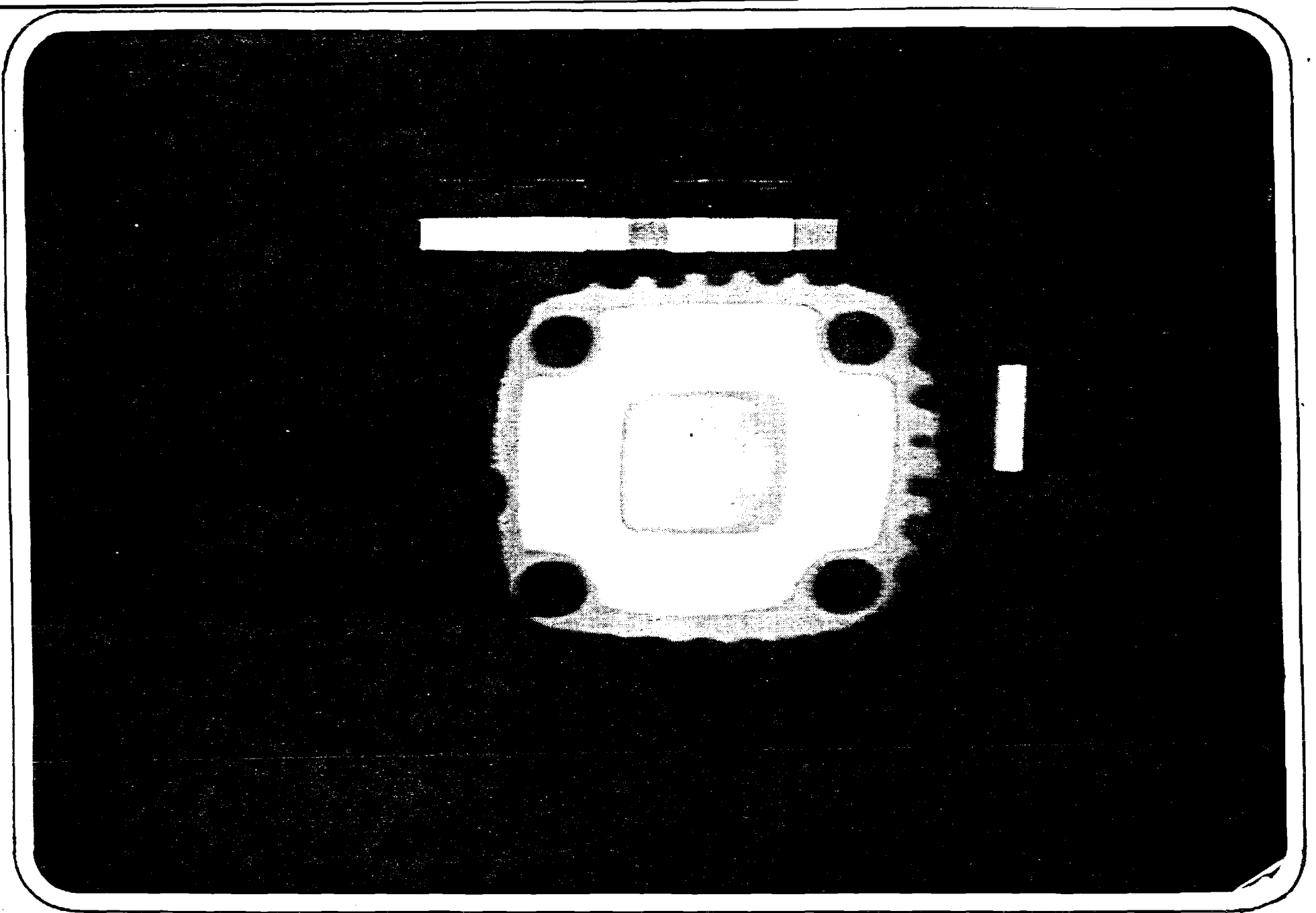


Fig. 3 Color Thermograph of Energized Motorola Test Chip with Glass Window Intact (scanned by normal lens).

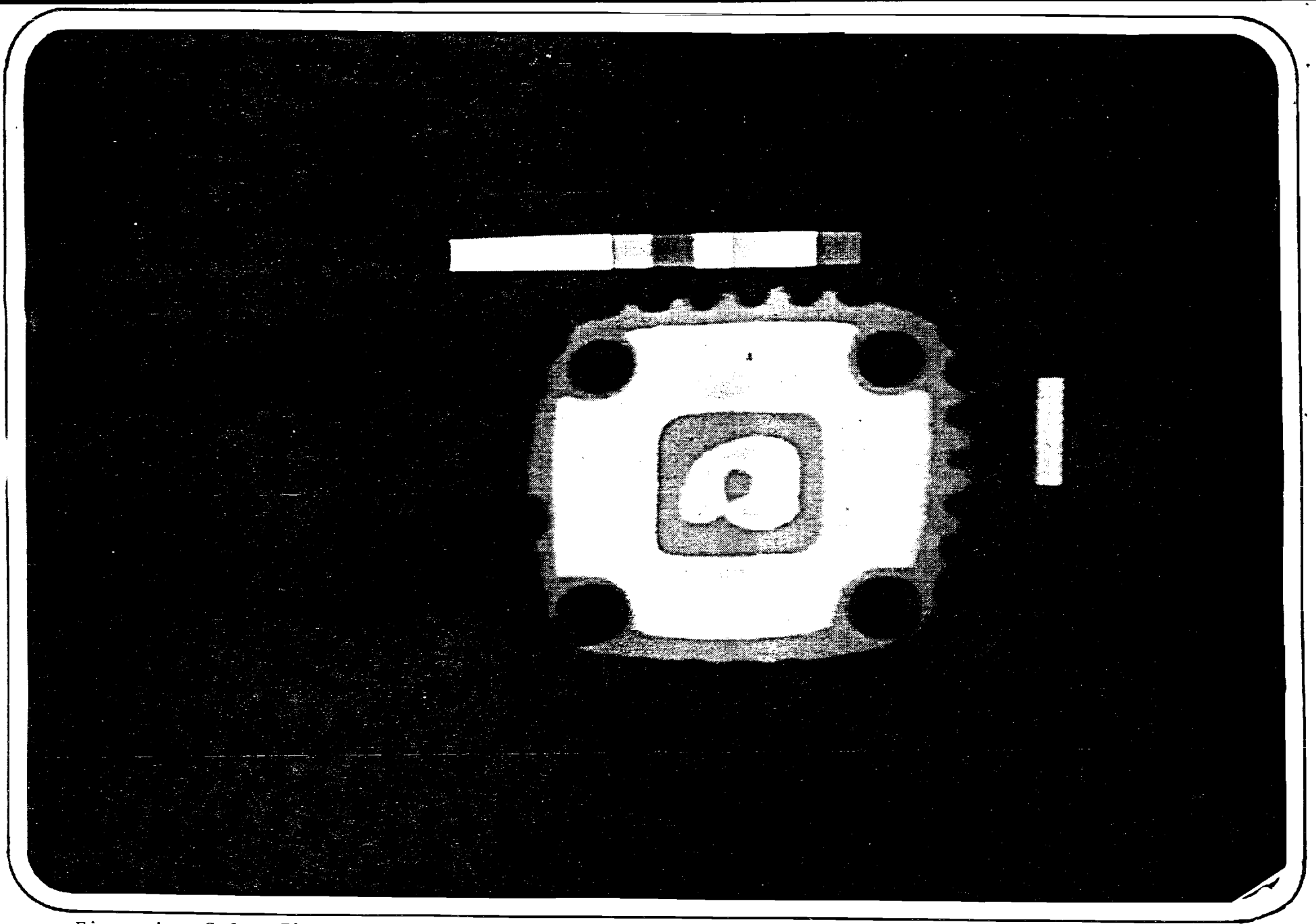


Fig. 4 Color Thermograph of Energize Motorola Test Chip Without Glass Window (scanned by normal lens).

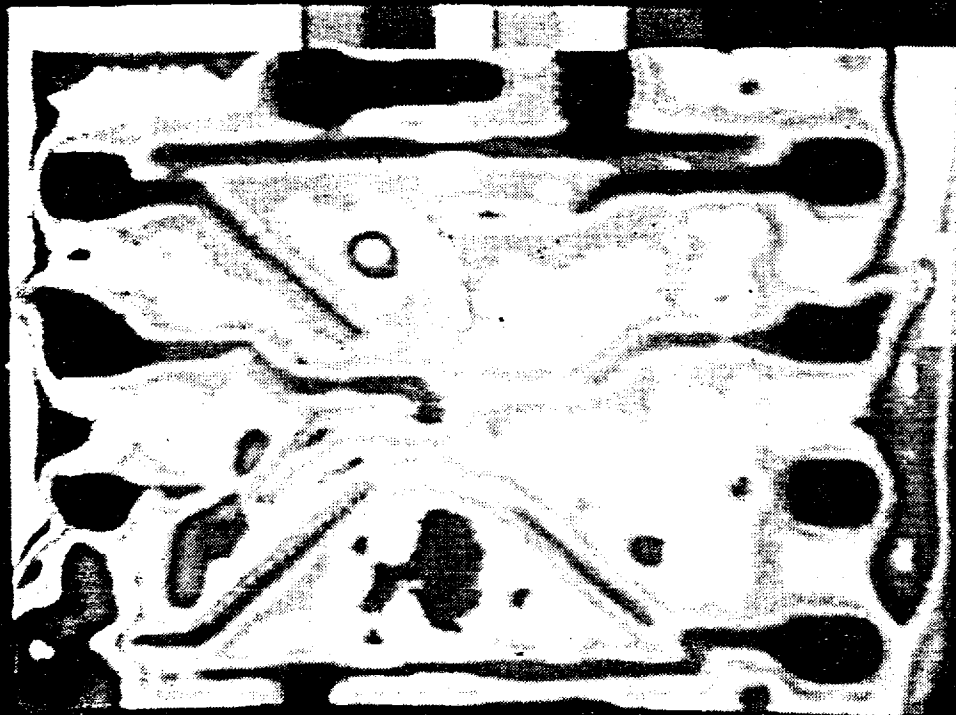


Fig. 5 Color Thermograph of Energized Motorola Test Chip Without Glass Window (Scanned by 3x Telescope Coupled to Microscope Objective).

The second problem involves calibration of the Imaging Radiometer so that it is capable of quantitatively measuring local temperatures on the surface of the chip. The operations manual received from Inframetrics at the time the equipment was originally delivered did not include the steps necessary to calibrate the radiometer. However, a more recent edition of the operations manual has a calibration section and a new version of the manual has been ordered. It is anticipated that this additional information will permit precise temperature measurements on the chip under transient heating conditions. Once the temperature distributions on the chip are measured, the values will be compared with the temperature calculated with the computer thermal model.

U. M. Z. Black
2/20/85

Heng Fook Geow



GEORGIA TECH 1885-1985

DESIGNING TOMORROW TODAY

E25-669

June 5, 1985

Dr. William F. Nelson
Director, Collaborative Research Programs
GTE Laboratories, Inc.
40 Sylvan Road
Waltham, Mass. 02254

Subject: Quarterly Progress Report - February through April 1985, "Thermal Model for Microelectronic Chips".

Accomplishments

Over the last three months, limited progress was made on the research project relating to the heat transfer from microelectronic chips, because the graduate student assisting in the project was preparing for his Ph.D. Preliminary Examinations. During the rest of the time, attention was focused on calibrating the Imaging Radiometer.

A more recent edition of the operations manual has been received which contains calibration information for the Model 525 Inframetrics Imaging Radiometer that will be used in this research project. Standard calibration curves referenced at $T_{cal} = 30^{\circ}\text{C}$ were provided by Inframetrics for this particular instrument. For the most accurate temperature measurements, Inframetrics recommended that calibration curves be prepared for the specific operating conditions under which the instrument will be used. However, for the purpose of analyzing temperature distribution of microelectronic devices, the temperature range of interest is between room temperature and about 150°C . Thus the 30°C referenced standard calibration curves are suitable for this application.

In the operations manual, Inframetrics states that two blackbody radiation sources with separately controllable temperatures are required for the calibration procedure. However, since only one such unit is available, a modified calibration procedure was adopted and used to check the validity of the standard calibration curves and also to periodically verify the instrument calibration. Basically, the calibration procedure involves associating Isotherm Units data measured by the instrument to differences in temperature.

Georgia Institute of Technology

School of Mechanical Engineering Atlanta, Georgia 30332

The calibration tests were conducted using three different modes to provide Isotherm Units data; (1) the Line Scan mode, (2) the Isotherm mode, and (3) the Color mode. The results obtained from all three modes for 10°C scale, 20°C scale, 50°C scale, 100°C scale, and 200°C scale were in good agreement (+ 2%) with the standard calibration curves provided by Inframetrics. A curve fitting routine utilizing Least Square Fit and Gauss-Jordan Reduction schemes was then used to process the data. The resulting polynomial expressions provide temperature as a function of Isotherm Units. A fourth degree polynomial was adopted,

$$T(I) = A_0 + A_1 I + A_2 I^2 + A_3 I^3 + A_4 I^4 \quad (1)$$

where

T = Temperature in Celsius

I = Isotherm Units

A_0, \dots, A_4 are coefficients whose value depend on the scale used. The coefficients A_0, \dots, A_4 for the different scales calibrated at a reference temperature 30°C are:

Scale	A_0	A_1	A_2	A_3	A_4
10°C	0.30×10^2		0.10×10^1	.0	.0
20°C	0.2997×10^2		0.2977×10^1	-0.1787	0.9907×10^{-2}
50°C	0.3003×10^2		0.6560×10^1	-0.5212	0.6208×10^{-1}
100°C	0.3020×10^2		0.1988×10^2	-0.2895×10^1	0.3146
200°C	0.3077×10^2		0.3883×10^2	-0.5612×10^1	0.6359
					-0.1748×10^{-3}
					-0.2564×10^{-2}
					-0.1241×10^{-1}
					-0.2640×10^{-1}

A plot of Isotherm Units as a function of temperature for 10°C and 20°C scales is given in Figure 1, and for 50°C, 100°C, and 200°C scales are given in Figure 2. The temperature of a "target" can now be obtained using either the standard calibration curves in Figures 1 and 2 or by using the polynomial expressions once the number of Isotherm Units between the target and the blackbody reference source is established.

Once the emissivity of the target has been determined, the procedure for quantitatively measuring the target temperature is relatively straight forward. The description which follows describes the manner in which the infrared equipment can be used to determine the target temperature. The procedure used depends upon whether the calibration temperature is equal to or different from the reference temperature.

If the temperature of the blackbody reference source used to determine the "target" temperature is equal to the temperature of the blackbody calibration reference source, i.e. $T_R = T_{cal} = 30^{\circ}\text{C}$, then the following procedure is used:

1. Determine the apparent difference in Isotherm Units, ΔI_{app} , between the 30°C reference source and the target by using the infrared equipment. The actual difference in Isotherm Units, ΔI , is given by

$$\Delta I = \frac{\Delta I_{app}}{\epsilon_t} \quad (2)$$

ΔI = actual difference in Isotherm Units
 ΔI_{app} = apparent difference in Isotherm Units

where

ϵ_t = emissivity of the target = 1.0 for blackbody target
 < 1.0 for "real" target.

Graphical Method

- 2A. Select the temperature scale curve corresponding to the TEMP RANGE setting at which the measurement was made.
- 2B. Referring to Figure 3, read the target temperature, T , corresponding to the number of Isotherm Units, ΔI , between the 30°C reference source and the target.

Computational Method

- 3A. Select the appropriate coefficients for Equation 1 corresponding to the TEMP RANGE setting at which the measurement was made.
- 3B. Set $I = \Delta I$ from Equation (2) and use Equation (1) to compute the target temperature corresponding to the number of Isotherm Units, ΔI , between the 30°C reference source and the target.

If the temperature of the blackbody reference source used to determine the "target" temperature is greater than the temperature of the blackbody calibration reference source, i.e. $T_R > T_{cal} = 30^{\circ}\text{C}$, then the following procedure is used:

1. Knowing the exact temperature of the blackbody reference source, T_R , determine the apparent Isotherm Units, ΔI_{app} , between the reference source and the target using the infrared equipment. The actual difference in Isotherm Units is obtained from Equation (2).

Graphical Method

- 2A. Referring to Figure 4, locate the reference source temperature, T_R , and move vertically up to point (1) on the temperature scale curve corresponding to the TEMP RANGE setting at which the measurement was made.
- 2B. Move horizontally to point (2), and then add the number of Isotherm Units, ΔI , as determined in Step 1 to establish point (3).
- 2C. Move horizontally across to point (4) on the temperature scale curve and read the corresponding target temperature, T .

Computational Method

- 3A. Select the temperature scale curve and the appropriate coefficients for Equation 1 corresponding to the TEMP RANGE setting at which the measurement was made.
- 3B. Determine the reference source Isotherm Units, I_R , corresponding to the reference source temperature, T_R , from the temperature scale curve (refer to Figure 4).
- 3C. Set $I = \Delta I + I_R$ (ΔI from Equation (2)) and use Equation (1) to compute the target temperature corresponding to the number of Isotherm Units, ΔI between the reference source and the target plus the number of Isotherm Units, I_R , between the 30°C calibration reference source and the reference source.

The graphical method can provide quick temperature data, but it is only accurate within the ability to read the calibration curves. When the temperatures at a large number of pixels are to be evaluated, the polynomial expressions used in conjunction with a computer program will be more suitable.

Summary

The accomplishments over the past three months have provided us with the capability to determine temperature using the infrared equipment for surfaces of known emissivities. Once the number of Isotherm Units between the "target" and a blackbody reference source has been established by the infrared equipment, the target temperature can be obtained from the standard calibration curves or polynomial expressions which are presented in this report.

Future Effort

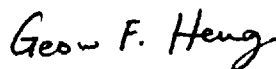
The primary interest over the next few months concerns the development of a procedure for determining the emissivity of the chip. Since a large number of microelectronic entities exist on a single chip, the appropriate approach is to analyze each pixel of the thermographic image to obtain the emissivity.

On the theoretical front, attention will be focused on the further development of the one-dimensional transient heat transfer model of the chip and its packaging. The adequacy of the completed 1-D model will be addressed.

Respectively Submitted,



Wm. Z. Black
Project Director



Geow F. Heng
Graduate Research Assistant

WZB:maw

cc: Dr. John Hooper
Dr. John Brighton

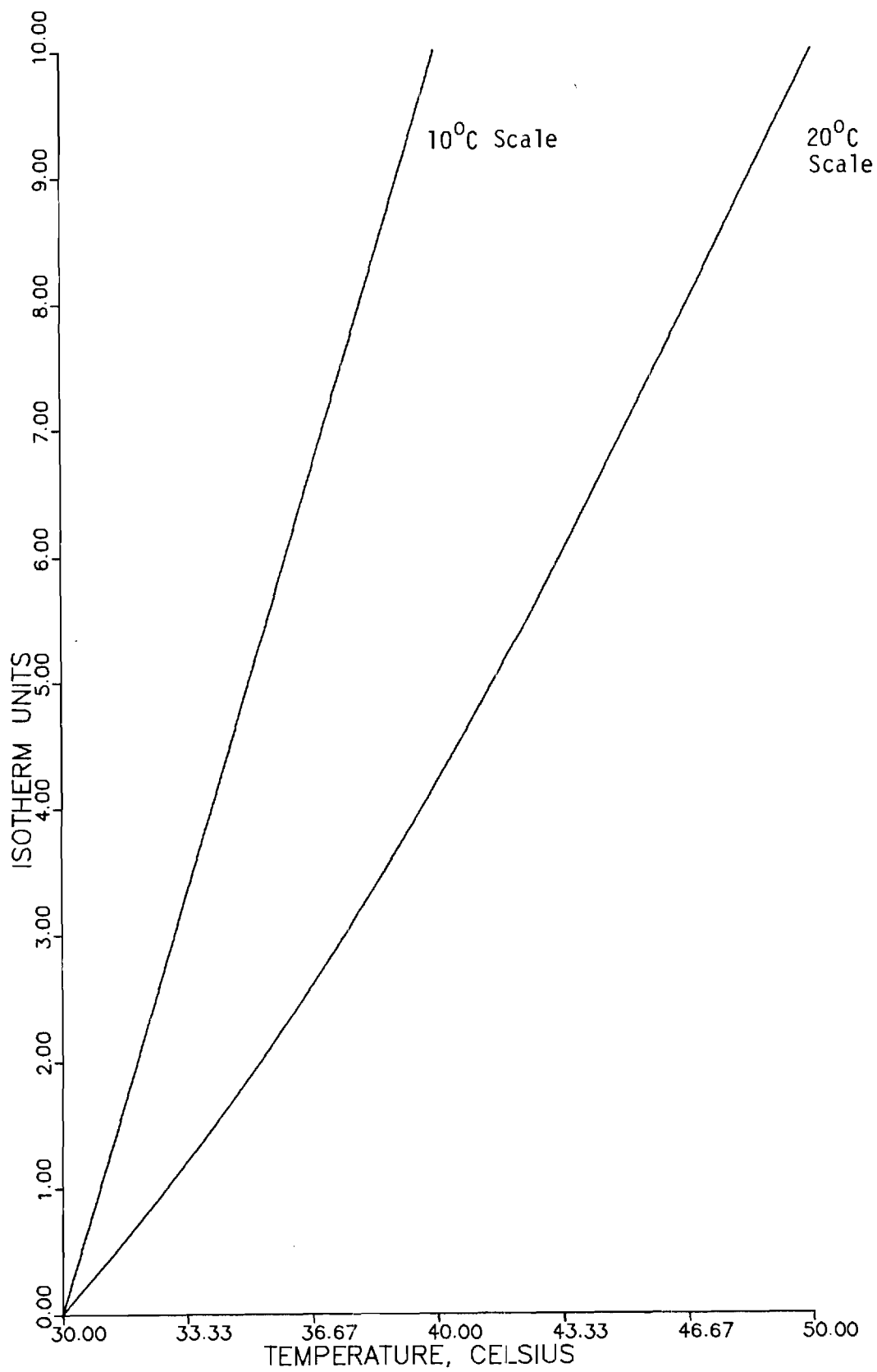


Figure 1. Standard Calibration Curves Referenced at 30°C for 10°C and 20°C Scales.

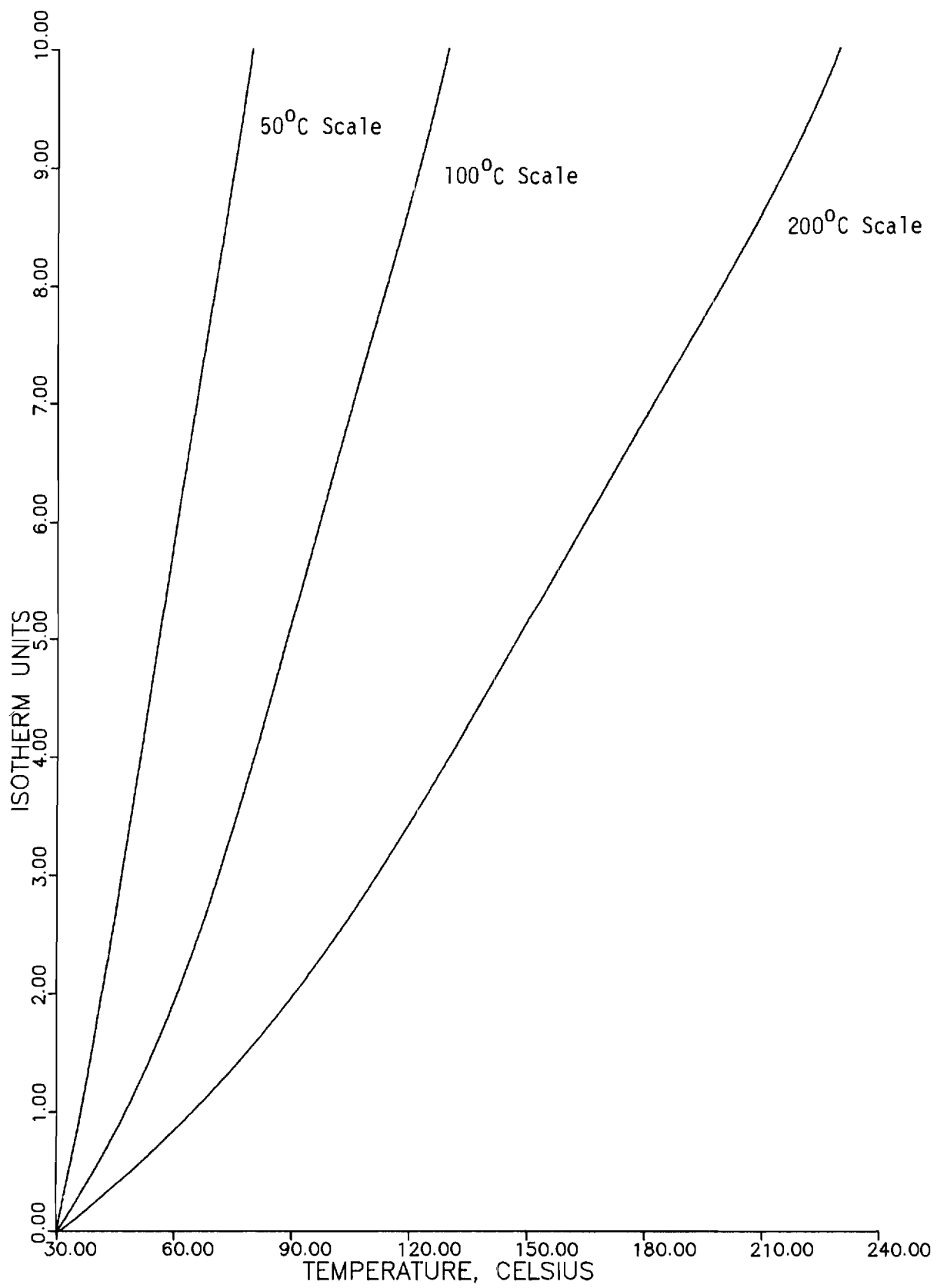


Figure 2. Standard Calibration Curves Referenced at 30°C for 50°C, 100°C and 200°C Scales.

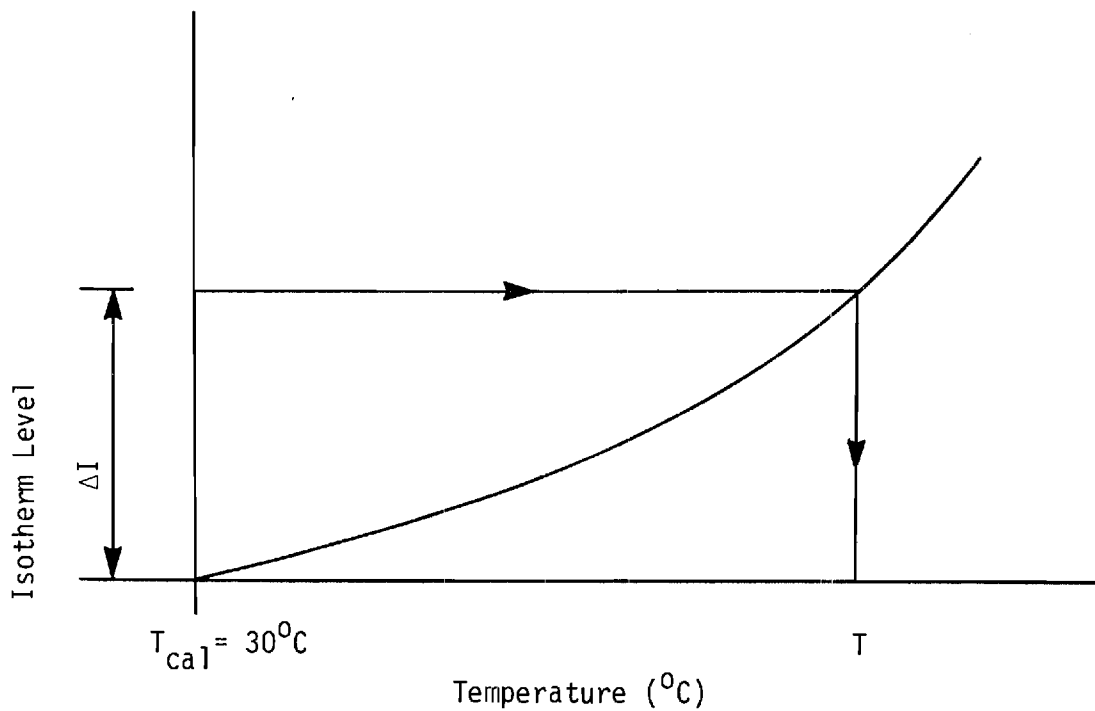


Figure 3. To Determine Target Temperature, T , Using a Reference Source, $T_R = 30^{\circ}\text{C} = T_{cal}$.

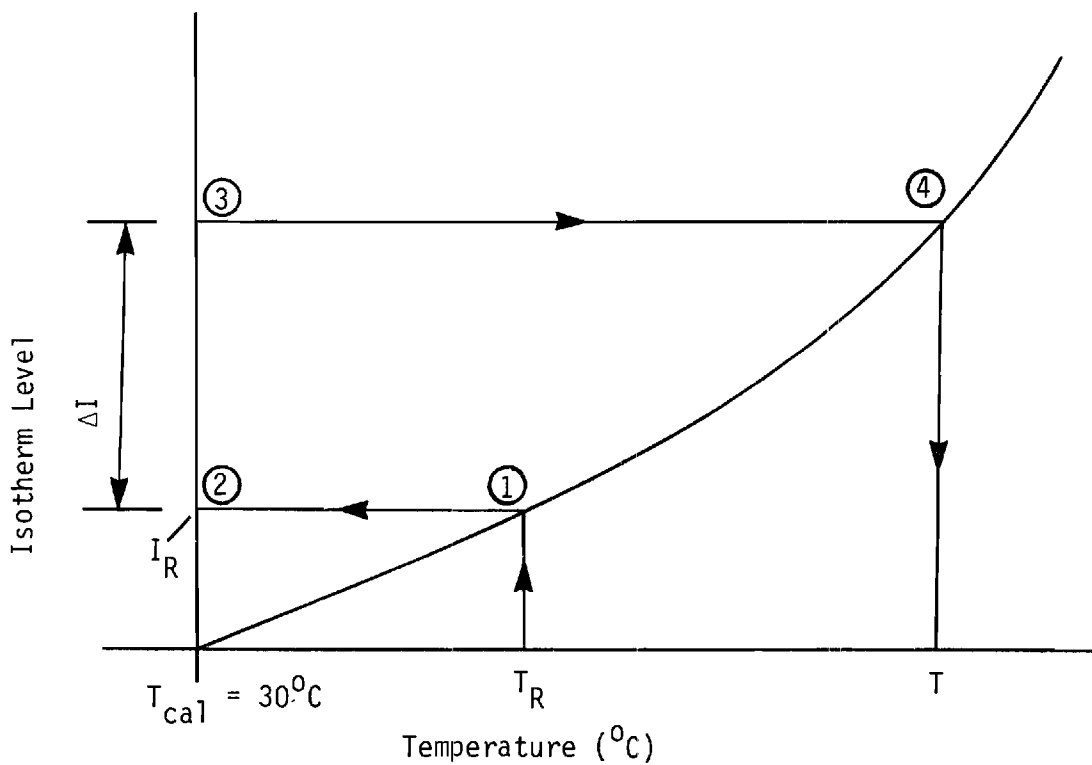


Figure 4. To Determine Target Temperature, T , Using a Reference Source, $T_R > 30^{\circ}\text{C} = T_{cal}$.



GEORGIA TECH 1985-1985

DESIGNING TOMORROW TODAY

September 3, 1985

Dr. William F. Nelson
Director, Collaborative Research Programs
GTE Laboratories Inc.
40 Sylvan Road
Waltham, Mass. 02254

SUBJECT: Quarterly Progress Report April-June, 1985 "Thermal Model
for Microelectronic Chips".

Dear Dr. Nelson:

During the past quarter a major decision was made to embark on a sophisticated three-dimensional model of the heat transfer from the VLSI package rather than to continue further development of the one-dimensional thermal model. The one-dimensional model will be retained and used as a simplified solution while the three-dimensional program will be used to provide detailed information on the location and magnitude of hot spot temperatures on the surface of the chip. Refinement of the infrared equipment will continue and eventually it will be used to verify the accuracy of the three-dimensional program.

Instead of facing the substantial task of writing a general three-dimensional thermal model, we have decided to adapt an available software package to the task of predicting the transient, three-dimensional temperature distribution in the chip and package. We have selected MITAS II (Martin Marietta Interactive Thermal Analysis System) as the most reasonable program for our task. The last several months have been spent in studying the reference manual and users guide and studying how MITAS must be modified so that it can be adapted to the thermal modeling of a microelectronic chip package.

MITAS is designed primarily to solve lumped-parameter networks of thermal systems. It can provide solutions to both steady-state and transient problems using any one of three finite differencing techniques. MITAS is capable of solving a thermal system problem consisting of up to 8191 nodes and over 12,000 unique conductors. These types of capabilities will permit the calculation of up to 100 discrete locations on the surface of a chip.

Georgia Institute of Technology

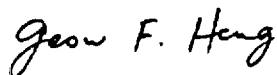
School of Mechanical Engineering Atlanta, Georgia 30332

MITAS is available in the Georgia Tech computer networks and we have begun to apply it to simple heat transfer problems with known solutions. Thus far results from MITAS compare identically with the classical solutions. In the coming months more complicated problems will be solved and finally MITAS will be adapted to the problem of predicting the temperatures for typical chip and package designs.

Respectfully submitted



William Z. Black
Project Director



Geow F. Heng
Graduate Research Assistant

WZB:v1

cc: Dr. John Hooper
Dr. John Brighton

Page 1

FINAL REPORT

THERMAL MODEL FOR MICROELECTRONIC CHIPS AND PACKAGES

Submitted by:

**Geow Heng
W. Z. Black**

FINAL REPORT

THERMAL MODEL FOR MICROELECTRONIC CHIPS AND PACKAGES

Submitted by:

Geow Heng
W. Z. Black

SCHOOL OF MECHANICAL ENGINEERING
GEORGIA INSTITUTE OF TECHNOLOGY

Submitted to:

John C. Gustafson
GTE Laboratories, Inc.
Waltham, MASS

August 1986

Summary

The Heat Transfer Laboratory in the School of Mechanical Engineering at Georgia Institute of Technology has been actively studying heat transfer from microelectronic components for the past three years. A large portion of that research effort has focused on the problem of measuring the temperature distribution over the surface of an energized microelectronic chip. The work has emphasized an experimental technique consisting of a computer software package coupled with a personal computer, an infrared imaging camera, digitizing equipment, image processing equipment and graphics display hardware. The system has evolved to such a degree that the technique can automatically adjust and accommodate for variations in surface emissivity of the chip, and the hardware/software package ultimately provides the true surface temperature of the chip. It is anticipated that surface temperatures can be measured to within 1°C at an average temperature of 100°C for a spot size of approximately 0.025mm.

The technique of measuring the surface temperature of a chip is a relatively simple one. The complex nature of the problem has been greatly simplified by the software which performs the detailed calculation and the process of surface emissivity mapping. After the surface of the chip has been scanned at a known reference temperature and the digitized signal has been compared to a reference blackbody, the emissivity map of the chip's surface is stored for future reference. Then the chip is energized in its operating environment and the output from the infrared camera is once again digitized. Each pixel of data is then automatically corrected for local emissivity values and the local

spot temperature calculated. The end result is therefore the spatial variation in temperature for the entire chip surface.

This experimental technique should prove to be a valuable tool for the designer of microelectronic circuitry. Local hot-spots can easily be identified and the maximum temperatures can be quantified. If the maximum temperature is considered to adversely affect the performance of the chip, corrective action can be taken. This technique can also be used to assess the changes in thermal performance of the chip as a result of changes in environmental conditions and changes in load on the chip. Areas within the chip that operate above their limiting temperatures can easily be identified. Areas of concentrated or excessive heat dissipation can be identified, and the influence on the local temperature can be assessed. By taking corrective measures, the chip design can be revised to produce one which is less likely to fail during operation.

Introduction

The objective of this proposed study is to model heat transfer from microelectronic devices. The drive towards higher functional density in microelectronic devices has already resulted in printed features on Very Large Scale Integration (VLSI) devices that are shrinking toward submicron dimensions. Further increase in microelectronic device density is currently constrained by the ability of the component to dissipate heat to the surroundings. As a result, the subject of heat transfer from microelectronic devices is vigorously being studied and analyzed by the thermal packaging community in the electronic industry.

The continuous increase in chip density (integration size) and reduction in chip separation distance can inevitably pose a thermal failure of the chip microcomponents if proper thermal analysis and design is not incorporated into the design of the chip and its packaging. The energy dissipated in a semiconductor device is associated with the passage of electrons through the transistor or diode emitter-base junction. From a thermodynamic point of view, transistor switching is an irreversible process, and the energy driving the switching action is eventually dissipated as heat. The energy dissipation generally occurs within 0.04 mm (1.6 mil) of the top surface of the chip. The resultant heat sources are highly localized, and the exact distribution is determined by the internal circuit layout of the chip [1-9].

For reliable operation of electronic systems, the heat dissipation must be accomplished effectively to maintain the junction temperatures below the maximum allowable component temperature of the chip. To obtain

the commonly accepted failure rates of 0.5 to 2.0 percent per thousand hours of operation, the semiconductor elements are generally operated at junction temperatures below 110 - 125°C [1,10]. For electronics systems that are required to operate with especially long operating life or with low maintenance and replacement-cost constraints, it is often desirable to have an average junction temperature as low as 60°C [1]. Usually a minor temperature increase above the maximum allowable component temperatures will result in a sharp decrease in reliability; however a large temperature excursion can produce a "thermal runaway" condition which may lead to thermal failure of the device [1,4,6]. When a semiconductor device is operated at or near its maximum power dissipation limits, the heat generated cannot be effectively dissipated by the accompanying heat sink hardware. As a result, an increase in the junction temperature above the maximum allowable temperature is imminent, and this will cause more current to flow through the junction, even though the voltage and other circuit values are kept constant. This behavior in turn causes the junction temperature to increase even further, producing a corresponding increase in current flow. If this cascading process, referred to as thermal runaway, is not stopped, then the temperature will continue to rise and the device will eventually fail [4,6]. The prevention of catastrophic thermal failure constitutes the primary motivation for the thermal control of semiconductor components. While present heat fluxes from microelectronic chips fall in the range of 2 to 3 W/cm², increasingly higher density chip designs of the future will have projected heat flux requirements on the order of 100 W/cm²[11]. These trends suggest that advanced thermal analysis/design and thermal

control techniques have to be applied to future chip designs in order to provide safe thermal operating limits.

The heat dissipation capability of semiconductor devices to a suitable heat sink (usually atmospheric air) is dependent on the total thermal resistance of the heat flow path. For microelectronic semiconductor systems, the thermal resistance from the component junction to the environment can be classified into three levels: i) the component level, ii) the package level, and iii) the system level [7]. The component level thermal resistance constitutes the resistance of the microelectronic entity that exists between the junctions and the outside surface of the case. The package level resistance consists of the resistance to heat flux from the surface of the case to a suitable reference point (e.g. temperature of air surrounding the component) in the entire system. The system level resistance refers to the heat transfer and fluid flow resistances that exist between the microelectronic packages and the ultimate heat sink which is the environment [7]. This proposed study will mainly be concentrated on the heat transfer from microelectronic chips at the component level.

Background to Proposed Research

The subject of heat transfer from microelectronic chips has been studied since the introduction of the first integrated circuit and numerous papers have been published on the subject. These papers have analyzed the thermal problem from either the component, package or system level. The majority of these papers can be classified into either theoretical or experimental studies, with the exception of a few major

studies which consider a combined theoretical and experimental analysis.

Theoretical:

Bar-Cohen et al. [10], Preston [12], Blodgett [13] and Oktay et al. [14] have summarized the problems associated with the continual miniaturization of microelectronic features, packaging, cooling techniques and other problems involved in the design of microelectronic devices. Bauer [15], Stafford [16] and Katronge and Northover [17] have discussed the application of very high packaging density chip carriers which improve the electrical and thermal performance of microelectronic devices. The advantages of using a chip carrier include its capability for achieving high pin counts for complex circuits and its closely coupled circuits which minimize signal propagation delays.

Adamain [18] and Emerald and Dewey [11] have provided relations to determine the allowable power dissipation levels at a given coolant temperature for simple package geometries. Procedures for determining thermal resistance and selection of heat sink hardware were given.

For a more detailed analysis of the temperature distribution in microelectronic devices, either an analytical or a numerical approach is necessary. Hein [19] has analyzed the three dimensional, steady-state problem for heat inputs from multiple sources on a substrate. He has considered heat transfer by convection and conduction from the chip.

Gray and Hamilton [20] and Gray [21] have presented a method for analyzing the transient temperature distributions in a silicon substrate using lumped or distributed heaters and sensors as the integrated chip. They have solved the two dimensional, transient conduction equation to provide the temperature distribution on the surface of a chip and they

have neglected heat losses from the chip due to convection and radiation.

Linsted and Surly [22] have solved the three dimensional, steady-state conduction problem for a chip with a constant heat flux source of finite area located at the center of the chip. The bottom surface of the chip was assumed to be isothermal and all the four chip edges and remainder of the nondissipating chip surface were assumed to be adiabatic.

Ellison [23,24] has provided three dimensional, steady-state solutions for chips mounted on composite substrates. He has considered problems with chips mounted on composite media with up to four layers of unequal thickness and different thermal conductivity.

Kokkas [25] has investigated the complete three dimensional, transient problem of heat flow in multilayer structures. He has assumed heat losses due to radiation and convection are negligible. Also, heat losses through wires bonded to the semiconductor chip were neglected.

David [26] has obtained the three dimensional, steady-state temperature distribution for hybrid circuits based on the solution of Laplace's Equation using Fourier techniques. He has assumed conduction to be the dominant heat transfer mechanism, and therefore neglected radiation and convection. Power generation in the hybrid device were assumed to be dissipated uniformly at the surface of a single chip.

Castello and Antognetti [27] and Antognetti [28] have presented the three dimensional, steady-state and transient solutions of a power integrated circuit mounted on a copper substrate. In order to permit the analytical solution of the heat-flow problem, they have simplified the structure of the component by assuming that most of the heat flows

through the portion of the substrate directly below the silicon chip. The heat spreading effects of the high conductivity copper was neglected.

Kadambi and Abuaf [29] have approached the problem by using two dimensional or axisymmetric approximations in their steady-state and transient analysis. They assumed a uniform heat flux over the chip area and convection from the bottom of the copper substrate. Heat spreading effects in the copper substrate were included in their analysis.

Since the interface between the chip and the substrate base is difficult to deal with analytically, many researchers have employed numerical methods in their thermal models. Thermal analyzer software that use finite difference or finite element techniques were utilized by Thompson and Blum [30], Wenthien [31], Boucher [32], Baxter [33], Baxter and Anslow [34], Cook et al. [35], Murtuza [36] and Pound [37] to model the thermal characteristics of semiconductor devices.

Blodgett and Barbour [38], Chu et al. [39] and Oktay and Kammerer [40] have reported an innovative conduction-cooling assembly called the Thermal Conduction Module. The TCM which uses Helium gas encapsulation contains 118 LSI devices mounted on a multilayer ceramic substrate. The thermal characteristics of the TCM at the chip and module levels were analyzed using numerical simulations.

Experimental:

McLaughlin and Fitzroy [41] summarized the various techniques for experimental measurements of temperature in integrated circuits. Because of the small dimension of microelectronic devices, noncontacting measurement methods must be used to avoid distorting the temperature field. In the defense industry, the testing procedures for the

determination of thermal characteristics of microelectronic devices in military equipment are in accordance with the guidelines given in MIL-STD-883C Method 1012.1 [42].

Goel and Gray [43] and Choudhury [44] reported on the use of liquid crystals for measuring temperatures of microelectronic devices. Liquid crystals react to changes in temperature by changing color, which provides a visual method for non-destructive testing and evaluation.

Sanders [45], Maher [46], Boulton and Siegal [47] and Boulton [48] have summarized the role of thermography in the design, development, production and in-use evaluation of microelectronic devices and assemblies. Infrared imaging systems are used to detect, isolate and quantify extreme temperature differences which usually indicate a defect in the component.

Martin [49], Weight [50], Egan [51] and Boulton [52] have reported the use of thermal imaging to detect temperature anomalies on PC Boards. Kallis et al. [53], and Boulton [54] have discussed the application of thermography for testing hybrid circuits. At the single component level, Yu [55] and Lidback [56] have presented temperature measurements of the surface of a chip using an infrared imaging technique. They have eliminated the difficulty of compensating for emissivities by coating the chip surface with a black velvet coating which has an emissivity close to unity.

Wickersheim [57] has presented a new thermometry technique for measuring component temperature of microelectronic devices. Fluoroptic thermometry utilized a small contact sensor constructed from insulating material which provides complete electrical isolation and minimal thermal

perturbation. Temperature measurements using Fluoroptic thermometry is based on the isolation and measurement of the relative intensities of two fluorescent emission lines which originated from an europium activated phosphor when illuminated by UV radiation.

In a combined theoretical and experimental analysis, Coats [58] numerically modeled the microelectronic device using a thermal analyzer program. Experimentally, he measured the substrate temperature using diode chips eutectically bonded to the surface of the substrate.

Sergent and Schuyler [59] described a numerical solution technique to predict the approximate temperature rise in hybrid microcircuits. Temperature measurements were made using an infrared microscope. They included emissivity corrections but primarily compare only temperatures of areas with equal emissivities.

A major study involving theoretical and experimental analysis was reported by Baxter [60,62], Baxter and Brouillette [61] and Anslow et al. [63]. These reports described the thermal characteristics and measurement techniques for microelectronic chips and packages. Computer simulations, infrared radiance measurements and electrical temperature sensitive parameters measurements were used to study the thermal characteristics of a thermal test chip. The problem of emissivity corrections for infrared radiation measurements and the use of various chip coatings to eliminate the chip translucence problem were discussed.

Proposed Research

The purpose of this research project is to develop a thermal model of a microelectronic semiconductor device at the component level. The

thermal model will be capable of predicting the transient, local temperatures over the entire surface of an energized chip. The proposed project can be broken into two distinct tasks:

1. Theoretical Model of the Heat Transfer from a Microelectronic Chip. The theoretical approach will result in a computer program capable of predicting the temperature distribution within a microelectronic package as a function of package design, power consumption of the chip, mounting techniques and materials used in the construction of the package.
2. Experimental Measurement of the Temperature Distribution Across the Surface of Microelectronic Chips. The bulk of the experimental measurement will be made with an infrared camera system used in conjunction with a digital video processor and a microcomputer for data acquisition and storage.

The experimentally measured temperature data will be used to verify the results of the computer-predicted temperature distribution.

Theoretical Model

Preliminary work on the thermal model has produced a conservative one-dimensional model of a microelectronic chip encased in a dual-in-line package (DIP). This transient one dimensional model was developed using an explicit finite difference formulation based on a typical DIP geometry configuration given in Figure 1.

The model assumes that the semiconductor chip is at a uniform temperature. The one dimensional assumption restricts the heat transfer

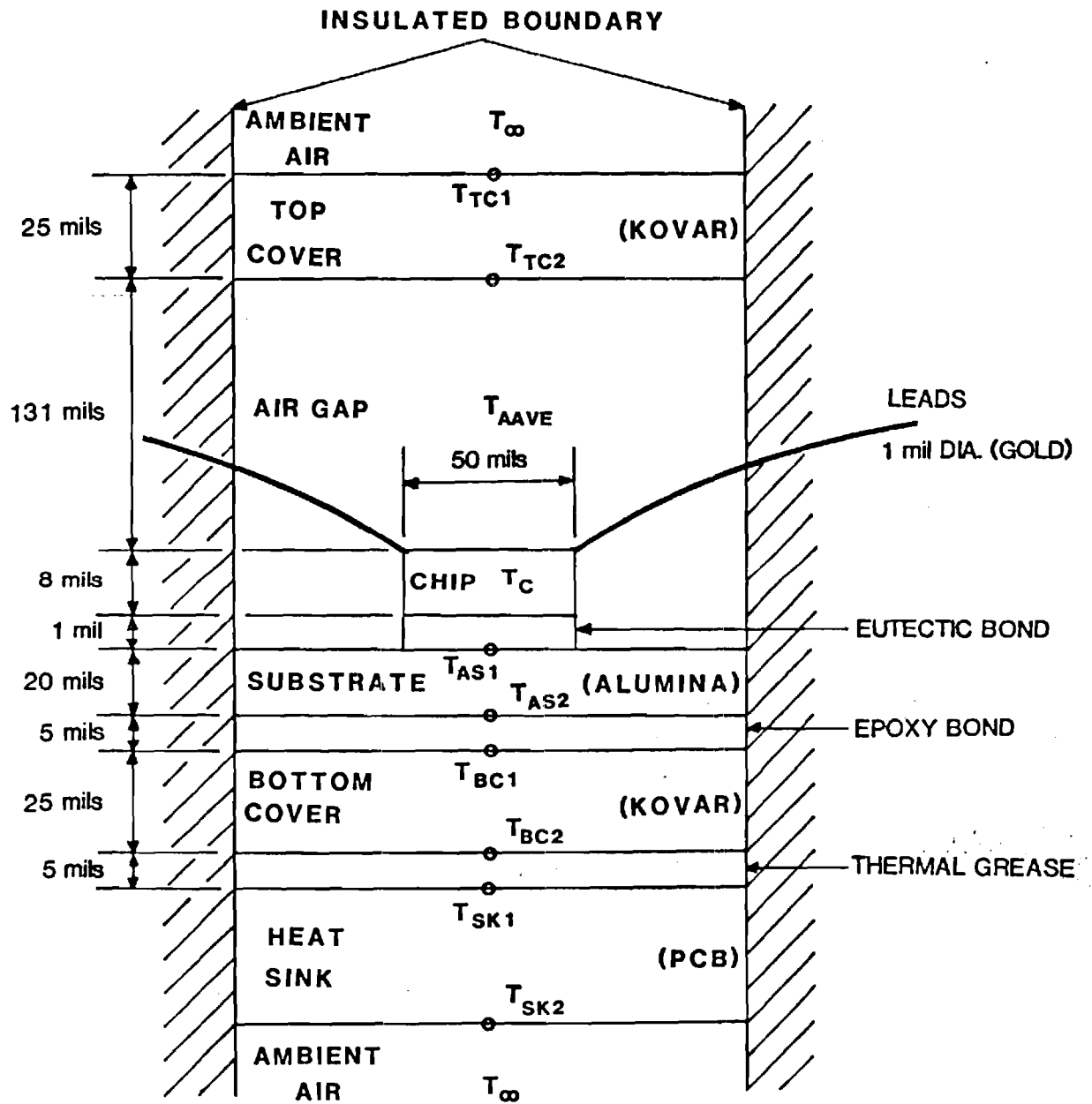


**FIG. 1 ONE DIMENSIONAL DIP PROFILE
(NOT TO SCALE)**

in the vertical direction only. The assumption of insulated sides will give a rather conservative preliminary approximation. Heat is assumed to be generated uniformly throughout the chip and it is dissipated through combinations of series-parallel thermal resistances to the outer surface of the package. A portion of the heat is conducted in series through the eutectic bond, ceramic substrate, epoxy bond and the cover material before reaching the outer surface of the bottom cover. Heat is also conducted from the chip through the lead wires. The remaining heat is dissipated by conduction (due to the small spacing of the air gap, convective cells cannot develop) and radiation in parallel through the air gap and then by conduction through the cover material to the outer surface of the top cover. At the outer surface of the top cover, heat is assumed to be transferred to the ambient surrounding by free convection and radiation. Heat removal from the outer surface of the bottom cover is more complicated, because it is dependent on the mounting configuration of the DIP onto the PCB and the heat sink configuration assumed in the model.

Preliminary results have been obtained using the 1-D transient model for various initial conditions, heat sink boundary conditions and dissipation rates. Figure 2 shows the temperature-time plot of the DIP for the following conditions: convective heat sink PCB [1,7,8], temperature dependent properties [64,65], adjustable time steps, initial temperature of 25°C, and a dissipation rate of 6.2 W/cm² in the chip.

The one dimensional thermal model is capable of providing a conservative approximation of the temperature distribution in a microelectronic package. However, preliminary infrared temperature

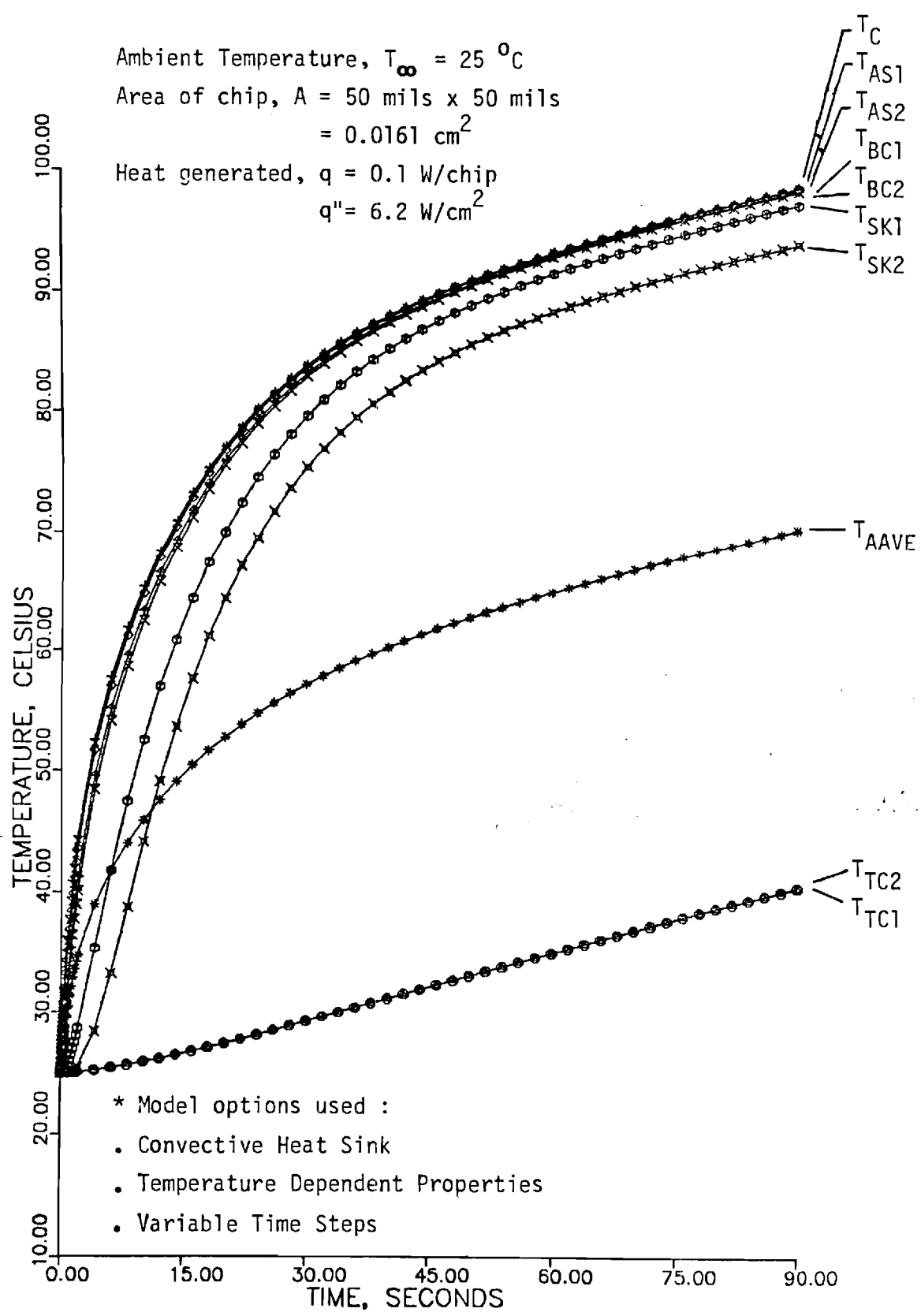


FIG. 2 TEMPERATURE DISTRIBUTIONS IN A DIP

measurements of a thermal test die provided by GTE indicates that local temperature variations exist across the surface of the chip. Thus, the assumption of uniform chip temperature in the one dimensional thermal model is inadequate for predicting localized hot spot temperatures. A three-dimensional model will be required to provide detailed information on the location and magnitude of hot spot temperatures on the surface of the chip. Instead of facing the substantial task of writing a general thermal model program, it was decided that time will be more efficiently utilized by adapting a commercially available software package for predicting the transient, three-dimensional temperature distribution in a microelectronic package. After a review of the available thermal model programs, MITAS-II [66] was selected for use in the theoretical modeling of the chip package. A portion of the proposed work will involve adapting MITAS-II to the task of predicting the transient, three dimensional temperature distribution in a microelectronic package.

MITAS-II has been used to solve several heat transfer problems with known analytical solutions. These initial applications serve to check the accuracy and applicability of MITAS-II. Initially, the temperature distribution for a steady-state classical fin with constant cross-sectional area was solved for the following cases: (i) convection from surface and end of fin; (ii) convection from surface of fin with insulated ends; and (iii) convection and radiation from surface of fin with insulated ends. The MITAS-II simulation results for all three cases agree identically with the analytical solutions (case (i) & (ii) [67], case (iii) [68]).

To further the understanding of MITAS-II's capability, the program

was applied to more complicated problems that resemble the heat transfer from a microelectronic chip and package. A one-dimensional model of a heater with internal generation (resembling heat dissipation in a chip) was selected and cases with increasing complexity were solved. The cases examined were as follows: (i) steady-state, constant properties ($k=\text{constant}$); (ii) steady-state, temperature dependent properties ($k=k(T)$); (iii) transient, constant properties ($k=\text{constant}$); and (iv) transient, temperature dependent properties ($k=k(T)$). The MITAS-II simulation results for cases (i), (ii), and (iii) agree identically with the analytical solutions [69] for the temperature distribution in the heater. For case (iv), a closed-form analytical solution is not available for comparison, however, transient simulation results for large time periods agree exactly with the steady-state analytical results of case (ii). A comparison of the MITAS-II simulation results with the analytical solution for case (iii) is shown in Figure 3.

Currently, a search is being conducted on the availability of a suitable thermal test chip that can duplicate the heat dissipation in a chip with a realistic design. Once the thermal test chip is obtained, MITAS-II will be adapted to model the heat transfer from the chip.

Experimental Measurements

The proposed experimental research involves measuring the temperature distribution on the surface of microelectronic chips. The equipment required for data collection centers around an infrared imaging radiometer that produces a thermograph video output, a digital video processor that digitizes the video output, and a microcomputer that controls the data acquisition process and provides data storage. A

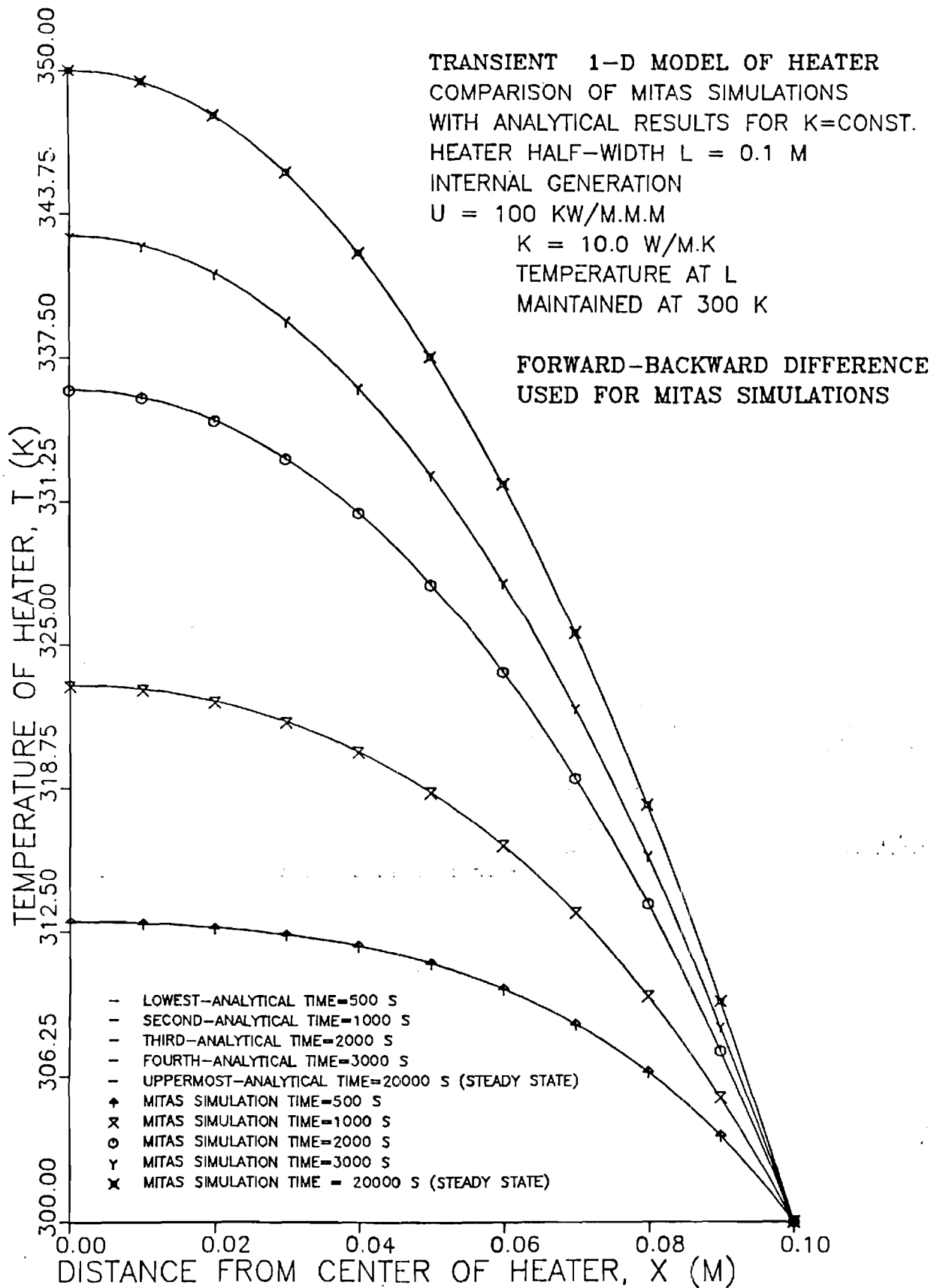


Figure 3. MITAS(FWDBCK)/ANALYTICAL RESULTS FOR $K=CONST.$

microcomputer specifically equipped for image processing is used to transform the test data to spatially match the master frame emissivity map. Either a main-frame computer or a microcomputer equipped with a Math Coprocessor can be used to process the spatially aligned data into a temperature distribution for the surface of the chip, which can then be displayed using Enhanced Graphics hardware.

Infrared Measurements

The infrared camera system, manufactured by Inframetrics, [70] produces a TV compatible video output signal of the thermal patterns radiated by a target. The scanner senses the infrared radiation emitted by the target using a liquid Nitrogen cooled Mercury-Cadmium-Telluride detector. The signal from the scanner is processed by the Control/Electronics unit into a video output which is proportional to the local radiant energy of the target. The black-and-white video output that is displayed on a TV monitor permits qualitative and quantitative data analysis by interpretation of gray tones or isotherm scale readings. In addition, a pseudo-color presentation of the video output can be generated by processing the output signal from the Control/Electronics unit with an Iso/Line Scan Colorizer. The resultant quantized color image representing different temperature ranges is obtained by superimposing eight discrete colors onto the black-and-white imagery.

The infrared camera is ideal for qualitative temperature detections. "Hot spots" within the target area can readily be detected. However, in order to determine a numerical temperature value for a region of interest, an involved manipulation and calibration of the equipment is required. The quantitative analysis is complicated by the non-blackbody

characteristics of the surfaces of microelectronic chips. The complexity of the temperature determination is compounded by the unknown emissivities of the materials which are distributed in micro proportions depending on the internal circuit layout of the chip.

The emissivity of a surface can be obtained using the following relation:

$$e_t = (\Delta I_{tr} - I_{ba}) / (I_t - I_{ba})$$

where

I_t = Absolute Isotherm Units of the target at T_e ;

ΔI_{tr} = Difference in Isotherm Units between target and reference at T_e ;

I_{ba} = Absolute Isotherm Units of the background;

e_t = emissivity of the target;

T_e = temperature of target
(target heated to a known temperature for emissivity mapping).

Once emissivity is known, the following relation is used to correct for emissivity and account for reflection from the background in an actual test.

$$I_t = (\Delta I_{tr} / e_t) + (1 - 1 / e_t) I_{ba}$$

After correction for emissivity, the Absolute Isotherm Units can be used to obtain temperature from the calibration curves (graphical method) or by substituting into polynomial functions expressing temperature as a function of Isotherm Units:

$$T = C31 + C32 I + C33 I^2 + C34 I^3 + C35 I^4$$

where

C3n's = calibration constant for infrared camera.

Preliminary measurements using the infrared camera system have been carried out for two types of chip packages. The first is an actual production chip consisting of a Motorola 6801 chip mounted in a 40-pin dual-in-line package (DIP). The other type of package examined consists of a Motorola Thermal Test die mounted in a leadless ceramic chip carrier (C³) package. These 16-lead Thermal Test chip packages, provided by GTE Packaging Technology Center, consist of two heater implants that duplicate the heat dissipation in an actual chip. Prior to measuring the chip temperature with the infrared equipment, temperature-resistance measurements of the chip were made for both type of packages. The temperature-resistance calibrations will provide an approximate check of the results obtained from the infrared radiation measurements.

Only the outer surface of the Motorola 6801 chip package can be analyzed using the infrared camera because the chip itself is encapsulated within the DIP. Since the outer surface of the package consists of a single material, the temperature distribution can readily be evaluated once the emissivity of the surface is known. The Thermal Test die, on the other hand, is sealed within the chip carrier package with a glass window. Since glass is opaque to infrared radiation, the video output obtained from the infrared camera when focused on the leadless chip carrier package was due to radiation emitted from the heated glass. After the glass window was removed to expose the chip, slight variations in temperature were observed when the chip area was scanned with the normal lens. However, when the chip was scanned with a 3X telescope coupled to a microscopic objective, the magnified image

revealed an "apparent" temperature variation on the surface of the chip. The terminology of an "apparent" temperature is used to denote results that have not been corrected for emissivity. Variations in the apparent temperature can be attributed to either actual temperature differences on the surface or they can arise from emissivity differences due to the different materials on the surface. The metallized regions are observed to produce lower apparent temperatures on the chip due to their high reflective properties (low emissivity). Figure 4 is a magnified video output showing the variation in surface apparent temperatures that exist on the Thermal Test die. The actual temperature distribution can be evaluated once the emissivities of the microstructures on the chip surface are known.

Digitizing and Graphics Display

The Isotherm Units calibration curve of the infrared camera can be used to determine the emissivity and ultimately the temperature. However, since the video image produced by the infrared camera indicates complex thermal patterns across the surface of the chip, the temperature at every pixel of the video image must be determined. Since the number of pixels for each frame of video image is very large, a computer is ideal for carrying out the necessary computations. Thus, the video output from the infrared equipment must be stored and made accessible to a computer which will perform the computations and provide the temperature results. The video output signal from the infrared camera can be read to and stored in the memory of the digital video processor at 512x512 addressable pixels per frame of video. The analog signal at each pixel location is digitized and assigned an integer number ranging from 0



Figure 4. Video Output from the Infrared Camera showing the Apparent Temperature Distribution Across the Surface of a Thermal Test Chip.

to 255, depending on the intensity level (0-black, 255-white).

The digitized signal can then be transferred from the digital video processor's memory to a PC and ultimately stored on floppy diskettes. Since the PC has limited memory capacity and low computational speed, the large number of digital video data can be more efficiently processed using a mainframe computer. A communication software package has been used to transfer files between the PC and the host computer. Figure 5 is a three dimensional plot of the infrared radiation intensity distribution on the surface of a Thermal Test chip. The original 512x512 digital video data have been reduced and averaged to produce the 100x100 "reduced" data used to generate the plot in Figure 5.

Using a personal computer equipped with the Enhanced Graphics Adapter and Monitor, the "processed" data can be displayed in high resolution graphics (640x350 pixels) using 16-color isotherm bands as shown in Figure 6 for the thermal test die. This capability permits the reconstruction of the "processed" data into a video image for comparison with the video output of the infrared camera. A reconstructed video image displayed using the same 8-color output by the infrared camera system is shown in Figure 7 for the thermal test die. Figure 8 and 9 are pictures of an actual chip used in the thermography experiment. A computer reconstructed video image of the energized chip is shown in Figure 10.

Emissivity Corrections

Due to the complex distribution of materials on the chip surface and the large number of pixels per video image, it would be impractical to identify the material, determine its emissivity and then input

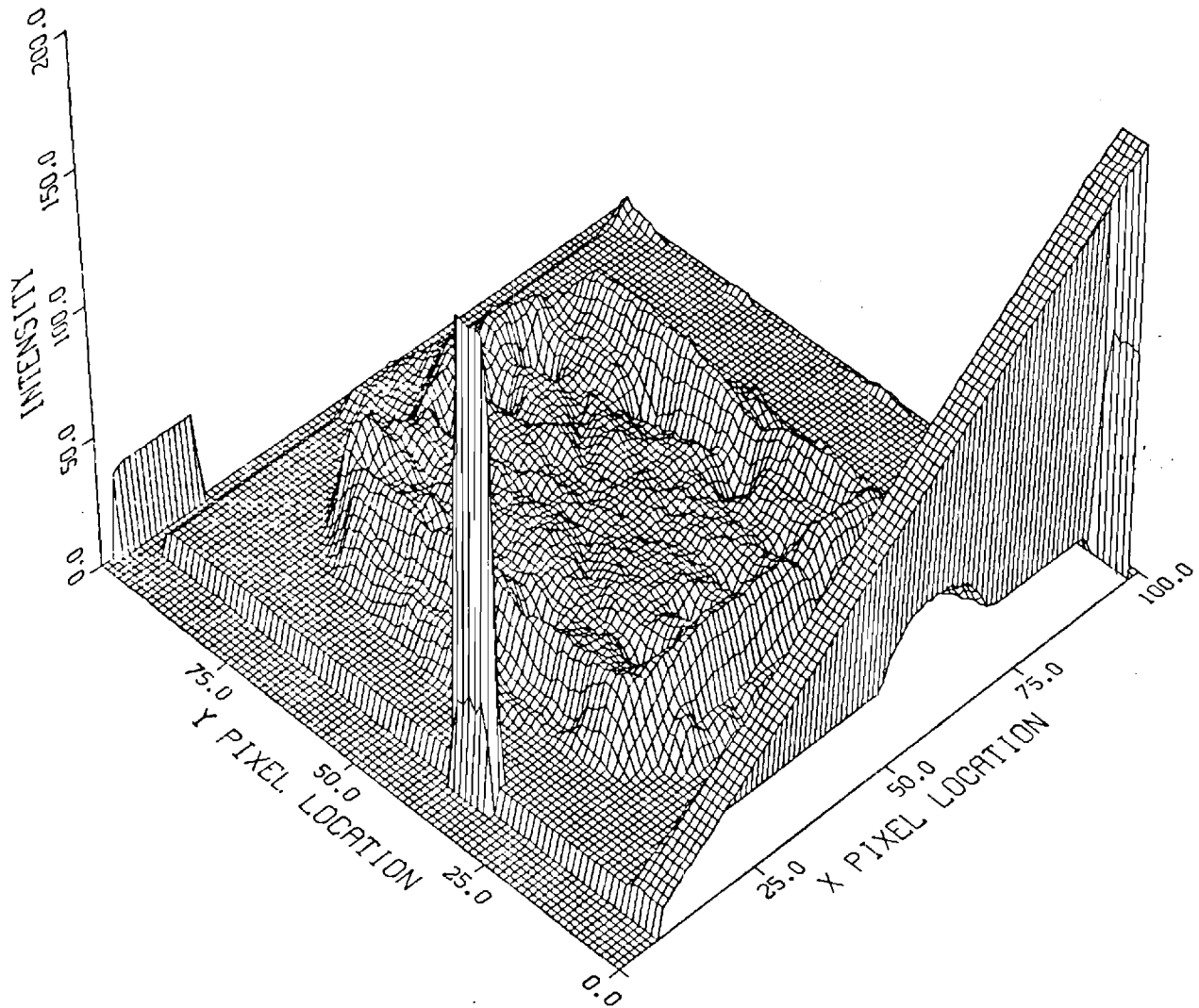


Figure 5. Infrared Intensity Level of a Thermal Test Chip.

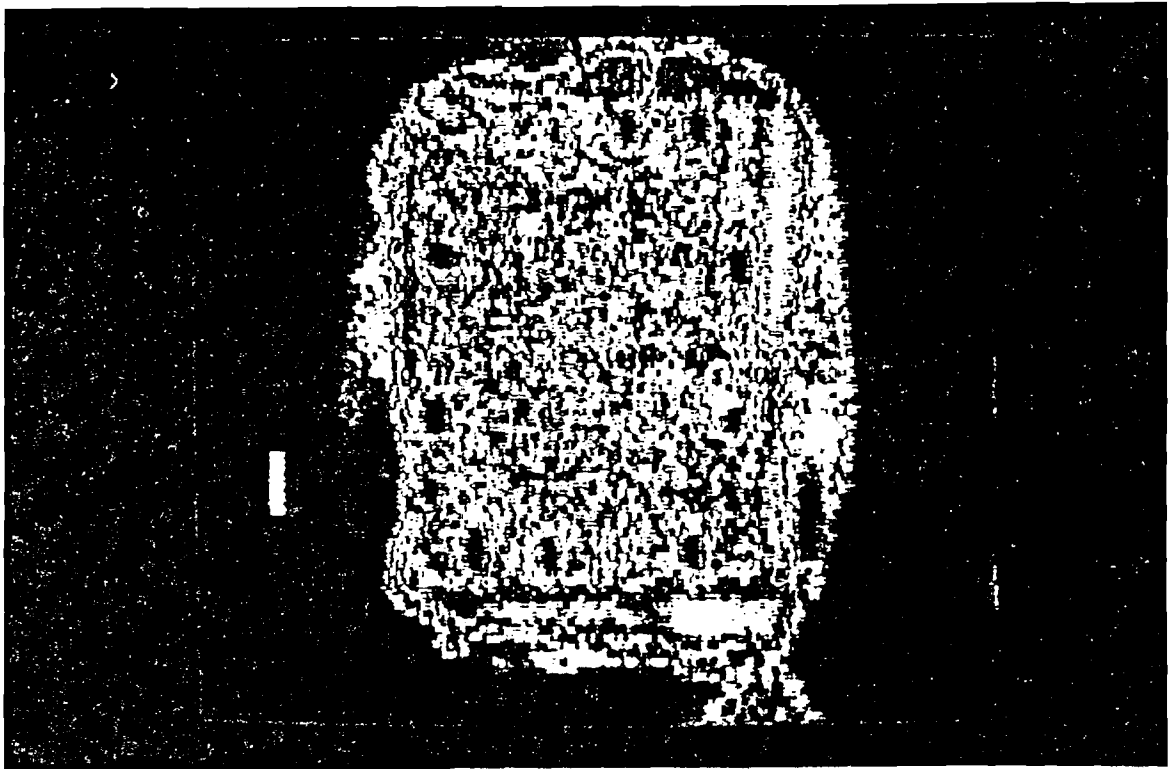


Figure 6. Computer Constructed Thermograph of a Thermal Test Chip in High Resolution (640 x 350 pixels) in 16 Colors Contour.

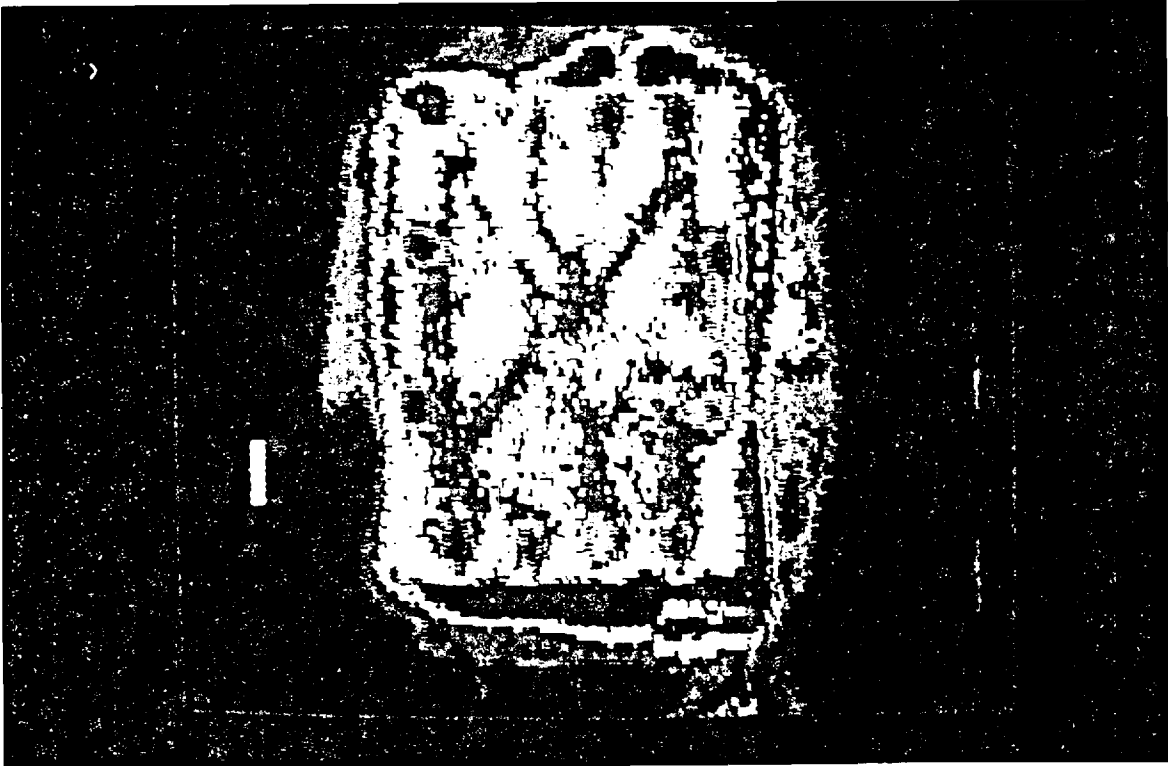


Figure 7. Computer Constructed Video Image of a Thermal Test Chip Displayed Using High Resolution Enhanced Graphics, with 8 Colors Contour (Duplicate IR Camera Output).

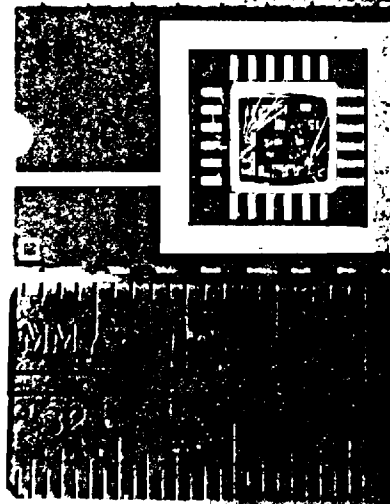


Figure 8. An Actual Chip Used in the Thermography Experiment.

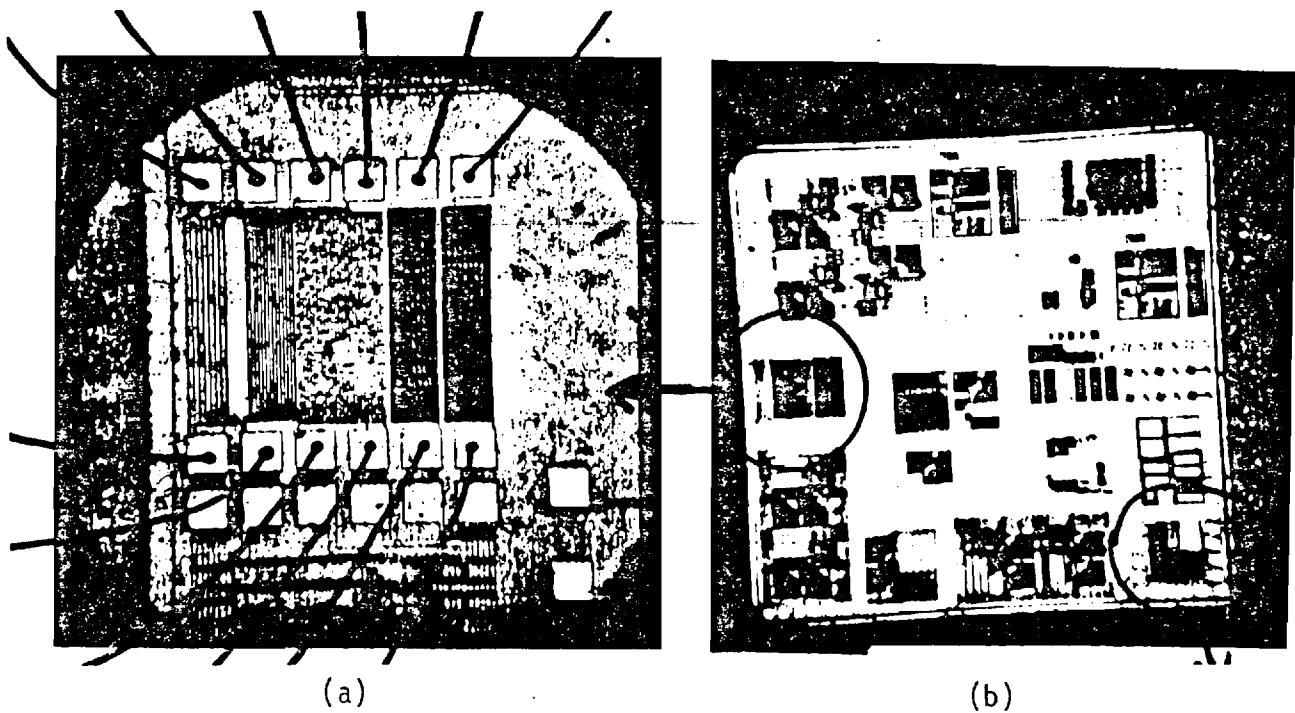


Figure 9. Detail of Microcomponents on the Actual Chip (4.8 mm x 4.8 mm).
 (a) Enlarged Portion of the Actual Chip that was Energized;
 (b) Entire Chip.

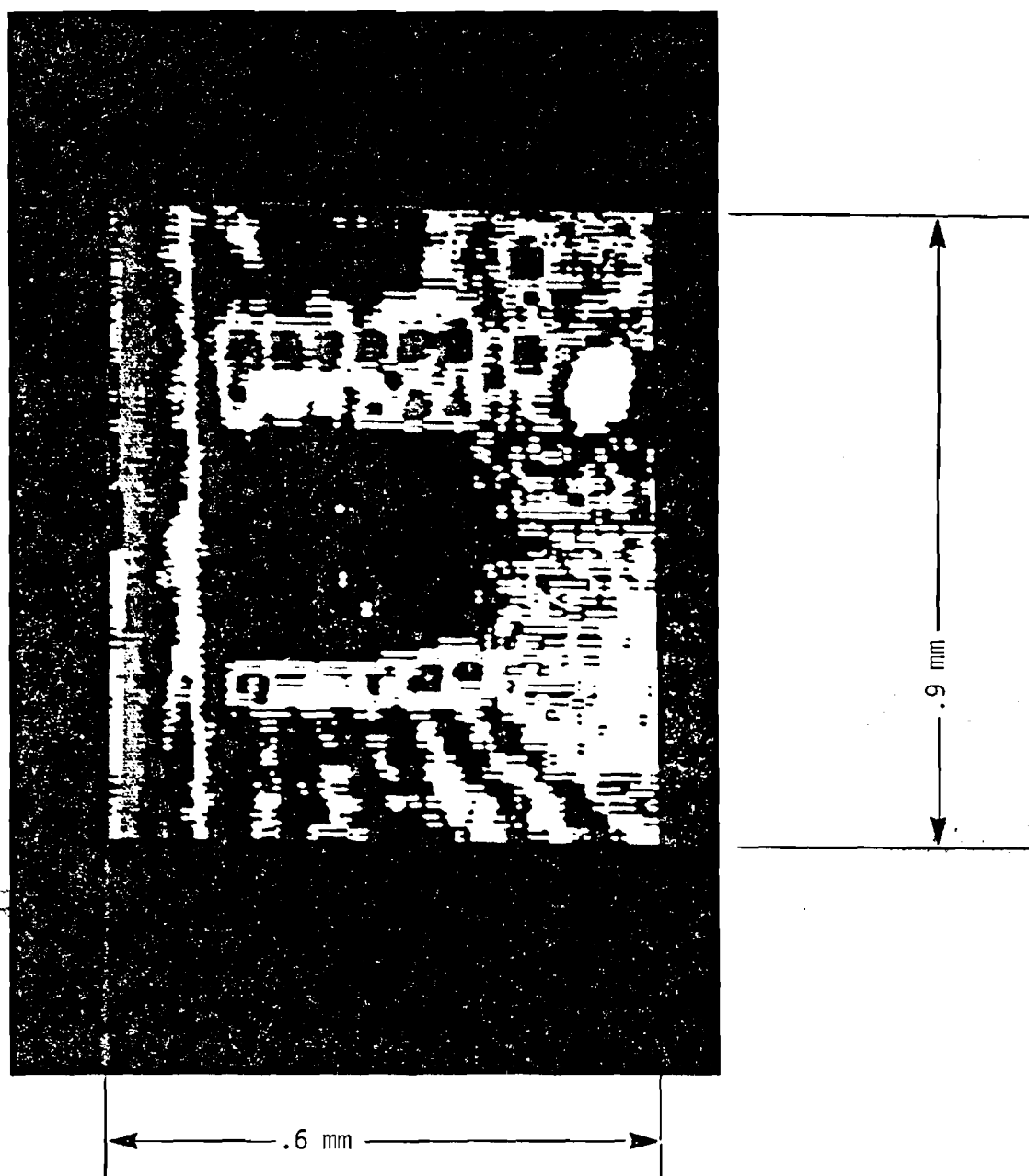


Figure 10. Computer Constructed Thermograph of the Enlarged Portion of the Actual Chip (Figure 6a). The Magenta Rectangular Area Represents the Energized Resistor on the Chip.

emissivity values for temperature calculations at all the pixel locations. An emissivity "mapping" process is proposed for the determination of emissivities at every pixel location of the video image. An isothermal cavity will be used to heat the chip to a constant known temperature. The radiation intensity of the chip surface will be compared to the radiation intensity of a blackbody source set at the same temperature of the chip. This information will be digitized and made accessible to a computer for the emissivity computation at every pixel location of the video image. Thus an emissivity map can be created for any chip and the respective pixel emissivity value can be retrieved to evaluate temperature in subsequent actual power-up testing of the same chip. However, due to the small spatial dimensions of microelectronic devices, it is impractical to align physically the image of a test frame with that of a previously stored emissivity master frame. Image processing hardware and software by Earth Resources Data Analysis System (ERDAS) will be used to geometrically transform the spatial locations of the test frame and align it with that of the master frame prior to temperature computation.

REFERENCES

1. Kraus, Allan D., and Bar-Cohen, Avram, Thermal Analysis and Control of Electronic Equipment, Hemisphere Publishing Corporation, Washington, 1983.
2. Kraus, Allan D., Cooling Electronic Equipment, Prentice-Hall, Inc., Englewood Cliffs, N.J., 1965.
3. Muroga, S., VLSI SYSTEM DESIGN When and How to Design Very-Large-Scale Integrated Circuits, John Wiley & Sons, New York, 1982.
4. Lenk, J. D., Handbook of Integrated Circuits: For Engineers and Technicians, Reston Publishing Company, Inc., Reston, Virginia, 1978.
5. Mannasse, F. K., Semiconductor Electronics Design, Prentice-Hall, Inc., Englewood Cliffs, N.J., 1977.
6. Bell, D. A. Fundamentals of Electronic Devices, Reston Publishing Company, Inc., 1975.
7. Seely, J. H., and Chu, R. C., Heat Transfer in Microelectronic Equipment, Marcel Dekker, Inc., New York, 1972.
8. Steinberg, D. S., Cooling Techniques for Electronic Equipment, John Wiley & Sons, New York, 1980.
9. Ellison, G. N., Thermal Computations for Electronic Equipment, Van Nostrand Reinhold Company, New York, 1984.
10. Bar-Cohen, A., Kraus, A. D., and Davidson, S. F., "Thermal Frontiers in the Design and Packaging of Microelectronic Equipment," Mechanical Engineering, June 1983.
11. Emerald, P. R., and Dewey, F. R., "Computing IC Temperature Rise," Machine Design, June 9, 1977.
12. Preston, G. W., "The Very Large Scale Integrated Circuit," American Scientist, Volume 71, September-October 1983.
13. Blodgett, A. J., "Microelectronic Packaging," Scientific American, July 1983.
14. Oktay, S., Hannemann, R., and Bar-Cohen A., "High Heat from A Small Package," Mechanical Engineering, March 1986.
15. Bauer, J. A., "Chip Carrier Packaging Applications," IEEE Transactions on Components, Hybrids, and Manufacturing Technology, March 1980.

16. Stafford, J. W., "Chip Carriers: Application and Future Direction," *Electronic Packaging and Production*, July 1980.
17. Katronge, G. A., and Northover, G., "Chip Carrier Applications," *IEEE Transactions on Components, Hybrids, and Manufacturing Technology*, June 1981.
18. Adamian, A., "Cooling Hot ICs with Heat Sinks," *Machine Design*, May 1977.
19. Hein, V. L., "Convection and Conduction Cooling of Substrates Containing Multiple Heat Sources," *The Bell System Technical Journal*, October 1967.
20. Gray, P. R., and Hamilton, D. J., "Analysis of Electrothermal Integrated Circuits," *IEEE Journal of Solid-State Circuits*, February 1971.
21. Gray, P. R., Hamilton, D. J., and Lieux, J. D., "Analysis and Design of Temperature Stabilized Substrate Integrated Circuits," *IEEE Journal of Solid-State Circuits*, April 1974.
22. Lindsted, R. D., and Surty, R. J., "Steady-State Junction Temperatures of Semiconductor Chips," *IEEE Transactions on Electron Devices*, January 1972.
23. Ellison, G. N., "The Effect of Some Composite Structures on the Thermal Resistance of Substrates and Integrated Circuit Chips," *IEEE Transactions on Electron Devices*, March 1973.
24. Ellison, G. N., "The Thermal Design of an LSI Single-Chip Package," *IEEE Transactions on Parts, Hybrids, and Packaging*, December 1976.
25. Kokkas, A. G., "Thermal Analysis of Multiple-Layer Structures," *IEEE Transactions on Electron Devices*, November 1974.
26. David, R. F., "Computerized Thermal Analysis of Hybrid Circuits," *IEEE Transactions on Parts, Hybrids, and Packaging*, September 1977.
27. Castello, R., and Antognetti, P., "Integrated-Circuit Thermal Modeling," *IEEE Journal of Solid-State Circuits*, June 1978.
28. Antognetti, P., Bisio, G. R., Curatelli, F., and Palara, S., "Three-Dimensional Transient Thermal Simulation: Application to Delayed Short Circuit Protection in Power IC's," *IEEE Journal of Solid-State Circuits*, June 1980.
29. Kadambi, V., and Abuaf, N., "An Analysis of the Thermal Response of Power Chip Packages," *IEEE Transactions on Electron Devices*, June 1985.

30. Thompson, R. R., and Blum, H. R., "Computer Simulation of the Thermal Environment of Large-Scale Integrated Circuits: Computer Time-Saving Techniques," IEEE Transactions on Parts, Hybrids, and Packaging, December 1971.
31. Wenthen, F. T., "Computer-Aided Thermal Analysis of Power Semiconductor Devices," IEEE Transactions on Electron Devices, September 1970.
32. Boucher, S., "Computer-Aided Thermal Design of LSI Packages," IEEE Transactions on Parts, Hybrids, and Packaging, April 1972.
33. Baxter, G. K., "Transient Temperature Response of a Power Transistor," IEEE Transactions on Parts, Hybrids, and Packaging, June 1974.
34. Baxter, G. K., and Anslow, J. W., "High Temperature Thermal Characteristics of Microelectronic Packages," IEEE Transactions on Parts, Hybrids, and Packaging, December 1977.
35. Cook, K. B., Kerns, D. V., Nagle, H. T., Slagh, T. D., and Ruwe, V. W., "Computer-Aided Thermal Analysis of a Hybrid Multistage Active Bandpass Filter/Amplifier," IEEE Transactions on Parts, Hybrids, and Packaging, December 1976.
36. Murtuza, M., "Computer-Generated Models Abridge Thermal Analysis of Packaged VLSI," Electronics, February 1982.
37. Pound, R., "Thermal CAD Brings Hot Spots Under Control," Electronic Packaging & Production, April 1984.
38. Blodgett, A. J., and Barbour, D. R., "Thermal Conduction Module: A High-Performance Multilayer Ceramic Package," IBM J. RES. DEVELOP., January 1982.
39. Chu, R. C., Hwang, U. P., and Simons, R. E., "Conduction Cooling for an LSI Package: A One-Dimensional Approach," IBM J. RES. DEVELOP., January 1982.
40. Oktay, S., and Kammerer, H. C., "A Conduction-Cooled Module for High-Performance LSI Devices," IBM J. RES. DEVELOP., January 1982.
41. McLaughlin, M. H., and Fitzroy, N. D., "Thermal Chip Evaluation of IC Packaging," IEEE Transactions on Parts, Hybrids, and Packaging, September 1972.
42. Military Standard, Test Methods and Procedures for Microelectronics, MIL-STD-883C, Method 1012.1, August 1977.
43. Goel, A., and Gray, A., "Liquid Crystal Technique as a Failure Analysis Tool," Reliability Physics, 1980.

44. Choudhury, M. A., "Heat Shows Its Colors for Testing," Electronic Packaging & Production, May 1983.
45. Sanders, J., "IR Imaging Systems for Quality Control," Electronic Packaging & Production, August 1979.
46. Maher, F. X., "The Growth of Thermal Imaging in Electronics Design and Test," ATE Central Seminar/Exhibit, Rosemont, Illinois, October 1982.
47. Boulton, H., and Siegal, B. S., "Integrating Temperature Test Equipment into Production ATE," Test Measurement World, March 1984.
48. Boulton, H., "Design Verification, Product Characterization and Production Testing of Hybrids and Printed Circuit Boards Using High-Sensitivity Thermography Systems, IEEE International Test Conference Proceedings, 1984.
49. Martin, K. J., "Using Infrared Signatures for PC Board Failure Analysis," Electronic Packaging and Production, March 1979.
50. Weight, M., "Thermography Testing of Production PC Boards," Electronic Packaging and Production, October 1981.
51. Egan, G., "Testing Heats Up," Quality, March 1982.
52. Boulton, H., "Thermography Systems for PCB Testing Applications," Electronics, April 1985.
53. Kallis, J. M., Egan, G. S., and Wirick, M. P., "Nondestructive Infrared Inspection of Hybrid Microcircuit Substrate-to-Package Thermal Adhesive Bonds," IEEE Transactions on Components, Hybrids, and Manufacturing Technology, September 1981.
54. Boulton, H., "Testing Hybrids Using Thermography," Hybrid Circuit Technology, July 1984.
55. Yu E. Y., "Determination of Temperature of Integrated-Circuit Chips in Hybrid Packaging," IEEE Transactions on Parts, Hybrids, and Packaging, June 1976.
56. Lidback, C. A., "Scanning Infrared Microscopy Techniques for Semiconductor Thermal Analysis," Reliability Physics, 1979.
57. Wickersheim, K. A., "New Thermometry Technique Measures Component Temperature," Electronic Packaging and Production, September 1981.
58. Coats T., "A Computer-Aided Thermal Analysis for Microcircuits," Electronic Packaging and Production, October 1975.
59. Sergeant, J., and Schuyler, D. R., "Thermal Analysis Helps Keep

Hybrid Microcircuits Cool," Electronic Packaging and Production, October 1982.

60. Baxter G. K., "Thermal Resistance of Microelectronic Packages: Part 1," RADC-TR-75-204, NTIS 1975.
61. Baxter, G. K., and Brouillette, W., "Thermal Resistance of Microelectronic Packages: Part 2," RADC-TR-75-204, NTIS 1975.
62. Baxter, G. K., "A Recommendation of Thermal Measurement Techniques for IC Chips and Packages," Reliability Physics, 1977.
63. Anslow, J. W., Baxter, G. K., and Brouillette, J. W., "Thermal Resistance of Microelectronic Packages," RADC-TR-77-321, NTIS 1977.
64. Touloukian, Y. S., et al., Thermophysical Properties of Matter, Thermophysical Properties Research Center, IFI/Plenum, New York, 1970.
65. Weast, R. C., Astle, M. J., Beyer, W. H., CRC Handbook of Chemistry and Physics, CRC Press, Inc., Boca Raton, Florida, 1983.
66. Martin Marietta Interactive Thermal Analysis System, Version 2.0, User's Manual, Martin Marietta Denver Division, ESO No. 7581, 1974.
67. Kreith, F., Black, W. Z., Basic Heat Transfer, Harper & Row, Publishers, New York, 1980.
68. Siegel, R., Howell, J. R., Thermal Radiation Heat Transfer, Hemisphere Publishing Corporation, New York, 1981.
69. Arpaci, V. S., Conduction Heat Transfer, Addison-Wesley Publishing Company, Reading, Massachusetts, 1966.
70. Inframetrics Instruction Manual, Model 525-Infrared Thermal Imaging System, Bedford, Massachusetts, June 1981.



GEORGIA TECH 1885-1985

DESIGNING TOMORROW TODAY

THE GEORGE W. WOODRUFF SCHOOL OF
MECHANICAL ENGINEERING

August 8, 1986

Dr. John C. Gustafson
Department Manager
Physical Electronics Tech Center
GTE Laboratories, Inc.
40 Sylvan Road
Waltham, MASS 02254

Dear Dr. Gustafson:

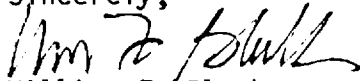
Geow Heng has made excellent progress on his thesis since the beginning of the year. He has advanced to the stage where he can now scan the surface of the chip or chip package with the infrared camera and process the data through a digitizer and PC to map the local surface temperature. He has also developed a technique that allows him to locally correct for the variations in the emissivity of the chip or package. The emissivity correction scheme utilizes an image processing software package that was originally developed for enhancing earth satellite photographs. The entire technique is a unique one which will permit local temperature measurements on a spot size as small as 0.025 mm to within 1 °C.

I have enclosed a summary report of Geow's accomplishments to date. This document will serve as a final report of work that GTE sponsored in the School of Mechanical Engineering through December 1985.

We would like to thank you for your financial support of the micro-electronic packaging project. We would not have been able to make any of this progress without your help. We will mail you a copy of Mr. Heng's Ph.D thesis when he completes it sometime next year.

If you have any comments or questions about the enclosed report, please feel free to call me.

Sincerely,


William Z. Black

WZB:rh
Enclosure

Georgia Institute of Technology
Atlanta, Georgia 30332-0405